**CHARLES UNIVERSITY IN PRAGUE**

**Faculty of Science**

Study programme: Biology

Field of study: Cell and Developmental Biology

**Bc. Tomáš Liďák**

# Characterisation of the mechanisms regulating 53BP1 nuclear transport

Charakterizace mechanismů jaderného transportu proteinu 53BP1

MASTER'S THESIS

Supervisor: MUDr. Libor Macůrek, Ph.D.

Prague, 2016

**Prohlášení:**

Prohlašuji, že jsem závěrečnou práci zpracoval samostatně a že jsem uvedl všechny použité informační zdroje a literaturu. Tato práce ani její podstatná část nebyla předložena k získání jiného nebo stejného akademického titulu.

V Praze, 8. 8. 2016

_____

Tomáš Liďák

# Acknowledgements

My greatest thanks go to my supervisor Libor Macůrek for his guidance during my experimental work and to all other members of the Laboratory of Cancer Cell Biology at Institute of Molecular Genetics of the ASCR. I would like to especially thank to Jan Benada for help with microscopy experiments, to Kamila Burdová for help with biochemical experiments and to Soňa Pecháčková for purification of GFP-TRAP®. I would like to acknowledge Roman Liška, from X-ray irradiation facility at Institute of Molecular Genetics of the ASCR, for γ-irradiation of cells. My sincere thanks goes to Tomáš Macháček, who helped me with statistics and language correction of this thesis. Last but not least, I would like to thank to my family for their continuous support during my studies.

# Abstract

Tumor suppressor p53-binding protein 1 (53BP1) is an integral part of a sophisticated network of cellular pathways termed as the DNA damage response (DDR). These pathways are specialized in the maintenance of genome integrity. Recently, it was reported that nuclear import of 53BP1 depends on importin ß. Here, I used fluorescence microscopy and co-immunoprecipitation experiments to identify its nuclear localization signal (NLS). Clusters of basic amino acids 1667-KRK-1669 and 1681-KRGRK-1685 were required for 53BP1 interaction with importin ß and for its nuclear localization. Short peptide containing these two clusters was sufficient for interaction with importin ß and targeting EGFP to the nucleus. Additionally, the effect of 53BP1 phosphorylation at S1678 on its nuclear import was examined. Mimicking the phosphorylation in the 53BP1-S1678D mutant decreased the binding to importin ß and resulted in a mild defect in 53BP1 nuclear import. However, 53BP1 entered the nucleus continuously during the cell cycle, suggesting that CDK-dependent phosphorylation of S1678 probably does not significantly contribute to the regulation of 53BP1 nuclear transport. Taken together, 53BP1 NLS meets the attributes of a classical bipartite NLS. Although no cell cycle-dependent regulation of its import was observed, the potential effect of other 53BP1 posttranslational modifications or cancer mutations on its nuclear localization can now be easily estimated.



Keywords: 53BP1, nuclear localization signal, nuclear import, phosphorylation, acetylation

# Abstrakt

Protein 53BP1 se významně podílí na buněčné odpovědi na poškození DNA a udržování integrity genomu. Nedávno bylo popsáno, že je transportován do jádra prostřednictvím importinu ß. Cílem této práce bylo identifikovat jaderný lokalizační signál proteinu 53BP1, a to s využitím metod fluorescenční mikroskopie a imunoprecipitace. Získané výsledky ukázaly, že protein 53BP1 váže importin ß prostřednictvím svých dvou úseků bohatých na bazické aminokyseliny (1667-KRK-1669 a 1681-KRGRK-1685). Tyto úseky byly rovněž nutné pro jeho vstup do jádra. Krátký polypeptid zahrnující tyto dva úseky vázal importin ß a umožnil transport GFP do jádra. Dále jsem se zaměřil na testování vlivu fosforylace serínu 1678 na transport proteinu 53BP1 do jádra. Mutanta 53BP1-S1678D, která mimikuje fosforylovaný serín na pozici 1678, měla výrazně sníženou schopnost vázat importin ß a byla hůře transportována do jádra. Nicméně žádné změny v transportu proteinu 53BP1 do jádra nebyly pozorovány, a tak se zdá, že fosforylace serínu 1678 cyklin-dependentními kinázami nebude významně regulovat jeho transport. Závěrem lze konstatovat, že protein 53BP1 má klasický bipartitní jaderný lokalizační signál. I když se transport proteinu 53BP1 do jádra nezdá být regulován v průběhu buněčného cyklu, může být regulován v odpovědi na jiné podněty. Výsledky předložené v této práci proto do budoucna výrazně usnadní předpověď vlivů dalších popsaných postranslančních modifikací a nádorových mutací na transport proteinu 53BP1 do jádra.



Klíčová slova: 53BP1, jaderný lokalizační signál, transport proteinů do jádra, fosforylace, acetylace

# Table of contents

# Abbreviations

| | |
|---|---|
| **4X SB** | 4X sample buffer |
| **53BP1** | tumor suppressor p53-binding protein 1 |
| **AID** | activation-induced cytidine deaminase |
| **alt-EJ** | alternative end joining |
| **ATM** | ataxia teleangiectasia mutated |
| **ATR** | ATM and Rad3-related |
| **BARD1** | BRCA1-associated RING domain protein 1 |
| **BRCA1** | breast cancer type 1 susceptibility protein |
| **BRCT** | BRCA1 C-terminal |
| **CDC25** | cell division cycle 25 |
| **CDK(s)** | cyclin dependent kinase(s) |
| **co-IP** | co-immunoprecipitation |
| **CSR** | class switch recombination |
| **DDR** | DNA damage response |
| **DNA-PKcs** | DNA-dependent protein kinase catalytic subunit |
| **DSBs** | double-strand breaks |
| **ELM** | eukaryotic linear motif |
| **G1** | gap1 |
| **G2** | gap2 |
| **GAP** | GTPase-activating protein |
| **GEF** | guanine nucleotide exchange factor |
| **H2AK15ub** | histone H2A ubiquitinated at K15 |
| **H4K20me2** | histone H4 dimethylated at K20 |
| **HNF-4** | hepatocyte nuclear factor 4 |
| **HR** | homologous recombination |
| **CHD3** | chromodomain 19 helicase-DNA-binding protein 3 |
| **Chk1** | checkpoint kinase-1 |
| **Chk2** | checkpoint kinase-2 |
| **IBB** | importin β binding |
| **IF** | immunofluorescence |
| **IgH** | immunoglobulin heavy chain |
| **IP** | immunoprecipitation |
| **IR** | ionizing radiation |
| **KAP-1** | KRAB-associated protein 1 |
| **K-W** | Kruskall-Wallis |
| **LINC** | linker of nucleoskeleton and cytoskeleton |
| **M** | mitotic |
| **MDC1** | mediator of DNA damage checkpoint protein 1 |
| **MRN** | Mre11-Rad50-Nbs1 |
| **MUM1** | mutated melanoma-associated antigen 1 |
| **NES** | nuclear export sequences |
| **NHEJ** | nonhomologous end joining |
| **NLS(s)** | nuclear localization signal(s) |
| **NPCs** | nuclear pore complexes |

| | |
|---|---|
| **NTF2** | nuclear transport factor 2 |
| **NUP153** | nucleoporin 153kDa |
| **PARP1** | poly(ADP-ribose) polymerase 1 |
| **PARPi** | PARP inhibitors |
| **PBS** | phosphate-buffered saline |
| **PCR** | polymerase chain reaction |
| **PIKK** | phosphatidylinositol 3-kinase related kinase |
| **PLK1** | polo-like kinase 1 |
| **PTIP** | Pax transactivation domain-interacting protein |
| **RIDDLE** | radiosensitivity, immunodeficiency, dysmorphic features, and learning difficulties |
| **Rif1** | Rap1-interacting factor 1 |
| **RNF168** | RING-finger ubiquitin ligase 168 |
| **RNF8** | RING-finger ubiquitin ligase 8 |
| **RPA** | replication protein A |
| **S** | synthesis |
| **SDSA** | synthesis-dependent strand annealing |
| **SSA** | single strand annealing |
| **UDR** | ubiquitylation-dependent recruitment |
| **USP28** | ubiquitin-specific protease 28 |
| **XLF** | XRCC4-like factor |
| **γH2AX** | histone H2AX phosphorylated at S139 |

**The Twenty Amino Acids**

| | | | |
|---|---|---|---|
| A | alanine | M | methionine |
| C | cysteine | N | asparagine |
| D | aspartic acid | P | proline |
| E | glutamic acid | Q | glutamine |
| F | phenylalanine | R | arginine |
| G | glycine | S | serine |
| H | histidine | T | threonine |
| I | isoleucine | V | valine |
| K | lysine | W | tryptophan |
| L | leucine | Y | tyrosine |

Single-letter amino acid code is used in the thesis, X represents any amino acid, pS stands for phosphorylated serine, pT stands for phosphorylated threonine, ub refers to ubiquitination and me refers to methylation.

# 1. Introduction

DNA damage response (DDR) is a sophisticated network of cellular pathways dedicated to maintain genome integrity. Primarily, these pathways detect and repair DNA lesions. Furthermore, they can activate DNA damage checkpoints to temporarily arrest cell cycle progression, induce senescence or definitively eliminate a cell by programmed cell death (apoptosis).

Of the various types of DNA lesions, DNA double-strand breaks (DSBs) are the most dangerous as they can cause cell death or genome rearrangements leading to genome instability. There are several sources of DNA DSBs: ionizing radiation (IR), reactive oxygen species, and DNA metabolisms itself. While DNA DSBs are usually accidental, some cellular processes generate DNA DSBs in a programmed way, such as during V(D)J recombination, class switch recombination (CSR) or meiosis (Pfeiffer et al., 2000). Defects in response to DNA DSBs are associated with various immunodeficiency and neurodegenerative disorders, infertility, premature aging, and cancer (Jackson and Bartek, 2009).

DNA DSBs can be repaired by several pathways and tumor suppressor p53-binding protein 1 (53BP1) is an important regulator of DNA DSBs repair pathway choice (Bothmer et al., 2010; Bunting et al., 2010). 53BP1 has a fundamental impact on outcome of DNA DSBs repair and genome integrity maintenance. Although its role in genome integrity has been studied extensively, much less is known about 53BP1 nuclear import. Import of 53BP1 to the nucleus is a prerequisite for its functions. Indeed, a defect in its nuclear import was shown to undermine DNA damage response and balance among DNA DSBs repair pathways (Lemaître et al., 2012; Moudry et al., 2012). Importantly, loss of 53BP1 can cause resistance to certain cancer therapies and it is also associated with tumorigenesis (Bouwman et al., 2010; Bunting et al., 2010). As inability of 53BP1 to localize to the nucleus is expected to mimic the loss of 53BP1, mechanisms of its nuclear transport and their potential regulation are of particular interest. Currently, it is not known whether import of 53BP1 to the nucleus is regulated. Within 53BP1 sequence, a nuclear localization signal (NLS) was mapped to its C-terminus (Jullien et al., 2002; Zgheib et al., 2009), but the precise position has not been determined. Herein, I present an identification of 53BP1 NLS and examination of potential ways of its regulation. The results may serve as a fundamental information resource for further exploration of 53BP1 nuclear transport.

# 2. Aims

The first aim was **to identify 53BP1 NLS**. This required:

- to predict the position of NLS within 53BP1 sequence;
- to design and prepare DNA constructs encoding 53BP1 mutants expected to be defective in nuclear import;
- to explore their defect in nuclear localization by immunofluorescence (IF);
- to examine their defect in binding to importin ß by co-immunoprecipitation (co-IP);
- to design and prepare DNA construct encoding the sequence of 53BP1 NLS fused to EGFP
- to confirm its nuclear localization and its binding to importin ß

The second aim was **to examine potential ways of 53BP1 NLS regulation**. This required:

- to select residues expected to be targeted by posttranslational modifications and thus regulate import of 53BP1 to the nucleus;
- to test the effect of selected posttranslational modification on nuclear import of 53BP1;
- to evaluate the ability of 53BP1 to be imported to the nucleus during different phases of the cell cycle.

# 3. Literature review

## 3.1. Cellular response to DNA DSBs

Three members of the phosphatidylinositol 3-kinase related kinase (PIKK) family orchestrate the response to DNA DSBs. Ataxia teleangiectasia mutated (ATM) kinase and DNA-dependent protein kinase catalytic subunit (DNA-PKcs) are activated in the vicinity of DNA DSBs. Activation of the ATM and Rad3-related (ATR) kinase requires single-stranded DNA coated by replication protein A (RPA), which can be also generated at DNA DSBs, especially in S and G2 phases of the cell cycle (Jazayeri et al., 2006). SQ/TQ motif is a common phosphorylation consensus sequence for these kinases (Kim et al., 1999). About 900 regulated phosphorylation sites encompassing over 700 proteins were identified in cells exposed to IR (Matsuoka et al., 2007). While DNA-PKcs is involved predominantly in DNA repair, ATM and ATR kinases initiate DNA damage checkpoints.

Checkpoint kinase-1 (Chk1) and checkpoint kinase-2 (Chk2) are effector kinases in DNA damage checkpoints. Active ATM kinase phosphorylates Chk2 at DNA DSBs, while active ATR kinase phosphorylates Chk1 at RPA-coated single-stranded DNA lesions. These phosphorylations lead to activation of Chk1 and Chk2. As both effector kinases are highly mobile, they enable quick spreading of the signal throughout the nucleus (Lukas et al., 2003; Smits et al., 2006). Various crosstalks between ATM-Chk2 and ATR-Chk1 signalling exist and both effector kinases share many substrates and perform partly redundant roles. Important processes controlled by Chk1 and Chk2 are cell cycle progression and apoptosis (Bartek and Lukas, 2003).

Proliferating cells repeatedly progress through the cell cycle to divide. The cell cycle consists of four subsequent phases: G1 (gap1), S (synthesis), G2 (gap2) and M (mitotic). Progression through the cell cycle is governed by different cyclin dependent kinases (CDKs) and their activating cyclin subunits. Cyclins activate CDKs by binding to them. While level of CDKs is constant during the cell cycle, the concentration of cyclins oscillates. Cyclin D-CDK4/6 and cyclin E-CDK2 regulate G1/S transition. Cyclin A-CDK2 promotes S phase. Cyclin A-CDK1 is active from late S to early M phase and cyclin B-CDK1 is essential for mitotic entry and progression. A plethora of CDK inhibitors can associate with cyclin-CDK complexes and inhibit their activity. Moreover, CDKs are regulated by activating and inhibitory phosphorylations. Cell division cycle 25 (CDC25) phosphatases are crucial for activation of CDKs by removing inhibitory phosphorylations (Arellano and Moreno, 1997). In response to DNA damage, rapid arrest of the cell cycle progression is achieved by inactivation of CDC25 phosphatases by Chk1 and Chk2 kinases (Falck et al., 2001; Jin et al., 2003; Peng et al., 1997; Sanchez et al., 1997).

Various stress-signalling pathways converge on transcription factor p53 and p53-dependent response can have various outcomes. Therefore, p53 is a central hub controlling the cell fate decision in response to potential threats. A principal negative regulator of p53 is an E3 ubiquitin ligase Mdm2.

In response to DNA damage, p53 is phosphorylated at serine and threonine residues by ATM, ATR, Chk1 and Chk2 kinases and acetylated at several lysine residues. These induced posttranslational modifications together disrupt interaction between p53 and Mdm2, stabilize p53 and recruit transcriptional co-activators (Dai and Gu, 2010). Importantly, p53 induces transcription of CDK inhibitor p21 (Dulić et al., 1994), which is crucial for checkpoint maintenance. Another important transcription targets of p53 are pro-apoptotic genes (Miyashita et al., 1994; Nakano and Vousden, 2001) and p53 can also induce replicative senescence (Kortlever et al., 2006).

Four distinct pathways (Figure 1) can repair DNA DSBs: classical nonhomologous end joining (NHEJ), homologous recombination (HR), alternative end joining (alt-EJ) or single strand annealing (SSA). Although DNA DSBs repair pathway choice is not completely understood, it is generally accepted that it is largely determined by DNA end resection and the extent to which it occurs. A process termed DNA end resection generates 3' single-stranded DNA overhangs by degradation of 5'-terminated DNA strands. The Mre11-Rad50-Nbs1 (MRN) complex and protein CtIP cooperate during the initial phase of DNA end resection to generate short 3' single-stranded DNA overhangs. Additional exonucleases and helicases can further expand these short overhangs into more extensive ones. DNA end resection is precisely regulated during the cell cycle progression, being limited in G1 phase and much more efficient in S and G2 phases. A crucial suppressor of DNA end resection is 53BP1, while CDK activity is responsible for a burst of DNA end resection in S and G2 phases of the cell cycle (Ceccaldi et al., 2016).

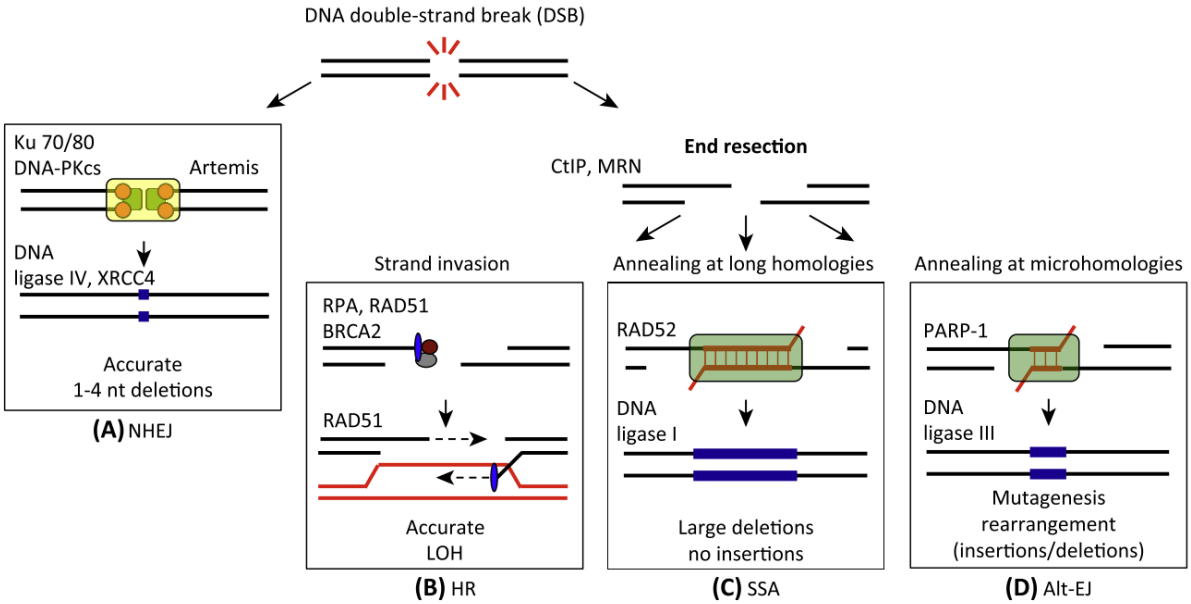


**Figure 1. DNA DSBs repair pathways.** When DNA end resection is blocked, NHEJ is favoured. However, when DNA end resection occurs, HR, SSA and alt-EJ can compete for the repair. NHEJ and HR are considered high-fidelity processes, whereas SSA and alt-EJ are intrinsically mutagenic. Adapted from Ceccaldi et al., 2016.

NHEJ has fast kinetics and mediates ligation of blunt-ended DNA DSBs. NHEJ is inhibited by and inhibitory to DNA end resection and not restricted to any certain phase of the cell cycle. Ku70/Ku80 heterodimers recognise DNA ends and immediately associate with DNA-PKcs to form active DNA-PK holoenzymes. DNA-PK holoenzymes further recruit other NHEJ factors to assist in holding and processing of DNA ends, if necessary. Finally, DNA ligase IV joins the blunt DNA ends together. The drawback of DNA repair by NHEJ is the DNA end processing step which can cause small deletion, substitution or insertion (Davis and Chen, 2013).

HR in mammalian somatic cells uses sister chromatid as a template. Therefore, it is restricted to S and G2 phases of the cell cycle and considered error-free mechanism. Among others, stalled or broken replication forks rely especially on HR. DNA repair by HR requires extensive resection. As any single-stranded DNA in cells, 3' single-stranded DNA overhangs are immediately bound by RPA. To initiate HR, RPA must be displaced from 3' single-stranded DNA overhang and replaced by RAD51 recombinase to generate RAD51 filament. In the next step, RAD51 filament performs a homology search and invades homologous duplex. DNA synthesis extends the invading 3' DNA end, thereby copying the sequence from the sister chromatid. At this point, several distinct subpathways can emerge. When both DNA ends are present, a subpathway termed synthesis-dependent strand annealing (SDSA) is predominant. SDSA terminates by annealing of the newly synthesised strand with a complementary sequence within the resected strand of the second DNA end (Heyer et al., 2010).

alt-EJ and SSA mediate end joining by annealing at microhomologies and long homologies, respectively. These processes are therefore inherently mutagenic and generate various genome rearrangements. alt-EJ depends on a limited DNA end resection by MRN complex and CtIP. Limited DNA end resection is sufficient to reveal single-stranded microhomologies, which are believed to be annealed by poly(ADP-ribose) polymerase 1 (PARP1). DNA ligase III finally joins processed DNA ends (Frit et al., 2014). Although alt-EJ can occur in the G1 phase, especially when NHEJ is compromised, alt-EJ is significantly increased when cells enter the S phase and is used at level of 10-20% of HR (Truong et al., 2013). Interestingly, alt-EJ also contributes to the repair of collapsed replication forks (Truong et al., 2013). SSA has been insufficiently explored in mammalian cells yet. SSA depends on extensive resection and anneals exposed complementary sequences in a RAD51-independent process which is mediated by RAD52 recombinase (Bennardo et al., 2008).

## 3.2. 53BP1

53BP1 is a scaffold protein (Figure 2), which assembles protein complexes to chromatin flanking the DNA DSBs. 53BP1 lacks any enzymatic activity and its multiple functions in DDR are executed by various components of protein complexes that are gathered at sites flanking DNA DSBs by 53BP1.

.

Plethora of various proteins accumulates at or near DNA DSBs to form distinct nuclear structures termed as DNA damage foci. 53BP1 recruitment to these foci (see Section 3.2.1.) is vital to its functions and requires its oligomerization domain, tandem Tudor domain and ubiquitylation-dependent recruitment (UDR) motif (Fradet-Turcotte et al., 2013; Zgheib et al., 2009).

Although tandem BRCA1 C-terminal (BRCT) domain at the C-terminus of 53BP1 can contribute to 53BP1 recruitment to DNA damage foci, it is mainly implicated in repair of DNA DSBs associated with heterochromatin (see Section 3.2.2.).

The N-terminal part of 53BP1 is unstructured and phosphorylated by ATM kinase in response to DNA damage at various SQ/TQ motifs, which then serve as docking sites for numerous downstream effectors of 53BP1 (see Section 3.2.3.). 53BP1 and its downstream effectors collaborate on promoting NHEJ by various means. Especially, they supress DNA end resection (Bothmer et al., 2010; Bunting et al., 2010) and increase DNA end mobility (Dimitrova et al., 2008; Lottersberger et al., 2015).

53BP1 is important for development of the immune system because its functions are necessary for CSR and V(D)J recombination (see Section 3.2.4.). Owing to its role in genome integrity maintenance, 53BP1 is an important genome caretaker and its loss is associated with cancer in several distinct contexts (see Section 3.2.5.).

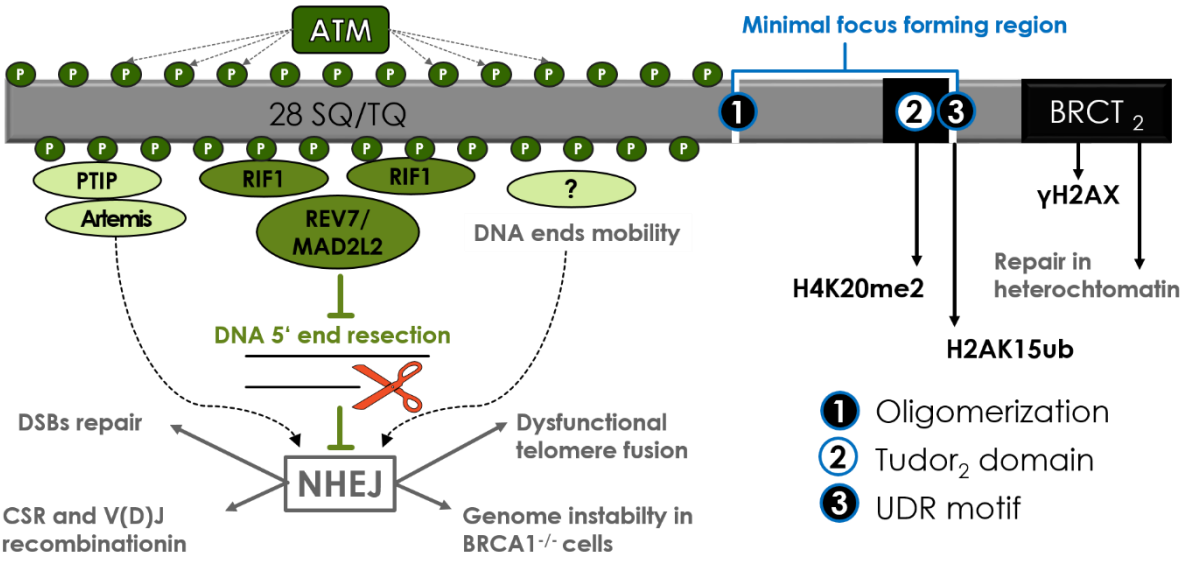


**Figure 2. Overview of structure and functions of 53BP1.** Oligomerization domain, tandem Tudor domain and UDR motif of 53BP1 are necessary for its recruitment to chromatin flanking DNA DSBs. Tandem BRCT domain of 53BP1 is required for repair of DNA DSBs associated with heterochromatin. N-terminal part is unstructured and phosphorylated at numerous SQ/TQ motifs in response to DNA damage. Phosphorylated SQ/TQ motifs serve as docking sites for downstream effectors of 53BP1, which generally promote NHEJ pathway. Importantly, 53BP1 together with its downstream effectors supress DNA end resection and thus regulate DNA DSBs repair pathway choice.

### 3.1.1. 53BP1 recruitment to DNA damage sites

In response to DNA damage (induced by IR and other DNA damaging agents), 53BP1 rapidly localizes to discrete nuclear foci flanking DNA DSBs and becomes hyperphosphorylated by ATM kinase (Anderson et al., 2001; Rappold et al., 2001; Schultz et al., 2000; Xia et al., 2001). Under replication stress, large 53BP1 bodies form around DNA lesions generated by mitotic transmission of under-replicated DNA to daughter cells. 53BP1 bodies sequester these DNA lesions throughout G1 phase and disappear in early S phase of the cell cycle (Harrigan et al., 2011; Lukas et al., 2011).

53BP1 recruitment to DNA damage sites depends on a chromatin-associated pathway. This pathway marks the chromatin flanking DNA DSBs and enables 53BP1 to be recruited there. Histone H2AX phosphorylated at S139 residue is termed γH2AX and occurs on chromatin flanking DNA DSBs (Rogakou et al., 1999, 1998). The phosphorylation is carried out by ATM kinase and DNA-PKcs (Stiff et al., 2004) and is a canonical marker of DNA DSBs. Recruitment of these two kinases and their subsequent activation rely on recognition of DNA DSBs by sensors, which are Ku70/Ku80 heterodimer in case of DNA-PK and MRN complex in case of ATM (Falck et al., 2005). The most important primary reader of γH2AX is the mediator of DNA damage checkpoint protein 1 (MDC1), which binds γH2AX *via* its BRCT domains (Stucki et al., 2005). Spreading of γH2AX is enabled by direct interaction between MDC1 and MRN complex, which associates with active ATM kinase (Hari et al., 2010).

RING-finger ubiquitin ligase 8 (RNF8) also directly interacts with MDC1 and is recruited to DNA damage sites *via* this interaction (Mailand et al., 2007). RNF8 in conjunction with ubiquitin-conjugating enzyme UBC13 (also known as UBE2N) generates K63-linked ubiquitin chains on H1-type linker histones (Thorslund et al., 2015). RING-finger ubiquitin ligase 168 (RNF168) recognises these chains and subsequently mediates monoubiquitination of K13 and K15 residues on histone H2A (Mattiroli et al., 2012; Thorslund et al., 2015). RNF8-RNF168 pathway is also implicated in unmasking of the histone H4K20me2 mark at sites flanking DNA DSBs. H4K20me2 is not induced after DNA damage and a competition over binding to H4K20me2 exists in unperturbed cells. Several proteins, which bind to H4K20me2, are described to be degraded or evicted from the chromatin by RNF8-RNF168 pathway (Acs et al., 2011; Mallette et al., 2012; Meerang et al., 2011).

A minimal region that is sufficient for localization to DNA damage foci, was narrowed down between amino acids 1231–1631 of 53BP1 (Zgheib et al., 2009). It contains oligomerization domain (1231-1277), tandem Tudor domain (1484-1603) and UDR motif (1604-1631), which are all necessary for recruitment of 53BP1 to chromatin flanking DNA DSBs (Fradet-Turcotte et al., 2013; Zgheib et al., 2009). Tandem Tudor domain specifically binds histone H4K20me2 and is important for association of 53BP1 with chromatin (Botuyan et al., 2006). UDR motif is responsible for specific recognition of DNA DSBs-flanking chromatin, because it binds histone H2AK15ub, which is induced by RNF8-RNF168 pathway in response to DNA damage (Fradet-Turcotte et al., 2013). Furthermore, tandem BRCT domain of

53BP1 can contribute to its recruitment to DNA damage sites. Tandem BRCT domain is outside the minimal focus forming region, but binds directly γH2AX, albeit with lower affinity than tandem BRCT domain of MDC1. Direct interaction between 53BP1 and γH2AX, albeit being dispensable, increases the efficiency of 53BP1 recruitment to DNA damage sites (Baldock et al., 2015; Kleiner et al., 2015).

53BP1 recruitment to DNA damage sites is inhibited in the M phase. Although the chromatin flanking DNA DSBs is marked by γH2AX and recognised by MDC1, other factors such as RNF8, RNF168 and 53BP1 are not recruited there (Giunta et al., 2010). This is achieved by a combined action of mitotic kinases CDK1 and polo-like kinase 1 (Plk1). CDK1 phosphorylate RNF8 to thwart interaction between RNF8 and MDC1. Furthermore, 53BP1 is phosphorylated within its UDR motif at T1609 by CDK1 and at S1618 by Plk1 to inhibit its binding to ubiquitinated histones (Benada et al., 2015; Lee et al., 2014; Orthwein et al., 2014). Nevertheless, S1678 outside the UDR motif was identified to be major phosphorylation target of cyclin B-CDK1 in *in vitro* kinase assays. It was hypothesised that this phosphorylation can also contribute to the inhibition of 53BP1 recruitment to the DNA damage sites (Benada et al., 2015). Reactivation of 53BP1 recruitment to DNA damage sites in the M phase results in telomere fusions and leads to chromosome segregation errors and aneuploidy (Orthwein et al., 2014).

### 3.1.2. 53BP1 functions associated with its BRCT domains

BRCT domains are often found in proteins involved in DNA metabolism or DDR and mediate interactions. They usually recognise short linear motifs phosphorylated by ATM or ATR kinases within their target proteins, but phospho-independent protein-protein interactions and binding to DNA or to poly(ADP-ribose) were described as well (Leung and Glover, 2011). 53BP1 possesses a tandem BRCT domain which is capable of both phospho-dependent and phospho-independent protein-protein interactions. A 53BP1 mutant that specifically abolished phospo-dependent binding to γH2AX but not phospho-independent binding to MRN complex was described (Baldock et al., 2015). Using this mutant, it is now possible to separate these two modes of 53BP1 tandem BRCT domain function. 53BP1 tandem BRCT domain are thought to have only minor role in DDR (Ward et al., 2006) and are believed to be required only when DNA DSBs are acquired in heterochromatin (Noon et al., 2010).

Tethering of active ATM kinase to the late repairing foci in the G1 phase depends on phospho-dependent interaction(s) mediated by tandem BRCT domain of 53BP1 (Baldock et al., 2015; Noon et al., 2010). Only γH2AX has been described to interact with 53BP1 tandem BRCT in phospo-dependent manner. Therefore, other so far undiscovered ligand or a complex mechanism involving γH2AX binding are likely responsible for this phenomenon. Late repairing foci are thought to correspond to DNA DSBs in heterochromatin (15–25% of DNA DSBs), which are repaired by slower kinetics than DNA DSBs in euchromatin and require ATM kinase activity (Goodarzi et al., 2008). Active ATM kinase is believed to

be concentrated at this late repairing foci in order to locally sustain the phosphorylation of the transcriptional co-repressor KRAB-associated protein 1 (KAP-1) at S824 for a period needed for completion of the repair (Noon et al., 2010). Phosphorylation of KAP-1 at S824 disrupts its interaction with the nucleosome remodeller chromodomain 19 helicase-DNA-binding protein 3 (CHD3), thereby causing heterochromatin relaxation and enabling repair of heterochromatic DNA DSBs (Goodarzi et al., 2011). Although these mechanisms were studied in G0/G1 cells, 53BP1 was also shown to be required for overcoming the barrier to DNA DSBs repair posed by heterochromatin in the G2 phase (Kakarougkas et al., 2013).

Hyperaccumulation of MRN complex at late repairing foci depends on phospho-independent interaction(s) mediated by tandem BRCT domain of 53BP1 (Baldock et al., 2015; Noon et al., 2010). The interaction between RAD50 (and therefore MRN complex) and tandem BRCT domain of 53BP1 was shown *in vitro* to stimulate ATM kinase activity and therefore was suggested to amplify ATM-dependent checkpoint signalling (Lee et al., 2010).

Other proteins recruited to DNA damage sites by 53BP1 tandem BRCT domains are EXPAND1 (also known as mutated melanoma-associated antigen 1 (MUM1)) and ubiquitin-specific protease 28 (USP28). 53BP1-EXPAND1 interaction was described to be phosphorylation-independent. Once recruited to DNA damage sites, EXPAND1 triggers chromatin relaxation, which is distinct from that KAP1-CHD3-dependent and plays an accessory role (Huen et al., 2010a). Although 53BP1-USP28 interaction is well documented, no significant role in DDR for this interaction has been addressed during interphase (Knobel et al., 2014).

### 3.2.3. 53BP1 functions associated with SQ/TQ motifs in its N-terminal part

The whole N-terminal part of 53BP1 preceding the minimal focus forming region is predicted to be unstructured and exposed to the solvent (Rost et al., 2004). This region contains 28 SQ/TQ motifs, which are potential targets of DNA-PK, ATR and ATM kinases. Indeed, some of these SQ/TQ motifs were shown to be phosphorylated by ATM kinase after exposure to IR and even by ATR kinase after exposure to UV (Jowsey et al., 2007). Importantly, fundamental roles of 53BP1 in DNA DSBs repair depend on its recruitment to DNA damage foci and these multiple phosphorylations at N-terminus of 53BP1 by ATM kinase.

These phosphorylations are often redundant in function. Therefore, a 53BP1-28A mutant, which has all 28 SQ/TQ motifs mutated and behaves as 53BP1 lacking the whole N-terminal part, has traditionally been used to study functions of 53BP1 in DNA DSBs repair (Bothmer et al., 2011; Lottersberger et al., 2013). In this way, roles of 53BP1 in supressing DNA ends resection during DNA DSBs repair, in promoting DNA DSBs mobility, in CSR, in fusion of dysfunctional telomeres and in genome instability caused by deficiency in the breast cancer type 1 susceptibility protein (BRCA1) were

associated with phosphorylations of these SQ/TQ motifs (Bothmer et al., 2011; Lottersberger et al., 2013). It is therefore generally accepted, that phosphorylated SQ/TQ motifs enable assembly of protein complexes at DNA damage sites, which bear distinct activities and cooperatively participates in the outcome of DNA repair.

A phospho-dependent interaction between 53BP1 and the Pax transactivation domain-interacting protein (PTIP) occurs after exposure to IR. It is mediated by the C-terminal tandem BRCT domains of PTIP and ATM-phosporylated S25 of 53BP1 (Munoz et al., 2007). Although PTIP itself can bind γH2AX via its BRCT tandem domain (Yan et al., 2011), its recruitment to DNA damage sites depends on interaction with 53BP1 (Callen et al., 2013). While the interaction is dispensable for CSR, it is required for fusion of dysfunctional telomeres (Callen et al., 2013). In BRCA1-deficient cells, 53BP1-PTIP interaction causes a defect in HR and a radial chromosome formation (Callen et al., 2013). Endonuclease Artemis, which trims overhangs at DNA ends and stimulates NHEJ (Mohapatra et al., 2013), was implicated to be the effector in the 53BP1-PTIP pathway (Wang et al., 2014). Endonuclease Artemis interacts with PTIP, recapitulates the phenotype of PTIP lost in BRCA1-deficient cells and its retention on DNA damage sites depends on the 53BP1-PTIP pathway (Wang et al., 2014).

A phospo-dependent interaction between 53BP1 and the Rap1-interacting factor 1 (Rif1) also occurs after exposure to IR. It is mediated by the HEAT repeats of Rif1 and multiple ATM-phoshorylated SQ/TQ motifs of 53BP1(Di Virgilio et al., 2013; Escribano-Díaz et al., 2013; Chapman et al., 2013; Zimmermann et al., 2013). This interaction is required for 53BP1-mediated inhibition of DNA end resection. It is required for CSR (Di Virgilio et al., 2013; Escribano-Díaz et al., 2013; Chapman et al., 2013) and fusion of dysfunctional telomeres (Chapman et al., 2013; Zimmermann et al., 2013), while being only partially responsible for a defect in HR caused by 53BP1 in BRCA1-deficient cells (Feng et al., 2013; Zimmermann et al., 2013). REV7 (also known as MAD2L2) is an additional member of the 53BP1-Rif1 pathway, which acts downstream of Rif1 to suppress DNA ends resection, to promote CSR and telomere fusions and to cause a HR defect in BRCA1-deficeint cells (Boersma et al., 2015; Xu et al., 2015).

Importantly, Rif1 and BRCA1 have mutually exclusive localization in DNA damage foci (Escribano-Díaz et al., 2013; Feng et al., 2013; Chapman et al., 2013). In the G1 phase, the 53BP1-Rif1 pathway inhibits BRCA1 recruitment to foci, while BRCA1 excludes Rif1 from DNA damage foci in the S and G2 phases (Escribano-Díaz et al., 2013; Chapman et al., 2013). At the moment, it is not clear whether the BRCA1 exclusion from DNA damage foci in the G1 phase mediated by 53BP1-RIF1 and the suppression of DNA end resection mediated by 53BP1-Rif1- REV7 are two distinct processes or cause and consequences of one particular process. Once a cell enters the S phase, DNA resection is enabled and BRCA1 is engaged in that. In the S phase, cyclin A-CDK2 phosphorylates E3 ubiquitin ligase UHRF1. Phosphorylated UHRF1 interacts with tandem BRCT domain of BRCA1 and the interaction is sufficient

for its recruitment to DNA damage sites, where UHRF1 adds K63-linked ubiquitin chains to Rif1. Ubiquitination of Rif1 causes its dissociation from 53BP1 and facilitates initiation of HR (Zhang et al., 2016). In the G2 phase, interaction between BRCA1 and CtIP contributes to the negative regulation of Rif1 (Zhang et al., 2016). Moreover, BRCA1 in conjunction with the BRCA1-associated RING domain protein 1 (BARD1) mediates ubiquitination of histone H2A to recruit chromatin remodeller SMARCAD1. Chromatin remodeller SMARCAD1 repositions 53BP1 to the periphery of DNA damage foci in the S and G2 phases (Densham et al., 2016). These BRCA1-dependent evets are believed to be sufficient to relieve the barrier to DNA end resection posed by 53BP1. Nevertheless, 53BP1 is thought to influence DNA end resection even in the S and G2 phases, as its loss leads to hyperresection and a switch in DNA DSBs repair from HR to SSA in the S and G2 phases (Ochs et al., 2016).

The third 53BP1 phospho-dependent interaction with important consequences is still elusive. 53BP1 promotes mobility of DNA DSBs and dysfunctional telomeres (Dimitrova et al., 2008; Lottersberger et al., 2015). Increased mobility of DNA ends promotes NHEJ-dependent formation of radial chromosomes in BRCA1-deficient cells treated with PARP inhibitors (PARPi) and NHEJ-dependent fusion of dysfunctional telomeres (Dimitrova et al., 2008; Lottersberger et al., 2015). This increased mobility depends on some of the 13 most C-terminal 28 SQ/TQ motifs in N-terminal part of 53BP1, SUN1/2 in the linker of nucleoskeleton and cytoskeleton (LINC ) complex and dynamic microtubules (Lottersberger et al., 2015). As Rif1 and PTIP are not involved in these processes (Lottersberger et al., 2015; Zimmermann et al., 2013), a link between phosphorylated SQ/TQ motifs of 53BP1 and SUN1/2 is still missing.

### 3.1.4. 53BP1 and immunodeficiency

53BP1-deficient mice are immunodeficient (Morales et al., 2003; Ward et al., 2003), exhibiting a significant defect in CSR (Manis et al., 2004; Ward et al., 2004) and a slight defect in V(D)J recombination (Difilippantonio et al., 2008). Both CSR and V(D)J recombination are processes occurring during the lymphocyte maturation. Programmed DSBs are generated during these processes and 53BP1 is, to different extent, required for their re-joining.

CSR occurs upon antigen stimulation in B cells in order to produce antibodies of different isotypes (and therefore different effector functions), while not altering their antigen binding specificity. CSR is a deletional recombination process happening between switch regions located upstream of each immunoglobulin heavy chain (IgH) constant regions (except for Cδ), which is initiated by activation-induced cytidine deaminase (AID). AID creates, by deamination of cytidines to uracils, dU:dG mismatches within switch regions which are subsequently processed to DNA DSBs by base excision repair and mismatch repair pathways. Donor and acceptor switch region are brought together and joined in

a process dependent on 53BP1 and NHEJ pathway, thereby deleting intervening sequence and resulting in production of different antibody isotype (Stavnezer et al., 2008).

Using B cells originating from 53B1-deficient mice, it was demonstrated that 53BP1 is required for CSR and that loss of 53BP1 leads to 5–10-fold decrease in serum concentration of switched IgH isotypes (Manis et al., 2004; Ward et al., 2004). Since the loss of 53BP1 enhanced intraswitch region recombination, it was proposed that 53BP1 favours long-range recombination by synapsis of distal switch regions (Reina-San-Martin et al., 2007). Furthermore, 53BP1 protects DNA ends during CSR against resection (Bothmer et al., 2010) by a mechanism dependent on Rif1 (Di Virgilio et al., 2013; Escribano-Díaz et al., 2013; Chapman et al., 2013) and REV7 (Boersma et al., 2015; Xu et al., 2015).

V(D)J recombination occurs during B and T cells development in order to produce diverse repertoire of immunoglobulin and T cell receptor antigen binding specificities. Similarly to CSR, V(D)J recombination is also a deletional recombination process happening between recombination signal sequences flanking each V, D and J segment. It is initiated by RAG1/2 recombinases. RAG1/2 recombinases introduce DNA DSBs at donor and acceptor recombination signal sequences, which are, after certain processing, joined by NHEJ pathway. As a result, the intervening sequence is lost and a new combination of V(D)J segments is created, potentially giving rise to functional immunoglobulin or T cell receptor bearing new antigen specificity (Dudley et al., 2005).

53BP1 facilitates only long-range DNA end joining during V(D)J recombination, being required for distal V-DJ joining and protection against degradation of DNA ends (Difilippantonio et al., 2008). Furthermore, 53BP1 and XRCC4-like factor (XLF) have overlapping functions in V(D)J recombination, which is therefore severely impaired only by combined 53BP1 and XLF deficiency (Liu et al., 2012; Oksenych et al., 2012).

To date, no human immunodeficiency was directly associated with the loss of 53BP1. However, the failure of 53BP1 to be localized to DNA damage sites is believed to be underlying cause of immunodeficiency in the human RIDDLE (radiosensitivity, immunodeficiency, dysmorphic features, and learning difficulties) syndrome, which is caused by mutations in the *RNF168* gene (Stewart et al., 2009, 2007). That is why it is expected that the loss of 53BP1 could cause human immunodeficiency and might be found in some patients suffering from immunodeficiency in the future.

### 3.1.5. 53BP1 and cancer

Cells derived from 53BP1-deficient mice exhibit enhanced radiation sensitivity and increased genome instability (Morales et al., 2003; Ward et al., 2003). One of 53BP1-deficient mouse models was prone to cancer, developing predominantly leukemia and lymphoma (Ward et al., 2005, 2003); however, the other was insufficient to develop malignancy during the first year (Morales et al., 2006, 2003). Never-

theless, when both of these mice were crossed with p53-null mice, 53BP1 and p53 cooperation in tumour suppression was observed since the combined deficiency accelerated tumorigenesis in both animal models leading predominantly to the development of T lineage and B lineage lymphoma (Morales et al., 2006; Ward et al., 2005). Furthermore, dose-dependent effect of 53BP1 loss was revealed in these experiments, suggesting that 53BP1 is haploinsufficient tumour suppressor in mice (Morales et al., 2006; Ward et al., 2005). Another mouse model combined the loss of 53BP1 with higher expression of AID in B cells to demonstrate that 53BP1 supresses AID-induced B-cell lymphoma (Jankovic et al., 2013). In human patients, 53BP1 single copy loss was reported in a subset of diffuse large B cell lymphomas (Takeyama et al., 2008).

For cancer research, a tight connection between 53BP1 and BRCA1 (see Section 3.2.2.) is the most serious issue. The germline mutations in BRCA1 are the most significant risk factors predisposing to breast and ovarian cancer (Miki et al., 1994). Women carrying these mutations have 57% and 40% risk of developing breast and ovarian cancer, respectively, by the age 70 (Chen and Parmigiani, 2007). BRCA1 is a multifunctional protein involved in various aspects of genome integrity maintenance. Among others, BRCA1 is an important positive regulator of DNA end resection and HR (Huen et al., 2010b).

Defect in HR in BRCA1-deficient cells is exploited in cancer therapy. PARP inhibitors (PARPi) efficiently kill BRCA1-deficient cells while exhibiting no effect on BRCA1-proficient cells (Bryant et al., 2005; Farmer et al., 2005). Importantly, PARPi proved to be useful in cancer therapy. PARP inhibitor olaparib (LynparzaTM) was approved for treatment of advanced ovarian cancer in 2014 and many others PARPi are currently in clinical trials (Sonnenblick et al., 2015). Nevertheless, resistance to therapy is often reported. BRCA1-deficient cells can partially restore HR and overcome hypersensitivity to PARPi by the loss of 53BP1 (Bouwman et al., 2010; Bunting et al., 2010). In a mouse model, BRCA1-mutated mammary tumours acquired resistance to PARPi by upregulating P-glycoprotein efflux pumps (Rottenberg et al., 2008) or indeed by losing 53BP1 (Jaspers et al., 2013), thereby transporting the drug out of the cell or restoring HR, respectively. Interestingly, the loss of 53BP1 also alleviates embryonic lethality in mice which lack both BRCA1 functional alleles, while the cells derived from these animals manifest genome instability (Cao et al., 2009). Furthermore, the loss of 53BP1 was associated with triple-negative and BRCA1-mutated breast cancers in human (Bouwman et al., 2010). It was hypothesised that the observed genome instability (Cao et al., 2009) and tumorigenesis (Bouwman et al., 2010) were due to an increase in usage of mutagenic SSA as the loss of 53BP1 redirects repair from HR to SSA. Consequently, viability of the cells lacking BRCA1 and 53BP1 depends on RAD52 (Ochs et al., 2016). This observation suggests a potential for inhibitors of RAD52 in cancer therapy.

## 3.3. Nuclear transport

A double-membraned nuclear envelope separates the cytoplasm and the nucleus. Nuclear pore complexes (NPCs) perforate the nuclear envelope and enable transport of molecules between the cytoplasm and the nucleus. NPCs consist of the central part embedded in the nuclear envelope, eight cytoplasmic filaments and the nuclear basket (structure formed by eight nucleoplasmic filaments converging in a distal ring). Components of NPCs are termed nucleoporins. Some nucleoporins contain FG (phenylalanine-glycine) repeats, which form a selective transport barrier in the central part of NPCs. While small molecules and proteins up to 40 kDa in size diffuse freely through NPCs, larger molecules require nuclear transport receptors to traverse the NPCs (Knockenhauer and Schwartz, 2016).

Nuclear transport receptors bind exposed nuclear localization signals (NLSs) or nuclear export sequences (NESs) of their cargos and interact with various nucleoporins to mediate nuclear import or export, respectively. Cargos having both NLS and NES can shuttle between the nucleus and the cytoplasm and the shuttling can be regulated by posttranslational modifications that affect the accessibility of NLS or NES for nuclear transport receptors. Majority of nuclear transport receptors belong to ß-karyopherin family. Members of ß-karyopherin family bind their cargos directly or through an adaptor protein and can mediate nuclear import, nuclear export or both (Chook and Süel, 2011).

Directionality of and energy for nuclear transport are provided by hydrolysis of GTP by a GTPase Ran. Guanine nucleotide exchange factor (GEF) for Ran is sequestrated in the nucleus and therefore GTP-bound Ran (RanGTP) predominates there, whereas GTPase-activating protein (GAP) for Ran and therefore GDP-bound Ran (RanGDP) are found in the cytoplasm. This creates a RanGTP gradient across the nuclear envelope, which is used for nuclear transport. Nuclear transport receptors that work as importins bind their cargos in the cytoplasm, where the concentration of RanGTP is low, and cargos dissociate from importins by RanGTP binding in the nucleus. Nuclear transport receptors that work as exportins bind their cargos only simultaneously with RanGTP in the nucleus and cargos are released by GTP hydrolysis in the cytoplasm (Cautain et al., 2015).

### 3.3.1 Nuclear transport of 53BP1

53BP1 is imported to the nucleus in a Ran-dependent process, which relies on the nucleoporin 153kDa (NUP153) and importin ß (Lemaître et al., 2012; Moudry et al., 2012). Disruption of importin ß pathway blocks nuclear import of 53BP1, causing accumulation of 53BP1 in the cytoplasm (Moudry et al., 2012). Intriguingly, import of 53BP1 (and not of several other DDR factors such as MDC1 or BRCA1) relies on NUP153 as NUP153 knockdown prevents 53BP1 from entering the nucleus (Lemaître et al., 2012; Moudry et al., 2012).

### 3.3.2. Importin ß import pathway

As it was established that import of 53BP1 to the nucleus is importin ß-dependent (Moudry et al., 2012), only importin ß import pathways is described here. Importin ß is a member of ß-karyopherin family. Its working cycle can be divided into four steps: cargo recognition in the cytoplasm, cargo translocation through the NPCs, cargo release in the nucleus and importin ß translocation back to the cytoplasm. Importin ß consists of 19 tandem HEAT repeats, each of which is composed of an A and B helix connected by a turn. A helices form a convex surface (extending outward), whereas a concave surface (extending inward) is formed by B helices (Cingolani et al., 1999).

Importin ß can recognise its cargo directly or through adaptor proteins that have both the importin β binding (IBB) domain and the cargo recognition domain. Numerous cargos bind directly to concave surface of importin ß to be imported to the nucleus. These cargos have complex non-classical NLSs, which cannot be easily predicted, because they are determined by numerous amino acids within the tertiary structure of cargo proteins (Cingolani et al., 2002; Choi et al., 2014; Lee et al., 2003). IBB domain that also binds concave surface of importin ß is found in importin α, snurportin 1 and XRIPα, which are all importin ß adaptor proteins (Lott and Cingolani, 2011). XRIPα recognises RPA and it is required for its nuclear import (Jullien et al., 1999). Snurportin 1 recognises 5'-2,2,7-terminal trimethylguanosine cap and serves as nuclear import receptor for small nuclear ribonucleoproteins (Huber et al., 1998).

The most important importin ß adaptor is importin α, which recognises cargos containing classical monopartite or bipartite NLSs. Importin α consists of an IBB domain needed for interaction with importin ß and 10 tandem armadillo repeats responsible for binding of the NLS (Cingolani et al., 1999; Conti et al., 1998). Armadillo repeats of importin α create two independent NLS binding grooves – the major and the minor (Conti et al., 1998). Classical monopartite NLSs are formed by one cluster of basic residues and bind to the minor or major binding groove. Classical bipartite NLSs contain two basic clusters separated usually by 10–12 amino acids and bind simultaneously to both the minor and the major binding groove (Conti and Kuriyan, 2000; Conti et al., 1998; Fontes et al., 2000; Kosugi et al., 2009a).

The convex surface of importin ß serves for interactions with various nucleoporins containing FG repeats (Bayliss et al., 2000). These interactions enable the cargo translocation through the NPCs by importin ß in a not fully understood process. In the nucleus, cargos are released. Binding of RanGTP to concave surface of importin ß changes importin ß conformation and leads to the dissociation of cargos or adaptor-cargo complexes from importin ß (Lee et al., 2005; Vetter et al., 1999). Adaptor-cargo complexes must be then dissociated as well. The dissociation of the cargo from importin α is the best described. IBB domain of importin α, which is rich in basic residues, works as an importin α autoinhibitory segment (Kobe, 1999). When importin α-cargo complex is released from importin ß, IBB

domain competes with NLS-bearing cargo for binding to the NLS binding grooves to facilitate cargo release (Kobe, 1999). In the dissociation step, nucleoporins at the nucleoplasmic side of NPCs are also actively involved in displacing of NLS-bearing cargos from importin α (Matsuura and Stewart, 2005). Importin ß bound to RanGTP returns to the cytoplasm itself, whereas nuclear export of its adaptors depends on distinct members of the ß-karyopherin family (Kutay et al., 1997; Paraskeva et al., 1999). In the cytoplasm, RanBP1 releases RanGTP from importin ß (and other members of ß-karyopherin family) and GAP for Ran subsequently stimulates the hydrolysis of GTP (Bischoff and Görlich, 1997). The recycling of importin ß and its adaptors is thereby finished. Nuclear transport factor 2 (NTF2) finishes the recycling of Ran by the translocation of RanGDP back to the nucleus (Ribbeck et al., 1998), where RCC1 (GEF for Ran) catalyses the GDP/GTP exchange (Bischoff and Ponstingl, 1991).

### 3.3.3. NUP153

Nuclear import of 53BP1 also depends on NUP153 (Lemaître et al., 2012; Moudry et al., 2012). NUP153 is a nuclear basket nucleoporin required for assembly of NPCs in interphase (Vollmer et al., 2015).

NUP153 consists of a N-terminal NPCs-targeting region (Bastos et al., 1996; Enarson et al., 1998), a central zinc finger domain (Sukegawa and Blobel, 1993) and C-terminal FG repeats (Sukegawa and Blobel, 1993). While N-terminal and central regions of NUP153 localize to the nuclear face of NPCs (central zinc finger domain specifically to distal ring of the nuclear basket), C-terminal part containing FG repeats is highly mobile and can localize to the nuclear basket as well as to the cytoplasmic face of NPCs (Fahrenkrog et al., 2002). Interestingly, association of NUP153 with NPCs is dynamic and NUP153 bound to NPCs exchanges rapidly with its soluble pool in the nucleoplasm (Daigle et al., 2001).

Various nuclear import pathways converge on NUP153 (Shah and Forbes, 1998) and NUP153 is also required for various nuclear export pathways (Bastos et al., 1996; Ullman et al., 1999). Importantly, NUP153 promotes importin α/ß-mediated nuclear import (Ogawa et al., 2012; Walther et al., 2001). Furthermore, NUP153 is implicated in the nuclear envelope breakdown (Prunuske et al., 2006) and in resolution of mitosis (Mackay et al., 2009).

### 3.3.4. Regulation of protein import by posttranslational modifications

**Regulation by phosphorylation**

Protein import is commonly regulated by phosphorylation, which can up-regulate or down-regulate the protein translocation to the nucleus. Numerous distinct mechanisms were described (Nardozzi et al., 2010). Phosphorylation adjacent to or within a classical NLS can decrease the affinity for importin α. This reduces nuclear import efficiency and causes the accumulation of the phosphorylated cargo in

the cytoplasm (Harreman et al., 2004). Alternatively, phosphorylation within NLS can increase the affinity for importin α and this accelerates nuclear import rate (Kitamura et al., 2006). Some NLSs are not accessible to importins prior to a phosphorylation-dependent conformation change (Kann et al., 1999; McBride et al., 2002). Import of proteins that shuttle between the cytoplasm and the nucleus can be also enhanced by phosphorylation-dependent inhibition of the nuclear export (Kondoh et al., 2006).

**Regulation by acetylation**

Regulation of nuclear transport by acetylation is less common. Acetylation of proteins can lead to both their cytoplasmic or nuclear localization. Nuclear import of several proteins (including c-Abl, IFI16 and E1A) is inhibited by acetylation within their NLSs (di Bari et al., 2006; Li et al., 2012; Madison et al., 2002). Acetylation of lysine residues within NLS can directly disrupt the interaction with importin α, thereby prevent the entry of a protein to the nucleus (Madison et al., 2002). Alternatively, acetylation within NLS can promote protein accumulation in the nucleus (Blanco-García et al., 2009; Soutoglou et al., 2000; Spilianakis et al., 2000). In case of the hepatocyte nuclear factor-4 (HNF-4), the protein retention in the nucleus is achieved by the inhibition of its export caused by acetylation-induced change in the protein conformation (Soutoglou et al., 2000).

# 4. Material and Methods

## 4.1. Buffers, media, solutions

**4X sample buffer (4X SB)**

- 250 mM Tris-HCl pH=6.8 (Applichem)
- 40% (v/v) glycerol (Lach-Ner)
- 8% (m/v) SDS (MP-Biomedicals)
- 400 mM DTT (Applichem)
- Bromphenol blue (Sigma-Aldrich)

**Annealing buffer**

- 10 µM Tris-Hcl pH=8
- 1 mM EDTA (MP-Biomedicals)
- 50 mM NaCl (Lach-Ner)

**Blotting buffer**

- 2.5 mM Tris
- 19.2 mM Glycine (VWR)
- 20% (v/v) Methanol (Lach-Ner)

**E1 resuspendation buffer**

- 50 mM Tris-HCl pH=7.5
- 10 mM EDTA pH=8.0
- 100 $\mu$g/mL RNase A (Applichem)

**E2 lysis buffer**

- 200 mM NaOH (MP-Biomedicals)
- 1% (w/v) SDS

**E3 neutralization buffer**

- 3.1 M KAc pH=5.5 (Applichem)

**Immunoprecipitation (IP) buffer**

- 150 mM NaCl
- 20 mM HEPES pH=7.5 (Sigma-Aldrich)
- 10% (v/v) glycerol
- 0.1% (v/v) Triton X-100 (Ambresco)

**Lower buffer**

- 1.5 M Tris pH=8.8
- 0.4% (w/v) SDS

**LB medium and LB agar**

- 25 g/1 L of LB Broth (Miller) powder (Sigma-Aldrich)
- + 15 g/1 L of agar (Sigma-Aldrich) when intended for agar plates

LB medium and agar plates could be supplemented with ampicillin (final concentration 100 µg/mL; Sigma-Aldrich) or kanamycin (final concentration 50 µg/mL; MP-Biomedicals).

**Mammalian cell culture medium**

- DMEM (#D6429; Sigma-Aldrich)
- 10% FBS (Sigma-Aldrich)
- 100 U/mL Penicillin – 100 $\mu$g/mL Streptomycin (Sigma-Aldrich)

**Phosphate-buffered saline (PBS)**

- 137 mM NaCl
- 2.7 mM KCl (MP-Biomedicals)
- 8.1 mM $Na_2HPO_4$ (PENTA)
- 1.5 mM $KH_2PO_4$ (PENTA)

**PBST**

- PBS
- 0.1% (v/v) Tween 20 (Ambresco)

**Ponceau S**

- 0.1% Ponceau S (MP-Biomedicals)
- 5% Acetic acid (Lach-Ner)

**Running buffer**

- 2.5 mM Tris
- 19.2 mM Glycine
- 0.1% (w/v) SDS

**SDS lysis buffer**

- 62.5 mM Tris-HCl pH=6.8
- 10% (v/v) glycerol
- 2% (m/v) SDS

**TAE buffer**

- 40 mM Tris
- 1 mM EDTA pH=8.0
- 20 mM Acetic acid

pH adjusted to 8.5.

**Upper buffer**

- 0.5 M Tris pH=6.8
- 0.4% (w/v) SDS

## 4.2. NLS prediction

Eukaryotic Linear Motif (ELM) prediction (Dinkel et al., 2016) and cNLS Mapper (Kosugi et al., 2009b) were employed to predict 53BP1 NLS(s).

ELM prediction uses sequence-based profiles of linear motifs. It searches for linear motifs corresponding to annotated ELM motif classes (which are defined by consensus sequences) based on sequence similarity. ELM prediction applies certain filters and displays identified putative instances in two tables, showing likely and unlikely result, respectively (Dinkel et al., 2016, 2012).

cNLS Mapper uses activity-based profiles. The profiles were obtained by extensive amino acid replacement analysis of different classes of classical NLSs (recognised by importin α) followed by nuclear import assays in budding yeast. In these assays, relative activities of altered NLS sequences were determined to assess contribution of each residue within an NLS to its activity. Thus, cNLS calculates NLS scores (expected NLS activities) to predict NLSs (Kosugi et al., 2009b).

## 4.3. DNA cloning

### 4.3.1. DNA cloning workflow

Desired changes were introduced into a plasmid DNA by mutagenic primers and standard polymerase chain reaction (PCR) or site-directed mutagenesis by Phusion PCR. Alternatively, desired changes were introduced into a plasmid DNA by ligation of annealed overlapping oligonucleotides, which carried them.

When the standard PCR protocol was used, PCR-amplified DNA fragments were separated by agarose gel electrophoresis, cut out of the gel and isolated. Next, they were ligated into PCR cloning plasmids (vectors), which were subsequently introduced into bacterial cells by heat shock transformation. Transformed bacteria were spread over LB agar plates and incubated overnight at 37°C. The following day, single colonies were picked up, inoculated into 3 mL of LB medium and grown overnight

in the shaking incubator at 37°C to further amplify plasmid DNA. The next day, plasmid DNA was isolated according to the miniprep protocol. Isolated plasmid DNA was used for screening by restriction enzyme digestion to verify that PCR fragment was successfully inserted into the PCR cloning plasmid. Once being confirmed, DNA fragments could be transferred (subcloned).

When the site-directed mutagenesis by Phusion protocol was applied, mutated plasmid DNA was directly introduced into bacterial cells by heat shock transformation and bacteria were grown overnight on LB agar plate at 37°C. Following day, single colonies were picked up, inoculated into 3 mL of LB medium and grown overnight in the shaking incubator at 37°C. The next day, plasmid DNA was isolated using the miniprep protocol. Isolated plasmid DNA was sequenced to verify that mutations were present. Once having positive results from sequencing, DNA fragment from mutated plasmid could be transferred (subcloned).

Annealed overlapping oligonucleotides were ligated into plasmid DNA, which had been digested by restriction enzymes, separated by agarose gel electrophoresis, cut out of the gel and isolated prior to DNA ligation. After DNA ligation, plasmid DNA was introduced into bacterial cells by heat shock transformation. Bacteria were plated on LB agar plate and grown overnight. Single colonies were then picked up, inoculated into 3 mL of LB medium and grown overnight in the shaking incubator at 37°C. The following day, plasmid DNA was isolated by the miniprep protocol and screened by restriction enzyme digestion.

Subcloning was performed by restriction enzyme double-digestion. Both the donor and the recipient plasmids were digested by the same two restriction endonucleases. In the case of the recipient plasmid, DNA ends were dephosphorylated to prevent self-ligation. DNA fragments were then separated by agarose gel electrophoresis. DNA fragments from both donor plasmid (inserts) and recipient plasmid (backbones) were cut out of the gel, isolated and ligated. To verify insertions, the series of aforementioned steps leading to the isolation of plasmid DNA and to subsequent screening by restriction enzyme digestion was performed.

Finally, when DNA constructs were validated by restriction enzyme digestion and sequencing, large amount of high-quality plasmid DNA was prepared according to the maxiprep protocol.

### 4.3.2. Particular steps of DNA cloning

**DNA amplification by PCR**

The following standard PCR protocol was employed to amplify any desired DNA fragment from plasmid DNA. When mutagenic primers were used, changes into plasmid DNA could have been introduced. These mutagenic primers were designed to carry desired changes and restriction sites, which enabled

subcloning and subsequent screening for positive clones by restriction enzyme. PCR mixture was prepared on ice in the total volume of 50 µL as follows:

- 31 µL of $dH_2O$
- 1 µL of 50 ng/µL template DNA
- 2 µL of 10 µM forward (fwd) primer
- 2 µL of 10 µM reverse (rev) primer
- 3 µL of 10 mM dNTPs Mix (Thermo Fisher Scientific)
- 10 µL of 5X Phusion HF Buffer (Thermo Fisher Scientific)
- 1 µL of 2 U/µl Phusion High-Fidelity DNA Polymerase (Thermo Fisher Scientific)

PCR was performed using T100TM Thermal Cycler (Bio-Rad Laboratoires) and following cycling conditions:

- Initial denaturation: 92°C, 2 min
- Denaturation: 92°C, 0.5 min
- Annealing: 0.5 min, temperature was calculated by Tm Calculator (Thermo Fisher Scientific)
- Extension: 72°C, time was calculated as follows: 1 min/1kbp
- Final extension: 72°C, 5 min

Thirty-five cycles were used.

**Site-directed mutagenesis by Phusion**

Site-directed mutagenesis by Phusion was used to make 1–3 point mutations in order to substitute one amino acid. Two mutagenic primers were used, both containing desired mutation(s) in the middle and being complementary to each other. The procedure was divided into two steps:

In the first step, mutated DNA plasmid was generated by PCR. PCR mixture was prepared on ice in the total volume of 50 µL as follows:

- 34 µL of $dH_2O$
- 1 µL of 50 ng/µL template DNA
- 1.25 µL of 10 µM sense primer
- 1.25 µL of 10 µM antisense primer
- 1.5 µL of 10 mM dNTPs Mix (Thermo Fisher Scientific)
- 10 µL of 5X Phusion HF Buffer (Thermo Fisher Scientific)
- 1 µL of 2 U/µl Phusion High-Fidelity DNA Polymerase (Thermo Fisher Scientific)

PCR was performed using T100TM Thermal Cycler (Bio-Rad Laboratoires) and following cycling conditions:

- Initial denaturation: 92°C, 3 min
- Denaturation: 92°C, 45 s
- Annealing: 54°C, 45 s
- Extension: 72°C, 8 min
- Final extension: 72°C, 10 min

Twenty cycles were used.

In the second step, 1 µL of 10 U/µL DpnI (Thermo Fisher Scientific) was added into the mixture to digest template DNA. Reaction mixture was incubated at 37°C for 4 h and then could be directly introduced into bacteria by heat shock transformation.

**Annealing oligonucleotides**

Sense and antisense oligonucleotides carrying desired changes were dissolved in $dH_2O$ to make 100 µM stock solutions. Annealing was then performed in the total volume of 100 µL, mixing 10 µL of each oligonucleotide (final concentration 10 µM each) and adding 80 µL of annealing buffer. The tube with mixed oligonucleotides was placed in heatblock (95°C) for 5 min and then slowly (for approximately 1 h) cooled down to room temperature.

**Restriction enzyme digestion**

Restriction enzyme digestion was performed to subclone DNA fragment from donor to recipient plasmid or for screening. The following restriction endonucleases and 10X buffers (all purchased from Thermo Fisher Scientific) were used: AgeI, BamHI, EcoRI, NheI, NotI, SacII, XbaI, XhoI, buffer O, buffer BamHI, buffer EcoRI, buffer Tango, buffer B and buffer R. When intented for subcloning, double digest reaction mixture was prepared in the total volume of 30 µL as follows:

- 5 µg of plasmid DNA
- 5 U of each restriction endonuclease
- 3 µL of 10X buffer
- $dH_2O$ up to 30 µL

Appropriate buffer was determined by DoubleDigest Calculator (Thermo Fisher Scientific). When intended for screening, only 0.5 U of one restriction enzyme was used. The mixture was incubated at 37°C at least for 1 h.

**Dephosphorylation of DNA ends**

When intended for subcloning, 5'-ends of recipient plasmid DNA were dephosphorylated. When digestion was completed, 1 U of FastAP Thermosensitive Alkaline Phosphatase (Thermo Fisher Scientific) was added directly into the restriction enzyme digest mixture and the mixture was then incubated for another 1–2 hours at 37°C.

**Agarose gel electrophoresis**

Agarose gel electrophoresis was used to separate DNA fragments according to their sizes. One-percent agarose gels, 1X TAE buffer, EnduroTM Horizontal Gel Boxes (Labnet International) and power supply PS 304 Minipec II (Apelex) were used for DNA separation. Ethidium bromide (0.5 µg/mL) was added to make the DNA visualisation possible. Samples were mixed with 6X DNA Loading Dye (Thermo Fisher Scientific) prior to loading into the wells. One kb DNA Ladder (Sigma-Aldrich) was also loaded to enable the estimation of molecular weights of DNA fragments. Voltage was set to 100 V. DNA was visualized using gel documentation system QUANTUM ST5 (Vilber Lourmat).

**DNA isolation from agarose gel**

DNA fragments were cut out of the gel and isolated using Agarose Gel Extraction Kit (Jena Bioscience).

**Determination of DNA concentration**

DNA concentration was determined using NanoDrop® ND-1000 Spectrophotometer (Thermo Fisher Scientific).

**DNA ligation**

DNA ligation reactions were performed in the total volume of 10 µL as follows:

- DNA insert
- 5-fold excess of recipient plasmid DNA
- 1 µL of T4 DNA Ligase (New England Biolabs)
- 1 µL of T4 DNA Ligase Reaction Buffer (New England Biolabs)

Required mass of DNA insert was calculated by NEBioCalculator™ (New England Biolabs). Reaction mixture was incubated at room temperature for 1–2 h.

**Heat shock transformation**

Plasmid DNA was introduced into DH5α™ Competent Cells (Thermo Fisher Scientific) by heat shock transformation. DH5α bacteria were thawed on ice, incubated with DNA ligation reaction mixture (which contains ligated plasmid DNA) for 15 min, placed in heatblock (42°C) for 1 min, returned on ice

and incubated here for 5 min. Finally, they were added into 1 mL of LB medium, incubated at 37°C in the shaking incubator for 1 h and spread over LB agar plate with appropriate antibiotic.

**Plasmid DNA isolation - Miniprep protocol**

After plasmid DNA amplification in bacteria, plasmid DNA was isolated from overnight-grown bacteria according to this Miniprep protocol, which is based on alkaline lysis. Briefly, bacteria were harvested by spinning at 4000 g for 10 min using Centrifuge 5810R (Eppendorf). While supernatant was discarded, bacteria in pellet were resuspended in 200 µL of E1 resuspendation buffer by vortexing and lysed in 200 µL of E2 lysis buffer for 5 min. Subsequently, 100 µL of chloroform and 350 µL of E3 neutralization buffer were added. After incubation (3 min), the mixture was centrifugated at 4000 g for 10 min using the same centrifuge. Plasmid DNA in supernatant was precipitated with isopropanol (500 µl), spun down at 21130 g (full speed), 4°C, 10 min using Centrifuge 5424R (Eppendorf), washed with 1,000 µL of ethanol (VWR), spun down again and air-dried. Finally, plasmid DNA was dissolved in 50 µL of $dH_2O$.

**DNA sequencing**

Plasmid DNA sequencing was done by SEQme company, which used Sanger sequencing approach.

**Plasmid DNA isolation – Maxiprep protocol**

When the DNA sequencing confirmed that DNA plasmid had desired changes, large amount of high-purity plasmid DNA was isolated from overnight-grown bacteria carrying the DNA plasmid using JetStar™ 2.0 Plasmid Maxiprep Kit (GENOMED).

### 4.3.3. DNA constructs

DNA constructs used in my experiments are listed below. If DNA constructs were neither purchased or obtained from Libor Macůrek, its preparation is described. All primers and oligonucleotides were purchased from Sigma-Aldrich.

**pEGFP-C2**

pEGFP-C2 plasmid encoding EGFP was purchased from Clontech Laboratories.

**pEGFP-TEV-FLAG-53BP1-wt**

pEGFP-TEV-FLAG-53BP1-wt encodes recombinant protein (2248 amino acids) comprising of human 53BP1 isoform 1 sequence (UniProt identifier: Q12888-1; 1972 amino acids) and HA tag-EGFP-TEV pro-

tease cleavage site-Flag tag sequence (276 amino acids) at N-terminus. As only EGFP tagging was employed in this work, the encoded protein was further termed EGFP-53BP1-wt. pEGFP-TEV-FLAG-53BP1-wt was a fundamental DNA construct from which all other DNA constructs encoding EGFP-53BP1 mutants were derived. pEGFP-TEV-FLAG-53BP1-wt itself was prepared by Libor Macůrek by cloning the protein coding sequence into HindIII/NotI sites of pcdna4/TO mammalian expression vector (Thermo Fisher Scientific).

**pEGFP-TEV-FLAG-53BP1-ΔNLS1**

pEGFP-TEV-FLAG-53BP1-ΔNLS1 encodes EGFP-53BP1 mutant which has the sequence 1626-KRKRR-1630 substituted by four alanines. The preparation was divided into two steps.

In the first step, intermediate DNA construct with desired substitution and lacking the whole downstream sequence was prepared. Substitution was created by PCR with pEGFP-TEV-FLAG-53BP1-wt as a template and following primers:

```
ΔNLS1-BamHI-fwd: 5’-AGAGAATGAGGCTCGAAGTGAGGATCC-3’
ΔNLS1-XhoI-rev: 5’-CTCGAGTTGCTAGCTTGCGGCCGCCCCTTCCACCAAATTGTCTAAG-3’
```

ΔNLS1-BamHI-fwd primer includes naturally occurring BamHI restriction site, while ΔNLS1-XhoI-rev primer is mutagenic and includes the substitution sequence and the segment consisting of NotI, NheI and XhoI restriction sites required for the second step of preparation. Amplified DNA fragment was ligated into pGEM®-T cloning vector (Promega) and subsequently subcloned into BamHI/XhoI sites of pEGFP-TEV-FLAG-53BP1-wt. NheI digestion was used for screening since positive clones were expected to have one more NheI site.

In the second step, the lacking downstream sequence was incorporated into the intermediate DNA construct. The sequence was amplified by PCR with pEGFP-TEV-FLAG-53BP1-wt as a template and following primers:

```
ΔNLS-NotI-fwd: 5’-GCGGCCGCAGCAAGTAACGTCAGCTCC-3’
53BP1fl-XhoI-rev: 5’-CTCGAGTTAGTGAGAAACATAATCGTGTTTA-3’
```

ΔNLS1-NotI-fwd and 53BP1fl-XhoI-rev primers include NotI and XhoI restriction sites, respectively. Amplified DNA fragment was ligated into pGEM®-T cloning vector (Promega) and subsequently subcloned into NotI/XhoI sites of the intermediate DNA construct prepared in the first step. NheI and EcoRV digestion was used for screening to confirm the loss of sequence between NotI and XhoI sites and the insertion of DNA fragment, respectively. DNA construct was validated by sequencing.

**pEGFP-TEV-FLAG-53BP1-ΔNLS1-3**

pEGFP-TEV-FLAG-53BP1-ΔNLS1-3 encodes EGFP-53BP1 mutant which has five alanines instead of 1626-1692 region. To enclose the DNA construct after deletion of desired sequence, an adapter with appropriate sticky ends had to be ligated into the plasmid. The following oligonucleotides were therefore annealed:

NotI-SacII-AgeI-sense:
5'-GGCCGCAGCAGCCGCGGTAGGGGCAGGAGAGTTTGTGAGCCCCTGTGAGAGTGGAGACAACA-3'
NotI-SacII-AgeI-antisense:
5'-CCGGTGTTGTCTCCACTCTCACAGGGGCTCACAAACTCTCCTGCCCCTACCGCGGCTGCTGC-3'

Annealed oligonucleotides were ligated into AgeI/NotI sites of pEGFP-TEV-FLAG-53BP1-ΔNLS1. SacII digestion was used for screening as annealed oligonucleotides carried SacII site. DNA construct was validated by sequencing.

**pEGFP-TEV-FLAG-53BP1-ΔNLS2**

pEGFP-TEV-FLAG-53BP1-ΔNLS2 encodes EGFP-53BP1 mutant which has the sequence 1667-KRK-1669 substituted by the sequence 1667-AAA-1669. Substitution was created by PCR with pEGFP-TEV-FLAG-53BP1-wt as a template and following primers:

ΔNLS-BamHI-fwd: 5'-AGAGAATGAGGCTCGAAGTGAGGATCC-3'
ΔNLS2-SacII-rev: 5'CCGCGGCAGGTTTTACTGTGGCAGACTTGCGACCTCGCTTGGCAGGG-GACCGTTCCTCTTCAGAAGTGATAAGTGCGGCCGCGCCTGAGAGAACTCCCATGG-3'

ΔNLS-BamHI-fwd primer includes naturally occurring BamHI site, while ΔNLS2-SacII-rev primer is mutagenic and includes desired substitution sequence, SacII and NotI restriction sites. Amplified DNA fragment was ligated into pCR™2.1-TOPO® cloning vector (Thermo Fisher Scientific) and subsequently subcloned into BamHI/SacII sites of pEGFP-TEV-FLAG-53BP1-ΔNLS1-3. SacII digestion was used for screening. DNA construct was validated by sequencing.

**pEGFP-TEV-FLAG-53BP1-ΔNLS3**

pEGFP-TEV-FLAG-53BP1-ΔNLS3 encodes EGFP-53BP1 mutant which has the sequence 1681-KRGRK-1685 substituted by the sequence 1681-AAAAA-1685. Substitution was created by PCR with pEGFP-TEV-FLAG-53BP1-wt as a template and following primers:

ΔNLS-BamHI-fwd: 5'-AGAGAATGAGGCTCGAAGTGAGGATCC-3'
ΔNLS3-SacII-rev: 5'-CCGCGGCAGGTTTTACTGTGGCAGATGCTGCGGCCGCTGCGGCAGGG-GACCGTTCCTCTTC-3'

ΔNLS-BamHI-fwd primer includes naturally occurring BamHI site, while ΔNLS3-SacII-rev primer is mutagenic and includes desired substitution sequence, SacII and NotI restriction sites. Amplified DNA fragment was ligated into pCR™2.1-TOPO® cloning vector (Thermo Fisher Scientific) and subsequently subcloned into BamHI/SacII sites of pEGFP-TEV-FLAG-53BP1-ΔNLS1-3. SacII digestion was used for screening. DNA construct was validated by sequencing.

**pEGFP-TEV-FLAG-53BP1-S1678A/S1678D**

pEGFP-TEV-FLAG-53BP1-S1678A and pEGFP-TEV-FLAG-53BP1-S1678D encode EGFP-53BP1 mutants which have S1678 substituted by alanine and aspartate, respectively. The preparation was divided into two steps.

In the first step, site-directed mutagenesis by Phusion protocol was employed to create desired substitutions. PCR was performed with pEP-BamHI-53BP1-AgeI plasmid (obtained from Libor Macůrek) as a template and with following primers:

```
S1678A-sense: 5’-CGCTTGGCAGGGGCCCGTTCCTCTTCA-3’
S1678A-anti:  5’-TGAAGAGGAACGGGCCCCTGCCAAGCG-3’

S1678D-sense: 5’-CCTCGCTTGGCAGGGTCCCGTTCCTCTTCAGA-3’
S1678D-anti:  5’-TCTGAAGAGGAACGGGACCCTGCCAAGCGAGG-3’
```

The mutated pEP-BamHI-53BP1-AgeI intermediate plasmids were directly used for bacterial transformation and plasmid DNA from selected clones was sequenced.

In the second step, DNA fragments from validated pEP-BamHI-53BP1-AgeI-S1678A and pEP-BamHI-53BP1-AgeI-S1678D intermediate plasmids were subcloned into BamHI/AgeI sites of pEGFP-TEV-FLAG-53BP1-wt. DNA constructs were validated by sequencing.

**pEGFP-TEV-FLAG-53BP1-T1609D-S1618D**

pEGFP-TEV-FLAG-53BP1-T1609D-S1618D encodes EGFP-53BP1 mutant which has T1609 and S1618 substituted by aspartate residues. Site-directed mutagenesis by Phusion protocol was employed as described above, however, one more mutagenesis step was included.

In the first step, pEP-BamHI-53BP1-AgeI plasmid was also used as a template for PCR with following primers:

```
S1618D-SENSE: 5’-CCTTCCACCAAATTGTCTAAGTCGATATCTGCTGCCTTTGTAAG-3’
S1618D-ANTI:  5’-CTTACAAAGGCAGCAGATATCGACTTAGACAATTTGGTGGAAGG-3’
```

In the second step, one more site-directed mutagenesis by Phusion was performed with pEP-BamHI-53BP1-AgeI-S1618D plasmid obtained in previous step as a template and with following primers:

```
T1609D-SENSE:    5’-CTGCTGCCTTTGTAAGAGGGTCTACTGCTTCATAGGGGCCAAG-3’
T1609D-ANTI:     5’-CTTGGCCCCTATGAAGCAGTAGACCCTCTTACAAAGGCAGCAG-3’
```

In the third step, DNA fragment from validated pEP-BamHI-53BP1-AgeI-T1609D-S1618D intermediate plasmid was subcloned into BamHI/AgeI sites of pEGFP-TEV-FLAG-53BP1-wt. DNA construct was validated by sequencing.

**pTON-EGFP-FLAG**

pTON-EGFP-FLAG encoding EGFP-FLAG was obtained from Libor Macůrek. EGFP-FLAG sequence was cloned into the same mammalian expression plasmid as EGFP-53BP1 is (pcdna4/TO).

**pTON2-EGFP-NLS**

pTON2-EGFP-NLS encodes recombinant protein, further referred as EGFP-NLS, consisting of EGFP fused N-terminally to 1658-RASMGVLSGKRKLITSEEERSPAKRGRKSA-1687 sequence derived from 53BP1. The following oligonucleotides, which encoded NLS and stop codon, were annealed:

```
XhoI-NLS-XbaI-fwd:
5’TCGAGCTAGCATGGGAGTTCTCTCAGGCAAAAGAAAACTTATCACTTCTGAAGAGGAAC-
GGTCCCCTGCCAAGCGAGGTCGCAAGTCTGCCTAGT-3’
XhoI-NLS-XbaI-rev:
5’CTAGACTAGGCAGACTTGCGACCTCGCTTGGCAGGGGACCGTTCCTCTTCAGAAGTGA-
TAAGTTTTCTTTTGCCTGAGAGAACTCCCATGCTAGC-3’
```

XhoI-NLS-XbaI-fwd and XhoI-NLS-XbaI-rev annealed oligonucleotides were ligated into XhoI/XbaI sites of pTON2-EGFP-FLAG-Wip-FL plasmid. NheI digestion was used for screening. DNA construct was validated by sequencing.

**pTON2-EGFP-NLS-S1678A/S1678D**

pTON2-EGFP-NLS-S1678A and pTON2-EGFP-NLS-S1678D encode EGFP-NLS mutants which have serine residue within NLS corresponding to S1678 of 53BP1 mutated to alanine and aspartate, respectively. Site-directed mutagenesis by Phusion protocol was employed to create desired substitutions. pTON2-EGFP-NLS was used as a template for PCR with following primers:

S1678A-sense: 5’-CGCTTGGCAGGGGCCCGTTCCTCTTCA-3’
S1678A-anti: 5’-TGAAGAGGAACGGGCCCCTGCCAAGCG-3’

S1678D-sense: 5’-CCTCGCTTGGCAGGGTCCCGTTCCTCTTCAGA-3’
S1678D-anti: 5’-TCTGAAGAGGAACGGGACCCTGCCAAGCGAGG-3’

The mutated plasmids were directly used for bacterial transformation and plasmid DNA from selected clones was sequenced. DNA fragments from validated pTON2-EGFP-NLS-S1678A and pTON2-EGFP-NLS-S1678D mutated plasmids were subcloned into AgeI/XbaI sites of non-mutated pTON2-EGFP-NLS. DNA constructs were validated by sequencing.

## 4.4. Cell culture

All experiments were performed using human osteosarcoma cell line, U2OS. Cells were cultivated in mammalian cell culture medium at 37°C in a humidified atmosphere with 5% $CO_2$. Cells were passaged three times per week, checked under inverted microscope Eclipse TS1000 (Nikon) and counted using Bürker counting chamber (Marienfeld).

## 4.5. Cell transfection with plasmid DNA

U2OS cells were transiently transfected with plasmid DNA using polyethylenimine (PEI) approach. When cells were growing on 10 cm plate and intended for IP/co-IP experiments, they were split a day before the transfection (to achieve 80% confluency the following day). The transfection mixture was prepared as follows:

1. 30 µL of 1 µg/µL PEI MAX 40000 (Polyscience) was diluted in Opti-MEM® I Reduced-Serum Medium (Gibco) to make the final volume of 250 µL
2. 5 µg of plasmid DNA was diluted in Opti-MEM® I Reduced-Serum Medium to make the final volume of 250 µL
3. These two mixtures were combined and incubated for 15 min

Transfection mixture was subsequently added to cells and the mammalian cell culture medium was exchanged 4 h after transfection. When intended for cell synchronization experiments, $1x10^6$ cells were seeded on 10 cm plate a day before the transfection. For microscopy experiments, $1.5x10^5$ cells were seeded in 6-well plate a day before the transfection and the transfection mixture contained 1 µg of plasmid DNA and 6 µg of PEI MAX 40000.

## 4.6. Cell synchronization techniques

### 4.6.1. Double thymidine block

The following protocol was employed when interaction between 53BP1 and importin ß was monitored during the cell cycle. Cells were transfected with plasmid DNA and grown for 24 h prior to the first thymidine block. During the first thymidine block, cells were arrested throughout the S phase by adding thymidine (Sigma-Aldrich) to the final concentration of 2 mM. After 16 h, cells were released from first thymidine block by washing three times with PBS. The fresh medium was added and cells were grown for 9 h. After that, cells were arrested at G1/S transition by adding thymidine (2 mM final concentration) and incubating for 15 h. While samples corresponding to the G1/S transition were harvested at this time point, the remaining cells were released from the second thymidine block by washing three times with PBS. The fresh medium was added and the sample corresponding to the S phase was harvested after 3 h. At this time point, RO-3306 (9 µM final concentration; GeneTiCA) or nocodazole (330 nM final concentration; Sigma-Aldrich) were added to prevent remaining cells escaping from the G2 or M phase, respectively. Samples corresponding to the G2 phase and the M phase were harvested after additional 11 h. Mitotic cells were always collected by mitotic shake-off so that only detached cells were present in mitotic sample.

### 4.6.2. Thymidine-nocodazole block and its modifications

Thymidine-nocodazole block was carried out when only mitotic cells were needed. Cells were transfected with plasmid DNA and grown for 24 h. Then, thymidine was added to final concentration of 2 mM. Cells were cultivated in the presence of thymidine for 24 h and subsequently released from thymidine block by washing three times with PBS and adding fresh medium. Nocodazole was added to cells 3 h after release and mitotic cells were collected after additional 13 h by mitotic shake-off.

Modifications of thymidine-nocodazole block were employed when cells only enriched in particular cell cycle phases were needed. Cells were processed as desribed above, however, more steps were done 3 h after release from thymidine. Cells harvested at this timepoint were used as a sample enriched in S phase cells. RO-3306 (9 µM final concentration) or nocodazole (330nM final concentration) were added at this timepoint to harvest samples enriched in G2 phase cells or mitotic cells, respectively, after additional 13 h. G1 cells were obtained by thymidine-nocodazole block followed by nocodazole release. Briefly, mitotic cells collected by mitotic shake-off were washed three times in warm PBS, fresh medium was added and cells were grown for additional 3 h in the tissue culture incubator.

## 4.7. γ-Irradiation of cells

γ-irradiation was performed using Orthovoltage X-ray instrument T-200 (WolfMedizintechnik) at the X-ray irradiation facility, Institute of Molecular Genetics of the ASCR. Cells growing in 6-well plate were exposed to 3 Gy of γ-irradiation (200 kV, 13 mA, 0.3 mm Al filter).

## 4.8. Immunoprecipitation techniques

### 4.8.1. Immunoprecipitation (IP) and co-IP of transiently expressed proteins

IP of transiently expressed EGFP-tagged proteins was performed in order to detect protein posttranslational modifications, while co-IP of EGFP-tagged proteins and proteins that are bound to them was performed in order to detect protein-protein interaction. For all these experiments, GFP-TRAP® (ChromoTek) was used. GFP-TRAP® was coupled to NHS-activated Sepharose™ 4 Fast Flow matrix (GE Healthcare) according to the manufacturer's instructions and stored as 50% slurry at 4°C. All steps were performed on ice.

In the first step, protein samples were prepared. Cells from 10 cm plate were lysed in 500 µL of pre-cooled IP buffer supplemented with PhosSTOP™ (Roche) and cOmplete™, Mini, EDTA-free Protease Inhibitor Cocktail (Roche). Samples were sonicated at 5 microns 3×15 s using Soniprep 150 Plus (MSE). After sonication, samples were spun using Centrifuge 5424R (Eppendorf) at 21130g (full speed) at 4°C for 15 min. The pellet was discarded. The concentration was determined using Bradford assay. Briefly, 1 µL of sample was resuspended in 1 mL of Quick Start Bradford protein 1X dye reagent (Bio-rad) and the concentration was determined using Boeco S 20 Spectrophotometer (Boeco). Protein samples were then diluted to the same concentration. At this time, inputs were prepared. Briefly, 90 µL of the sample was mixed with 30 µL of 4X SB and heated at 95°C for 5 min.

In the second step, the same volumes of protein samples (usually 400 µL) were incubated with GFP-TRAP® matrix. Appropriate amount of GFP-TRAP® matrix suspension was washed and suspended in IP buffer to make 50% slurry again. Twenty-five microliters of the slurry was added into each sample and the mixture was incubated for 1 h with gentle rotation.

In the third step, GFP-TRAP®matrix was washed four times in IP buffer. When intending for evaluation of posttranslational modification, GFP-TRAP®matrix was washed two times with IP buffer supplemented with additional NaCl to make final 1 M NaCl solution and then two times with IP buffer. Bound proteins were eluted by adding 20 µL 4X SB and heating at 95°C for 5 min.

### 4.8.2. co-IP of endogenous 53BP1

Co-IP of endogenous 53BP1 was performed in order to monitor the interaction between 53BP1 and importin ß during the cell cycle. In the first step, lysates were prepared as described above. In the

second step, 2 µg of 53BP1 or control normal rabbit IgG (Santa Cruz) were added into the lysate and the mixture was incubated for 4 h. In the next step, 20 µL of the 50% Pierce Protein A/G UltraLink Resin (Thermo Fisher Scientific) slurry was added and the mixture was incubated for 2 h. After incubation, the resin was washed four times and bound proteins were eluted by 20 µL 4X SB.

## 4.9. Lambda phosphatase assays

Lambda phosphatase assays were performed in order to gain more insight into the interaction between 53BP1 and importin ß in the M phase. The phospho-dependent increase or decrease in the interaction was tested.

To test whether there is a phospho-dependent increase in the interaction, the co-IP was performed as described in Section 4.8.1. with modifications in the third step. GFP-TRAP®matrix with bound proteins was washed four times in IP buffer and then one more wash in phosphatase buffer (10X NEBuffer for PMP (New England BioLabs), 10X $MnCl_2$ (New England BioLabs), diluted in $dH_2O$) was included. 100 µL of phosphatase buffer with 1 µL of Lambda Protein Phosphatase (New England BioLabs) was added to GFP-TRAP®matrix with bound proteins. Control sample was treated in the same way, but PhosSTOP™ (Roche) was added instead of Lambda Protein Phosphatase. The mixtures were incubated at 30°C for 1 h with agitation, washed three times in IP buffer and eluted by 20 µL 4X SB.

To test whether there is a phospho-dependent decrease in the interaction, the lysate was dephosphorylated prior to the co-IP. The first step of co-IP protocol decribed in Section 4.8.1 was therefore slightly modified. Cells were lysed in IP buffer supplemented with cOmplete™, Mini, EDTA-free Protease Inhibitor Cocktail (Roche) and $MnCl_2$ (final concentration 1 mM). Samples were then divided into two tubes. Into the first tube, 3 µL of Lambda Protein Phosphatase (New England BioLabs) was added, while PhosSTOP™ (Roche) was added into the other. The mixture was incubated at 30°C for 1 h. After incubation, samples were processed in the same manner as in Section 4.8.1.

## 4.10. Preparation of whole cell lysates (denaturated)

To obtaind whole cell lysates under denaturing conditions, cells were washed in PBS and lysed in SDS lysis buffer (500 µL/10 cm plate). Whole cell lysates were then heated at 95°C for 5 min, sonicated at 5 microns 3×15 s using Soniprep 150 Plus (MSE) and protein concentration was determined using Pierce™ BCA Protein Assay Kit (Thermo Fisher Scientific) and Multiskan EX (Thermo Fisher Scientific) acording to the manufacturer's intructions. Prior to protein separation by SDS-PAGE, the lysates were mixed with 4X SB.

## 4.11. SDS PAGE, Western blotting, immunodetection

### 4.11.1. SDS PAGE

Protein samples were separated by SDS-PAGE using handcast polyacrylamide gels (1.5 mm, 10 wells, see Table 1 for composition) and running buffer described in section 4.1. Separation was performed with Mini-PROTEAN® Tetra Vertical Electrophoresis Cell (Bio-Rad) and PowerPacTM Basic Power Supply (Bio-Rad) at constant current of 50 mA/1 gel. The samples were loaded as follows: 30 µg of total protein per well in case of whole cell lysates or approximately 5% of lysate volume dedicated to co-IP or IP experiment in case of inputs. The PageRuler™ Prestained Protein Ladder (Thermo Fisher Scientific) was used to estimate molecular weights.

**Table 1. Composition of 1.5 mm polyacrylamide gels.**

| **SEPARATING GELS** | **6 %** | **8 %** | **10 %** | **12 %** | **14 %** | **15 %** | **STACKING GEL** | |
|---|---|---|---|---|---|---|---|---|
| dH2O (mL) | 7.1 | 3.6 | 3.1 | 2.6 | 2.1 | 1.9 | dH2O (mL) | 1.8 |
| Acrylamide/BIS*(mL) | 1.5 | 2 | 2.5 | 3 | 3.5 | 3.75 | Acrylamide/BIS*(mL) | 0.45 |
| Lower buffer (mL) | 1.9 | 1.9 | 1.9 | 1.9 | 1.9 | 1.9 | Upper buffer (mL) | 0.75 |
| 10% APS (µL) | 50 | 50 | 50 | 50 | 50 | 50 | 10% APS (µL) | 24 |
| TEMED (µL) | 12.5 | 12.5 | 12.5 | 12.5 | 12.5 | 12.5 | TEMED (µL) | 6 |

*30% (w/v) acrylamide/BIS solution, 29:1 (Serva)

### 4.11.2. Western blotting

Following gel electrophoresis, the proteins were transfered onto nitrocellulose membrane (Amersham Protran 0.45 NC; GE Healthcare). Wet transfer system was used employing Criterion™ Blotter (Bio-Rad) and PowerPAc™ HC Power Supply (Bio-Rad). The composition of blotting buffer is described in section 4.1. The voltage was set to 100 V for 1 h. Successful protein transfer was confirmed by reversible Ponceau S staining.

### 4.11.3. Immunodetection

After western blotting, the membrane was incubated with 5% (w/v) non-fat dry milk in PBST for 20 min in order to prevent non-specific antibody binding. After blocking, the indirect chemiluminescent detection was carried out. Briefly, the membrane was incubated with unlabelled primary antibodies (listed in Table 2) diluted in 3% (w/v) non-fat dry milk in PBST overnight at 4°C. Next day, the membrane was washed three times in PBST, incubated with HRP-labelled secondary antibodies (listed in Table 2) diluted in 3% (w/v) non-fat dry milk in PBST for 1 h and again three times washed. All these steps were performed with gentle agitation. Finally, the membrane was incubated with Pierce™ ECL Western Blotting Substrate (Thermo Fisher Scientific) for 5 min and exposed to the medical X-ray film (AGFA), which was subsequently developed by OPTIMAX 2010 (Protec).

**Table 2. List of antibodies used for immunodetection.**

| Primary antibody | Source, clonality | Purchased from | Cat. No. | Working dilution |
|---|---|---|---|---|
| **53BP1** | Rabbit, poly | Santa-Cruz | Sc-22760 | 1:2000 |
| **53BP1-pS1618** | Rabbit, mono | Cell Signalling | 6209 | 1:1000 |
| **Acetylated lysine** | Rabbit, poly | Cell Signalling | 9441 | 1:1000 |
| **CDC27** | Mouse, mono | BD Bioscience | 610454 | 1:1000 |
| **Cyclin A** | Rabbit, poly | Santa-Cruz | Sc-751 | 1:1000 |
| **Cyclin B1** | Rabbit, poly | Abcam | ab7957 | 1:500 |
| **GFP** | Mouse, mono | Roche | 11814460001 | 1:5000 |
| **Histon H3-pS10** | Rabbit, poly | Millipore | 06-570 | 1:1000 |
| **Importin ß** | Mouse, mono | Santa-Cruz | Sc-137016 | 1:6000 |
| **Nup153** | Rat, mono | Abcam | Ab81463 | 1:1000 |
| **Phospho-MAPK/CDK Substrates** | Rabbit, mono | Cell Signalling | 2325 | 1:1000 |
| **Plk1** | Rabbit, poly | Prepared in-house, for details see Macůrek et al., 2008 | | 1:2000 |
| **α-Tubulin** | Rabbit, poly | Genetex | GTX102078 | 1:10000 |

| Secondary antibody | Source | Label | Purchased from | Dilution |
|---|---|---|---|---|
| **Anti-mouse IgG** | goat | HRP | Bio-RAD | 1:5000 |
| **Anti-rabbit IgG** | goat | HRP | Bio-RAD | 1:5000 |
| **Anti-rat IgG** | goat | HRP | Santa-Cruz | 1:1000 |
| **Anti-rabbit IgG *** | mouse | HRP | Jackson | 1:5000 |

*Light Chain Specific

## 4.12. Microscopy experiments

### 4.12.1. Immunofluorescence (IF)

Cells were grown on glass coverslips, fixed with 4% (w/v) paraformaldehyde in PBS (VWR) for 5 min, permeabilized with 0.5% (v/v) TritonX-100 (Ambresco) in PBS for 5 min and blocked with 3% BSA in PBST for 30 min. Next, cells were incubated with primary antibodies (listed in Table 3) diluted in PBST for 1 h, washed three times with PBST, incubated with a proper secondary antibody (listed in Table 3) in PBST for 1 h and again three times washed in PBST. Finally DNA was stained with DAPI (Sigma-Aldrich) diluted 1:1000 in milliQ $H_2O$ for 2 min. After DNA staining, cells were washed in milliQ $H_2O$ for 2 min, air-dried, mounted in Vectashield reagent (Vector Laboratories). All steps were performed at room temperature. For image acquisition, Leica DM6000 fluorescence microscope with HCX PL Apo 63x/1.40 oil PH3 CS objective (Leica) was employed.

**Table 3. List of antibodies used for Immunofluorescence.**

| Primary antibody | Source, clonality | Purchased from | Cat. No. | Working dilution |
|---|---|---|---|---|
| **53BP1** | Rabbit, poly | Santa-Cruz | Sc-22760 | 1:1000 |
| **γH2AX** | Mouse, mono | Millipore | 05-636 | 1:1000 |

| Second. antibody | Source | Label | Purchased from | Working dilution |
|---|---|---|---|---|
| **Anti-rabbit IgG** | Goat | Alexa Fluor® 568 | Thermo Fisher Sc. | 1:1000 |
| **Anti-mouse IgG** | Goat | Alexa Fluor® 568 | Thermo Fisher Sc. | 1:1000 |

### 4.12.2. Analysis of nuclear import defect

Cells were transfected with plasmid DNA encoding EGFP-53BP1-wt or EGFP-53BP1-S1678A/S1678D mutants and grown on glass coverslips for 24 h. Then, the cells were fixed, stained with DAPI and mounted onto glass slides as described in Section 4.12.1. The images were acquired using high-content screening station Scan^R (Olympus) connected to Olympus IX81 microscope with 40x/1.3 UPLFLN oil objective. Analysis was then performed using Scan^R analysis software. Briefly, the main objects (nuclei) were detected based on DAPI signal. Gate was set so that only cells having nuclei with proper circularity and area were further analysed. Then, based on mean GFP signal, another gate was applied to exclude overexpressing cells and cells with background non-specific signal. Remaining cells were then termed as GFP+ cells. Subsequently, a random gallery of 100 GFP+ cells was generated by the software. The cells with GFP signal only in the nucleus or with GFP signal in both the nucleus and the cytoplasm were counted based on naked-eye evaluation. The results from three independent experiments were then statistically analysed.

### 4.12.3. Quantification of DNA damage foci after γ-Irradiation

Cells were transfected with plasmid DNA encoding EGFP-53BP1-wt or EGFP-53BP1 mutants, grown on glass coverslips for 48 h and γ-irradiated (3 Gy). After 3 h, cells were fixed and processed (with γH2AX primary and Alexa Fluor® 568 secondary antibodies) as described in Section 4.12.1. Images were then acquired using high-content screening station Scan^R (Olympus) connected to Olympus IX81 microscope with 40x/1.3 UPLFLN oil objective. Analysis was performed by Scan^R analysis software. Briefly, the main objects (nuclei) were detected based on DAPI signal and sub-objects (foci) based on GFP (EGFP-53BP1 mutans) and Alexa568 (γH2AX) signal using spot detection module. At least 300 GFP+ cells per a coverslip were analysed. EGFP-53BP1 foci co-localizing with γH2AX were counted and the proportion of the cells with >5 foci was calculated. The results from three independent experiments were statistically analysed.

### 4.12.4. Laser microirradiation followed by live cell imaging

Cells were transfected with plasmid DNA encoding EGFP-53BP1-wt or EGFP-53BP1 mutants. After 24 h, 40 000 cells were seeded in 1µ-Slide 8-well (Ibidi) and grown in the presence of 10 µM BrdU for 24 h to pre-sensitize the cells. Prior to imaging, the medium was replaced with Leibovitz's L-15 medium (Gibco) supplemented with 10% FBS. Laser microirradiation and imaging was performed in climate

chamber (37°C), employing confocal microscope Leica TCS SP5 with HC PL APO 63x/1.40 OIL CS2 objective. Laser of wavelength 405 nm (100% power) was used to microirradiate defined stripes (tracks) in selected nuclei. Subsequently, the recruitment of EGFP-tagged proteins into these laser-induced tracks of DNA damage was monitored by capturing images at 30 s intervals for 5 min.

## 4.13. Statistical analysis

Statistical analysis was performed with GraphPad Prism software (version 6). Due to a low number of repetitions (3 in each case), data normality was not assumed. Thus, non-parametric Kruskall-Wallis (K-W) test followed by Dunn's multiple comparisons test were used to compare EGFP-53BP1- mutants to EGFP-53BP1-wt. p-values lower than 0.05 were considered statistically significant.

# 5. Results

## 5.1. Identification of 53BP1 NLS

ELM prediction and cNLS Mapper were employed to search for potential NLS within 53BP1 sequence (see Section 5.1.1.). The results obtained from these *in silico* searches were then used to design DNA constructs that were subsequently prepared in order to identify NLS used by 53BP1 (see Section 5.1.2.). For NLS identification, two different approaches were applied: (1) direct visualization of either EGFP-53BP1 mutants (see Section 5.1.3.) or EGFP-NLS sequence itself (see Section 5.1.4) and (2) co-IP of either EGFP-53BP1 mutants and importin ß (see Section 5.1.3.) or EGFP-NLS and importin ß (see Section 5.1.4.).

### 5.1.1. Prediction of 53BP1 NLS

ELM consensus sequence search identified 10 variants of classical NLSs as summarized in Table 4. However, some of these variants differed only in amino acids surrounding the crucial basic stretches (highlighted in bold). Therefore, the prediction results indicated the presence of only two different monopartite and two different bipartite NLSs. Furthermore, the results suggested that the region between amino acids 1625 and 1685 should be solely responsible for 53BP1 nuclear import.

**Table 4. The putative instances of 53BP1 NLSs obtained from ELM prediction.**

| ELM class | Putative instance |
|---|---|
| **TRG_NLS_Bipartite_1**<br>Definition: [KR][KR].{7,15}[^DE]((K[RK])\|(RK))(([^DE][KR])\|([KR][^DE]))[^DE] | 1651-**RK**ITESPRASMGVLSG**KRK**LI-1671<br>1667-**KRK**LITSEEERSPA**KRGRK**-1685<br>1668-**RK**LITSEEERSPA**KRGRK**-1685 |
| **TRG_NLS_MonoCore_2**<br>Definition: [^DE]((K[RK])\|(RK))[KRP][KR][^DE] | 1625-G**KRKRR**-1630<br>1626-**KRKRR**S-1631 |
| **TRG_NLS_MonoExtC_3**<br>Definition: [^DE]((K[RK])\|(RK))(([^DE][KR])\|([KR][^DE]))(([PKR])\|([^DE][DE])) | 1625-G**KRKRR**-1630<br>1680-A**KRGRK**-1685 |
| **TRG_NLS_MonoExtN_4**<br>Definition: (([PKR].{0,1}[^DE])\|([PKR]))((K[RK])\|(RK))(([^DE][KR])\|([KR][^DE]))[^DE] | 1626- **KRKRR**SN-1632<br>1627-**RKRR**SN-1632<br>1679-PA**KRGRK**-1685 |

cNLS Mapper proposed five variants of classical NLSs (the score cut-off was set at 3) which are summarized in Table 5. Only 1666-GKRKLITSEEERSPAKRGRKS-1686 bipartite NLS had the score >8 and therefore could be responsible for nuclear localization of 53BP1. Based on the scores, the remaining predicted NLSs could not be strong enough to handle 53BP1 import themselves.

**Table 5. Predicted NLS sequences obtained from cNLS Mapper.**

| Predicted bipartite NLS | Score* |
|---|---|
| 1666-G**KRK**LITSEEERSPA**KRGRK**S-1686 | 13.0 |
| 1668-**RK**LITSEEERSPA**KRGRK**S-1686 | 5.3 |
| **Predicted monopartite NLS** | **Score*** |
| 1677-RSPA**KRGRK**S-1686 | 4.5 |
| 1624-EG**KRKRR**SNVS-1634 | 4.0 |
| 1623-VEG**KRKRR**S-1631 | 3.0 |

*cNLS Mapper calculates NLS activity scores (see Section 4.2.). If the score is >8, the NLS sequence is expected to localize exclusively to the nucleus. The score of 6 or 7 suggests partial nuclear localization, while the score of 3–5 implies localization to both the nucleus and the cytoplasm (Kosugi et al., 2009b).

### 5.1.2. Preparation of DNA constructs for 53BP1 NLS identification

Based on NLS predictions, several DNA constructs described in Table 6 were designed, prepared and validated by restriction enzyme digestion and sequencing.

**Table 6. DNA constructs prepared for 53BP1 NLS identification and differences in the protein sequence between EGFP-53BP1-wt and EGFP-53BP1-ΔNLS mutants.**

| DNA construct | Modification (deletion, substitution) |
|---|---|
| **pEGFP-TEV-FLAG-53BP1-ΔNLS1-3** | Δ1626-1692 |
| **pEGFP-TEV-FLAG-53BP1-ΔNLS1** | 1626-KRKRR-1630 → 1626-AAAA-1629 |
| **pEGFP-TEV-FLAG-53BP1-ΔNLS2** | 1667-KRK-1669 → 1667-AAA-1669 |
| **pEGFP-TEV-FLAG-53BP1-ΔNLS3** | 1681-KRGRK-1685 → 1681-AAAAA-1685 |

### 5.1.3. Localization of EGFP-53BP1-ΔNLS mutants

Nuclear localization of prepared EGFP-53BP1-ΔNLS mutants was evaluated by fluorescence microscopy (Figure 3). The same expression of EGFP-53BP1-ΔNLS mutants was confirmed (see Suppl. Figure 1A). EGFP-53BP1-wt localized to the nucleus, thereby validating no deleterious effect of EGFP-tagging on 53BP1 nuclear localization. EGFP-53BP1-ΔNLS1 also localized to the nucleus, while EGFP-53BP1-ΔNLS1-3, EGFP-53BP1-ΔNLS2, EGFP-53BP1-ΔNLS3 were present exclusively in the cytoplasm.

### 5.1.4. Binding of EGFP-53BP1-ΔNLS mutants to importin ß

The ability of EGFP-53BP1-ΔNLS mutants to bind importin ß was assessed by co-IP (Figure 4). EGFP-53BP1-wt was able to bind importin ß specifically, thereby validating no deleterious effect of EGFP-tagging on 53BP1-importin ß interaction. EGFP-53BP1-ΔNLS1 also interacted with importin ß, while EGFP-53BP1-ΔNLS1-3, EGFP-53BP1-ΔNLS2, EGFP-53BP1-ΔNLS3 did not.

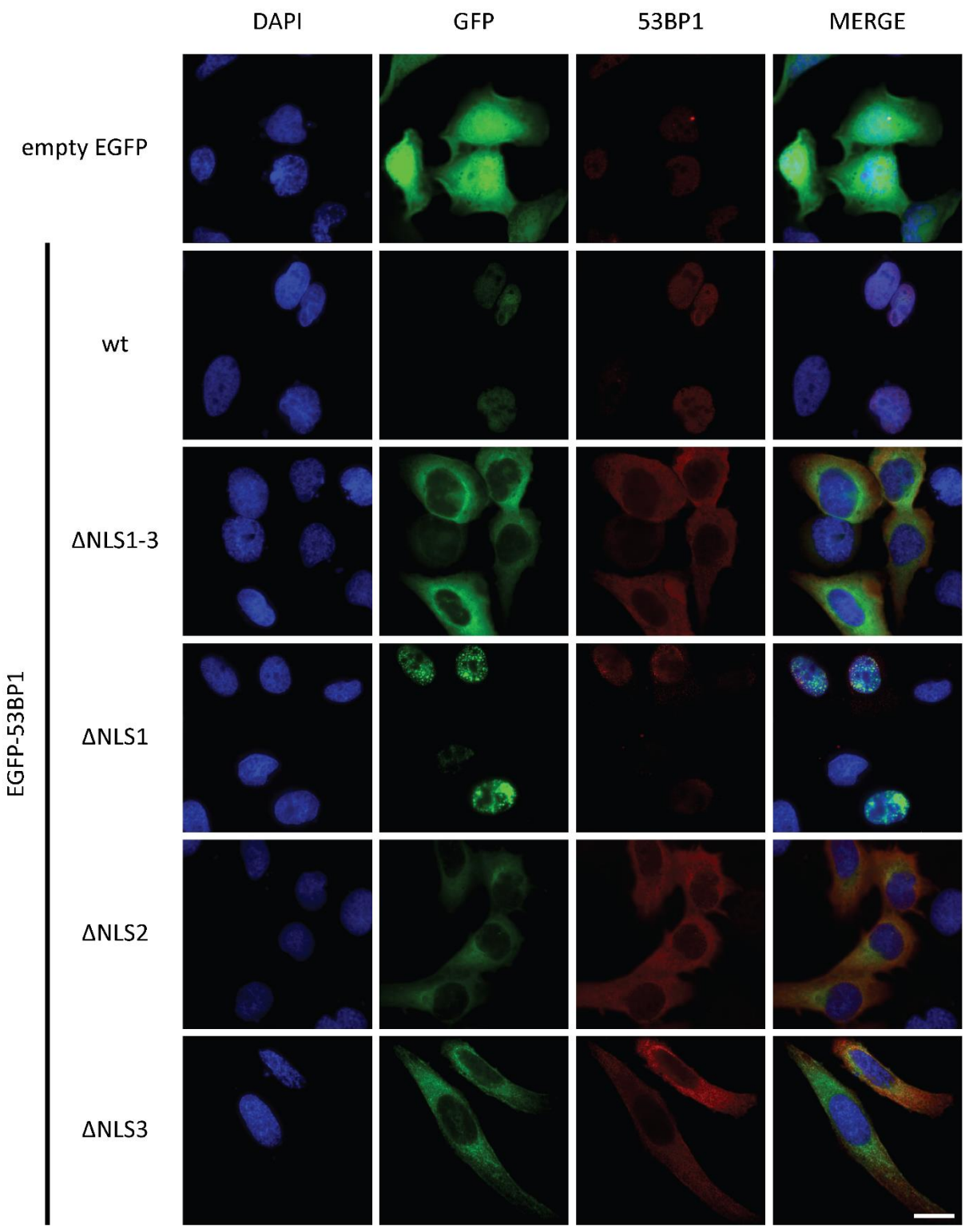


**Figure 3. Localization of EGFP-53BP1-ΔNLS mutants.** U2OS cells were transfected with DNA constructs encoding indicated EGFP-53BP1 mutants or empty EGFP as a control. Cells were fixed 48 h after transfection and stained with 53BP1 antibody (to confirm that EGFP signal corresponds to 53BP1). DAPI was used to visualize nuclei. The results indicated that KRK and KRGRK motifs, absent in EGFP-53BP1-ΔNLS2 and EGFP-53BP1-ΔNLS3 mutants, respectively, are both necessary for 53BP1 nuclear localization. Scale bar 20 μm.

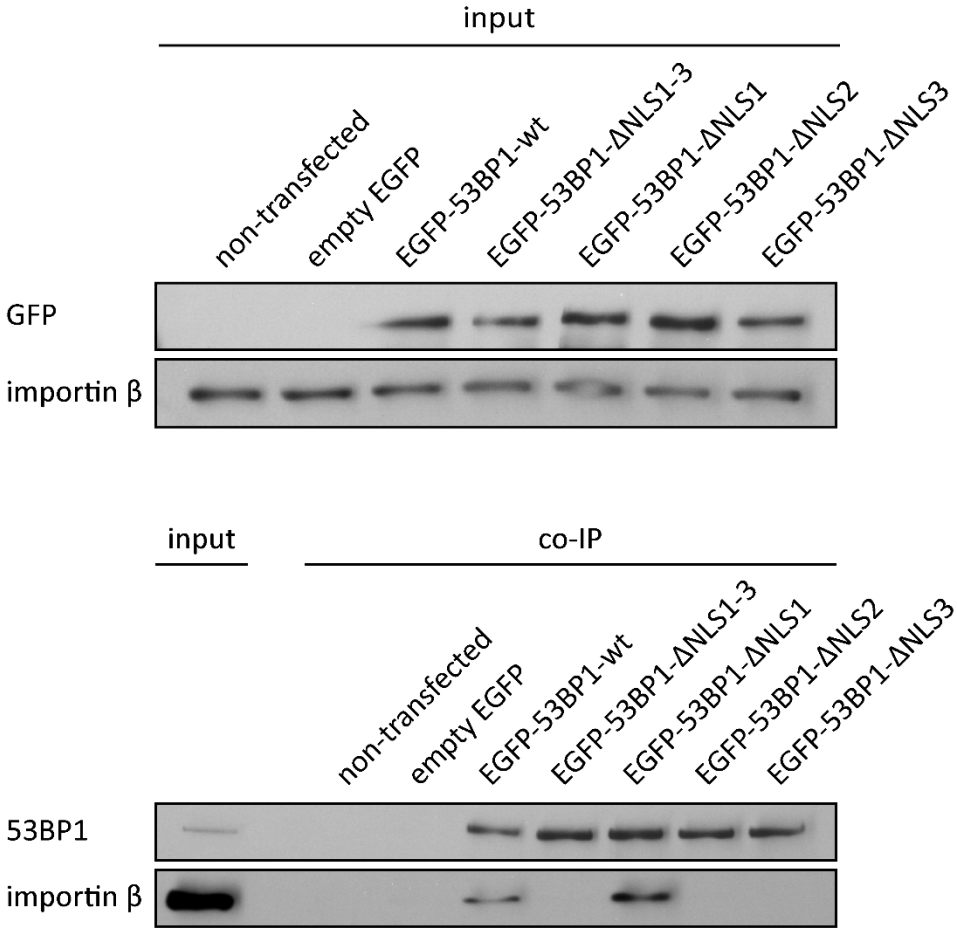


**Figure 4. Binding of EGFP-53BP1-ΔNLS mutants to importin ß.** U2OS cells were transfected with DNA constructs encoding indicated EGFP-53BP1 mutants. Empty EGFP-transfected and non-transfected cells were used as a control. The cells were lysed 24 h after transfection. co-IP of EGFP-tagged proteins and importin ß was performed. The results indicated that KRK and KRGRK motifs, absent in EGFP-53BP1-ΔNLS2 and EGFP-53BP1-ΔNLS3 mutants, respectively, are both necessary for interaction of 53BP1 with importin ß.

### 5.1.5. Localization of EGFP-NLS itself and its binding to importin ß

As previous results suggested that both KRK and KRGRK motifs (which are missing in EGFP-53BP1-ΔNLS2 and EGFP-53BP1-ΔNLS3, respectively) are necessary for 53BP1 nuclear import, the DNA construct encoding the sequence 1658-RASMGVLSG**KRK**LITSEEERSPA**KRGRK**SA-1687 fused to the EGFP was prepared and validated by restriction enzyme digestion and sequencing. EGFP-NLS localization was evaluated by fluorescence microscopy (Figure 5A) and its ability to bind importin ß was assessed by co-IP (Figure 5B). EGFP-NLS localized exclusively to the nucleus and interacted with importin ß.

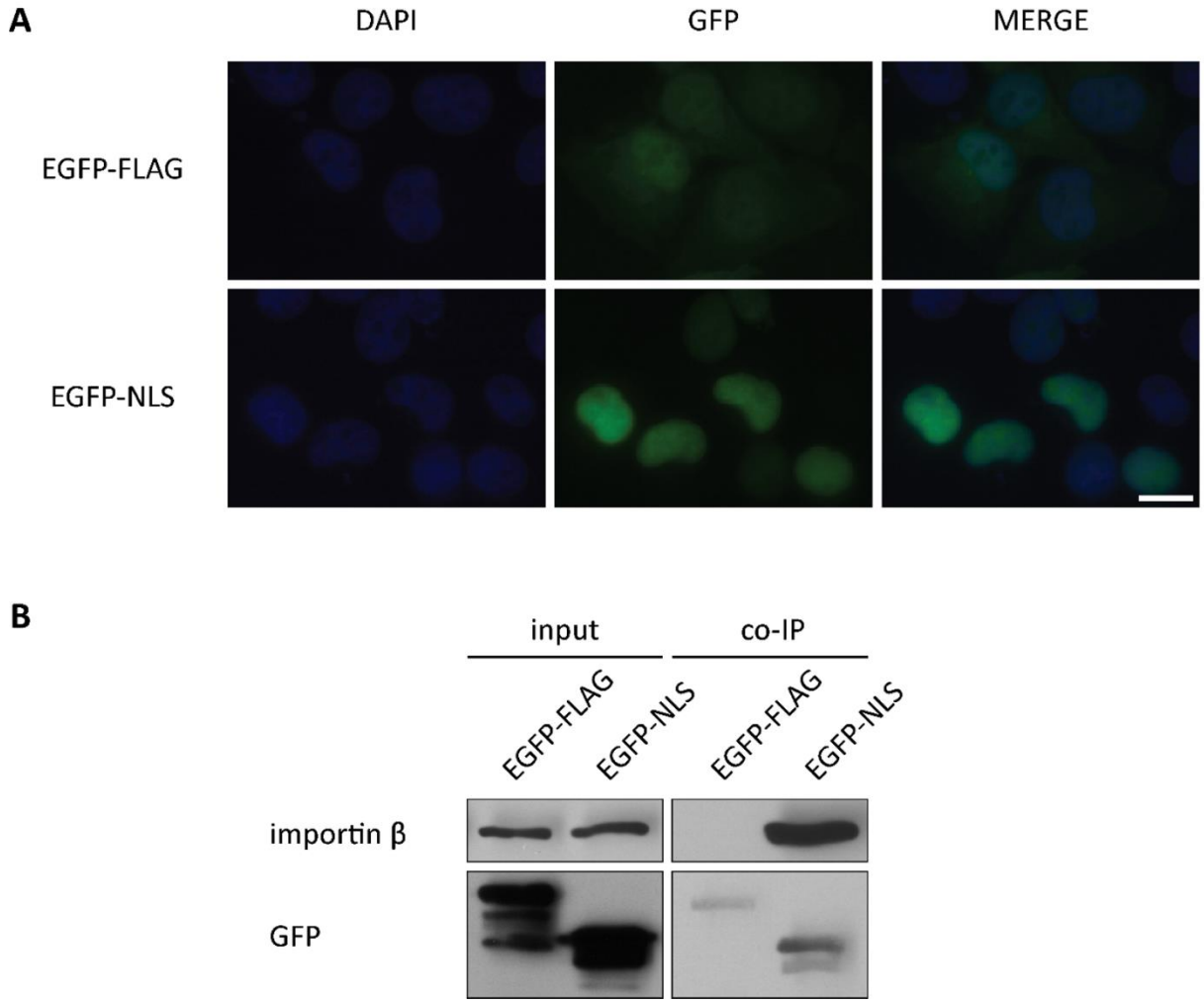


**Figure 5. Localization of EGFP-NLS itself and its binding to importin ß.** U2OS cells were transfected with DNA construct encoding EGFP-NLS or EGFP-FLAG. Cells were fixed 48 h after transfection and processed for fluorescence microscopy examination (A) or lysed 24 h after transfection to perform co-IP (B). The results of both approaches demonstrated that 1658-RASMGVLSGKRKLITSEEERSPAKRGRKSA-1687 sequence itself localizes to the nucleus and is sufficient for interaction with importin ß. DAPI was used to visualize nuclei. Scale bar 20 µm.

## 5.2. Potential regulation of 53BP1 NLS by phosphorylation

Identification of 53BP1 NLS facilitated the examination of its potential regulation by phosphorylation. Amino acids that can be phosphorylated and are within or adjacent to 53BP1 NLS were taken into consideration. S1678 was selected for further exploration for following reasons:

1. Among the residues within or adjacent to 53BP1 NLS, S1678 had the highest number of mass spectrometry analysis records, in which this site was assigned to be phosphorylated, in PhosphoSitePlus database (Hornbeck et al., 2015).

2. S1678 is followed by P1679, A1680 and K1681. This sequence corresponds to the CDK phosphorylation consensus sequence, which was defined as [pS/pT]PX[K/R] (Songyang et al., 1994). That is why CDK-dependent phosphorylation of S1678 was expected to regulate nuclear transport of 53BP1.
3. S1678 is the major cyclin B-CDK1 complex phosphorylation site in the C-terminal part of 53BP1 (1483-1972) *in vitro*, as shown in Benada et al. 2015.

To study the potential effect of phosphorylation at S1678 on 53BP1 nuclear import, DNA constructs encoding EGFP-53BP1-S1678A, EGFP-S53BP1-1678D, EGFP-NLS-S1678A and EGFP-NLS-S1678D were designed, prepared and validated by restriction enzyme digestion and sequencing.

Non-phosphorylatable mutants (EGFP-53BP1-S1678A and EGFP-NLS-S1678A) were used for determination of S1678 phosphorylation status in cells (see Section 5.2.1.). Interaction betwen 53BP1 and importin ß was examined during the cell cycle progression (see Section 5.2.2.). Phosphomimetic (EGFP-53BP1-S1678D and EGFP-NLS-S1678D) and non-phosphorylatable (EGFP-53BP1-S1678A and EGFP-NLS-S1678A) mutants were further employed to test the effect of the phosporylation on 53BP1 nuclear localization (see Section 5.2.3. and 5.2.5.) and its binding to importin ß (see Section 5.2.4. and 5.2.5.). As the phosphorylation at S1678 was believed to contribute to the inhibition of 53BP1 binding to ubiquitinated histones in the M phase (see Section 3.1.1.), the recruitment of EGFP-53BP1-S1678A and EGFP-53BP1-S1678D to DNA damaged sites was examined (see Section 5.2.6.).

### 5.2.1. Detection of S1678 phosphorylation status in cells

As there was no antibody againts pS1678-53BP1 available, the phospho-MAPK/CDK substrates antibody, which recognised PXpSP or pSPXR/K, was used to investigate S1678 phoshorylation status in cells. Within EGFP-53BP1-wt and EGFP-NLS sequences, there were 11 and 1 consensus sequences, respectively, potentially recognized by the antibody. When EGFP-53BP1-wt and EGFP-53BP1-S1678A were immnunoprecipitated from cells synchronized in different cell cycle phases, strong signal was noticed in mitotic samples but no difference in signal between EGFP-53BP1-wt and EGFP-53BP1-S1678A was recognised (Figures 6). When the same experiment was perfomed with EGFP-NLS and EGFP-NLS-S1678A, no or very weak and non-specific signal was obtained (not shown).

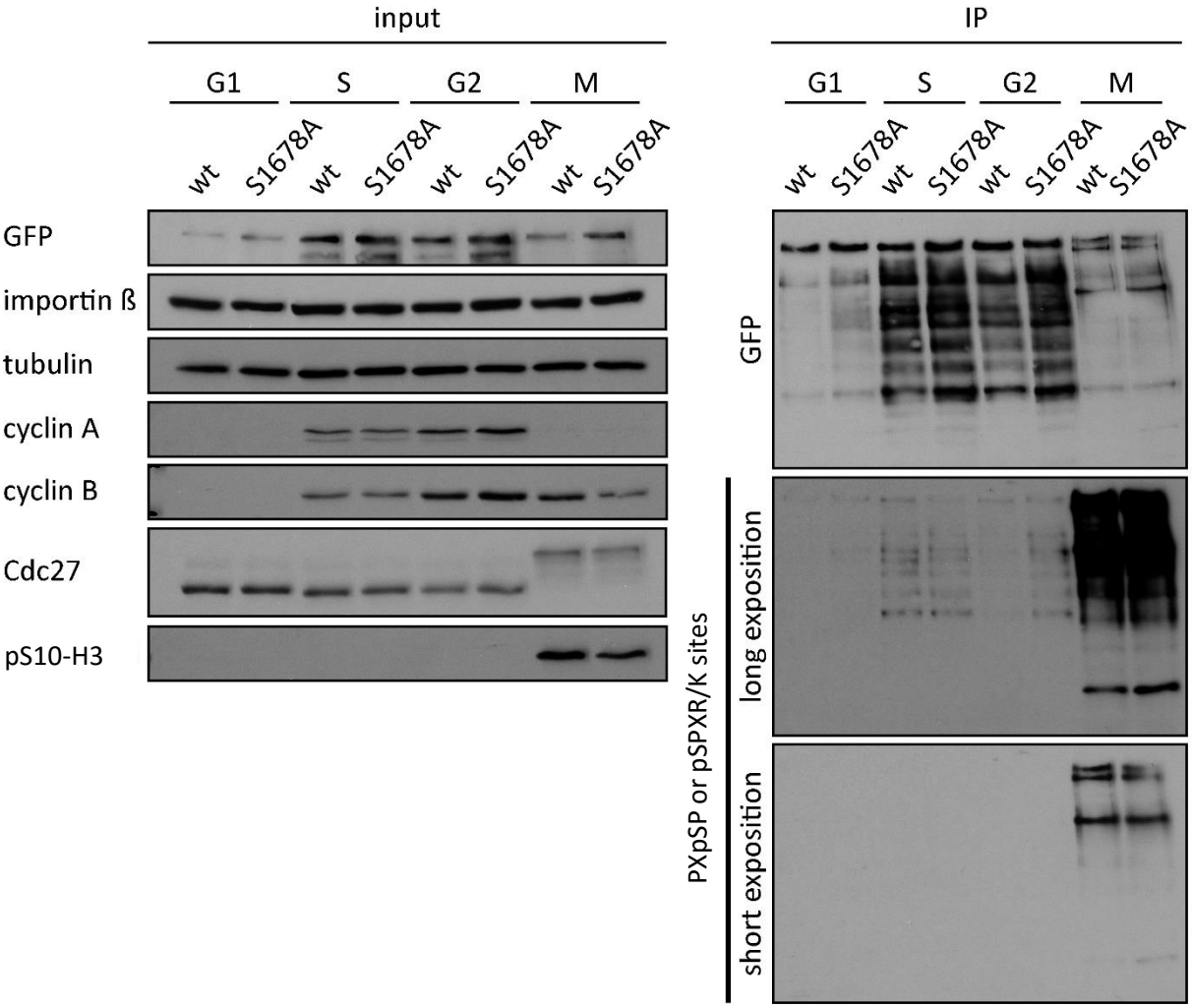


**Figure 6. Detection of 53BP1-S1678 phosphorylation status in cells.** U2OS cells were transfected with EGFP-53BP1-wt or EGFP-53BP1-S1678, synchronized by the modified thymidine-nocodazole block in G1, S, G2 and M phases of the cell cycle. Cell samples corresponding to these cell cycle phases were used for IP of EGFP-tagged proteins. The results illustrated the unsuitability of phospho-MAPK/CDK substrates antibody for detection of S1678 phosphorylation status when the full-length EGP-53BP1-wt was immunoprecipitated.

### 5.2.2. Import of 53BP1 to the nucleus during the cell cycle

53BP1 interactions with importin ß and NUP153 were monitored by co-IP during the cell cycle progression to determine whether 53BP1 is imported to the nucleus continuously or whether nuclear import of 53BP1 only occurs/is (in)decreased in particular cell cycle phases.

As co-IP of endogenous 53BP1 and importin ß failed to detect specific interactions, transiently overexpressed EGFP-53BP1-wt and EGFP-53BP1-ΔNLS1-3 were used. When cells were synchronized by double thymidine block and subsequently released to complete their cell cycle, no changes in EGFP-53BP1-wt interactions with importin ß and NUP153 were observed from the G1/S transition to the M phase (Figure 7). Cells were also synchronised by thymidine-nocodazole block, subsequently released and harvested after 1 h, 2 h and 3 h. In this setting, no changes in interactions were observed from the

M phase to the early G1 phase (not shown). EGFP-53BP1-wt interacted with NUP153 at the G1/S boundary and in the S and M phases to the same extent (Figure 7). The NUP153 antibody failed to recognise its epitope in the M phase.

It was believed that S1678 is phosphorylated in the M phase. To test the potential phospho-dependent increase in interaction between 53BP1 and importin ß in the M phase, the co-IP followed by dephosphorylation was performed (Suppl. Figure 2A). Lambda phosphatase dephosporylated majority of EGFP-53BP1-wt at S1618, but no decrease in interaction between EGFP-53BP1-wt and importin-ß was noticed. To test the potential phospho-dependent decrease in interaction between EGFP-53BP1-wt and importin ß in the M phase, lysate from mitotic cells was dephosphorylated prior to the co-IP. Lambda phosphatase dephosporylated the majority of EGFP-53BP1-wt at S1618, but non-specific binding of proteins to GFP-TRAP® matrix was observed (not shown).

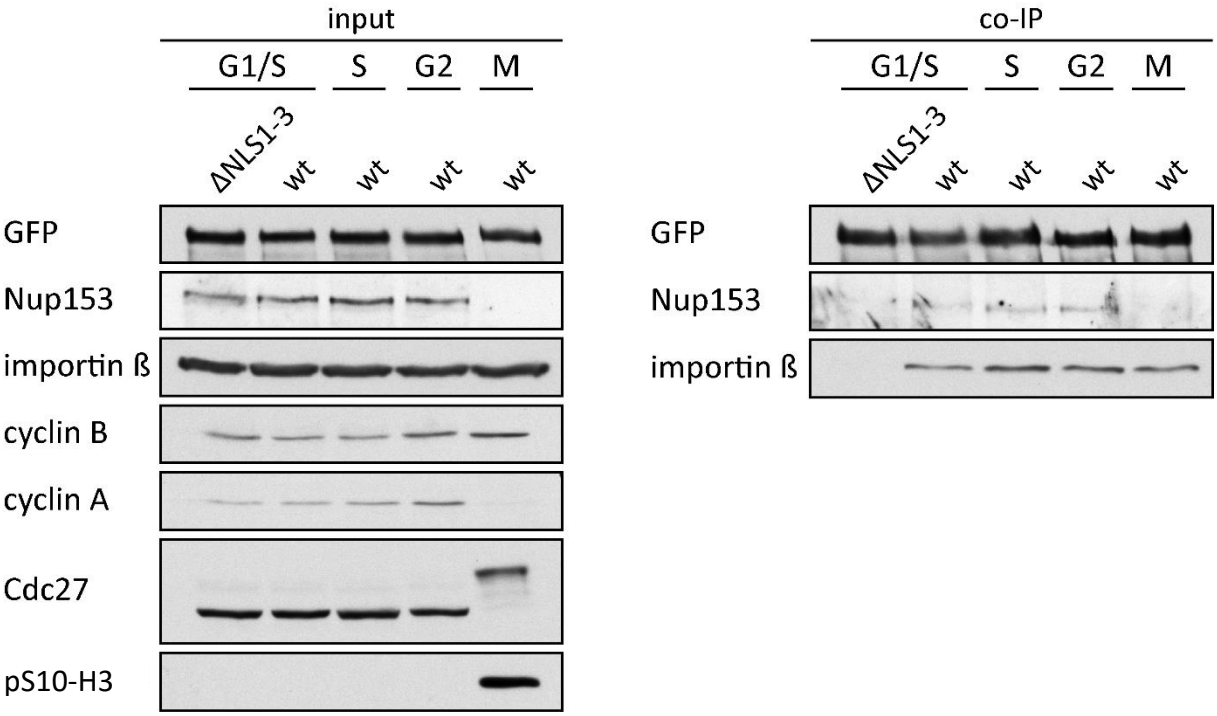


**Figure 7. Import of 53BP1 to the nucleus during the cell cycle.** U2OS cells were transfected with DNA constructs encoding EGFP-53BP1-wt or EGFP-53BP1-ΔNLS1-3, synchronized by double thymidine block, harvested at different stages of the cell cycle and co-IP was performed. The results suggested that there are no changes in the import of EGFP-53BP1-wt to the nucleus from the G1/S to M phase.

### 5.2.3. Localization of EGFP-53BP1-S1678A and EGFP-53BP1-S1678D

Expression of EGFP-53BP1-S1678A and EGFP-53BP1-S1678D mutants was the same in my experiments (Suppl. Figure 1B). They had ability to localize to the nucleus as demonstrated by IF (Suppl. Figure 3), but more cells in which 53BP1 was present in both the nucleus and the cytoplasm were observed if compared to EGP-53BP1-wt. That was particularly apparent 24 h after transfection. That is why the

quantification and statistical evaluation of the defect in nuclear transport was performed at this time point (Figure 8). On average, EGFP-53BP1-wt had nucleocytoplasmic distribution in 11% of cells, EGFP-53BP1-S1678A in 21% of cells and EGFP-53BP1-S1678D in 36% of cells. If compared to EGFP-53BP1-wt, EGFP-53BP1-S1678A was found even in the cytoplasm two-folds more often, which was not significantly different (p = 0.47, K-W), and EGFP-53BP1-S1678D three-folds more often which appeared to be of a significance (p = 0.03, K-W).

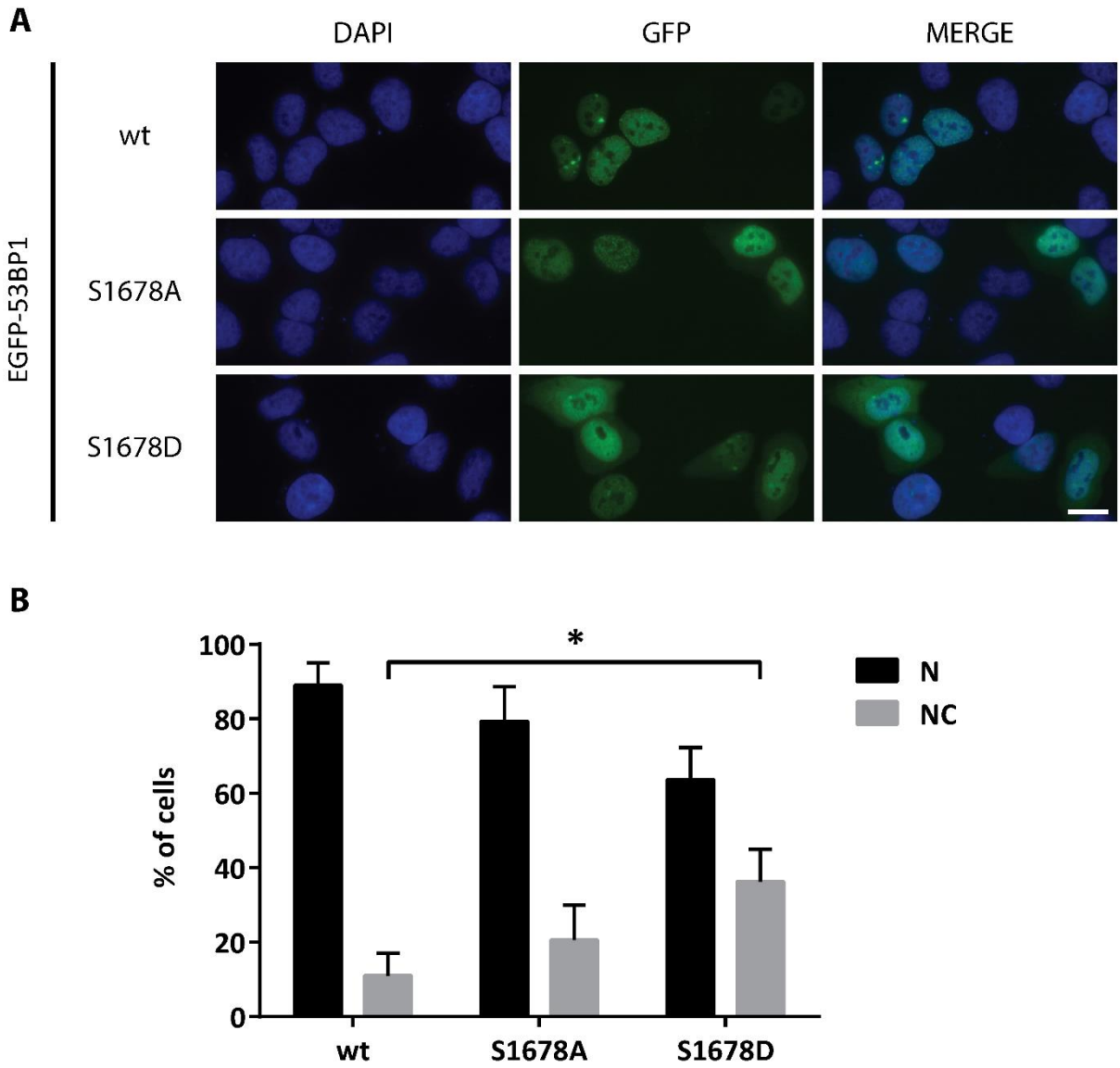


**Figure 8. Quantification of EGFP-53BP1-S1678A and EGFP-53BP1-S1678D distribution in cells.** U2OS cells were transfected with DNA constructs encoding indicated EGFP-53BP1 mutants. Cells were fixed 24 h after transfection, stained by DAPI to visualize nuclei and the nuclear/nucleocytoplasmic pattern of EGFP-53BP1 mutants was quantified. Representative images are shown in (A). Average percentage of cells with only nuclear (N) and nucleocytoplasmic (NC) distribution (100 cells/condition were counted, n = 3, error bars indicate standard deviation, * $p < 0.05$) is shown in (B). The quantification revealed that EGFP-53BP1-S1678D has a defect in nuclear import. Scale bar 20 µm.

### 5.2.4. Binding of EGFP-53BP1-S1678A and EGFP-53BP1-S1678D to importin ß

Binding of EGFP-53BP1-S1678A and EGFP-53BP1-S1678D mutants to importin ß was assessed by co-IP (Figure 9). Interaction between EGFP-53BP1-S1678A and importin ß was weaker than interaction between EGFP-53BP1-wt and importin ß. Surprisingly, no interaction between EGFP-53BP1-1678D and importin ß was observed in asynchronous cells. As the phosphorylation, which is mimicked in EGFP-53BP1-S1678D mutant, was believed to appear at least in the M phase, the interactions between EGFP-53BP1-S1678 mutants and importin ß were evaluated in nocodazole-arrested cells (Suppl. Figure 2B). In the M phase, the same results were obtained except for EGFP-53BP1-S1678D that showed weak interaction with importin ß.

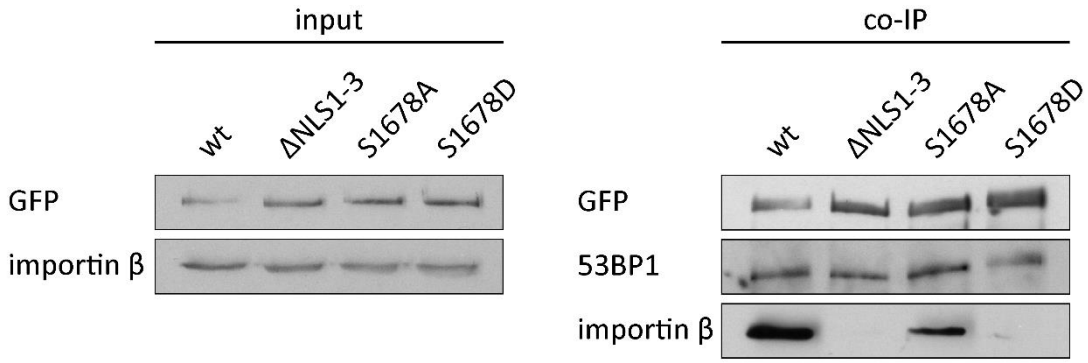


**Figure 9. Binding of EGFP-53BP1-S1678A and EGFP-53BP1-S1678D to importin ß.** U2OS cells were transfected with DNA constructs encoding indicated EGFP-53BP1 mutants and lysed 24 h after transfection. co-IP of EGFP-53BP1 mutants and importin ß was performed. The results showed that EGFP-53BP1-S1678A has weaker affinity for importin ß than EGFP-53BP1-wt. EGFP-53BP1-S1678D did not detectable interact with importin ß in asynchronous cells.

### 5.2.5. Localization of EGFP-NLS-S1678A and EGFP-NLS-S1678D and their binding to importin ß

Nuclear localization of EGFP-NLS-S1678A and EGFP-NLS-S1678D was evaluated by fluorescence microscopy (Figure 10A) and its binding to importin ß was assessed by co-IP (Figure 10B). EGFP-NLS-S1678A and EGFP-NLS-S1678D both localized to the nucleus and interacted with importin ß. However, EGFP-NLS-S1678A seemed to have weaker affinity for importin ß than EGFP-NLS and EGFP-NLS-S1678D had the lowest affinity for importin ß among these.

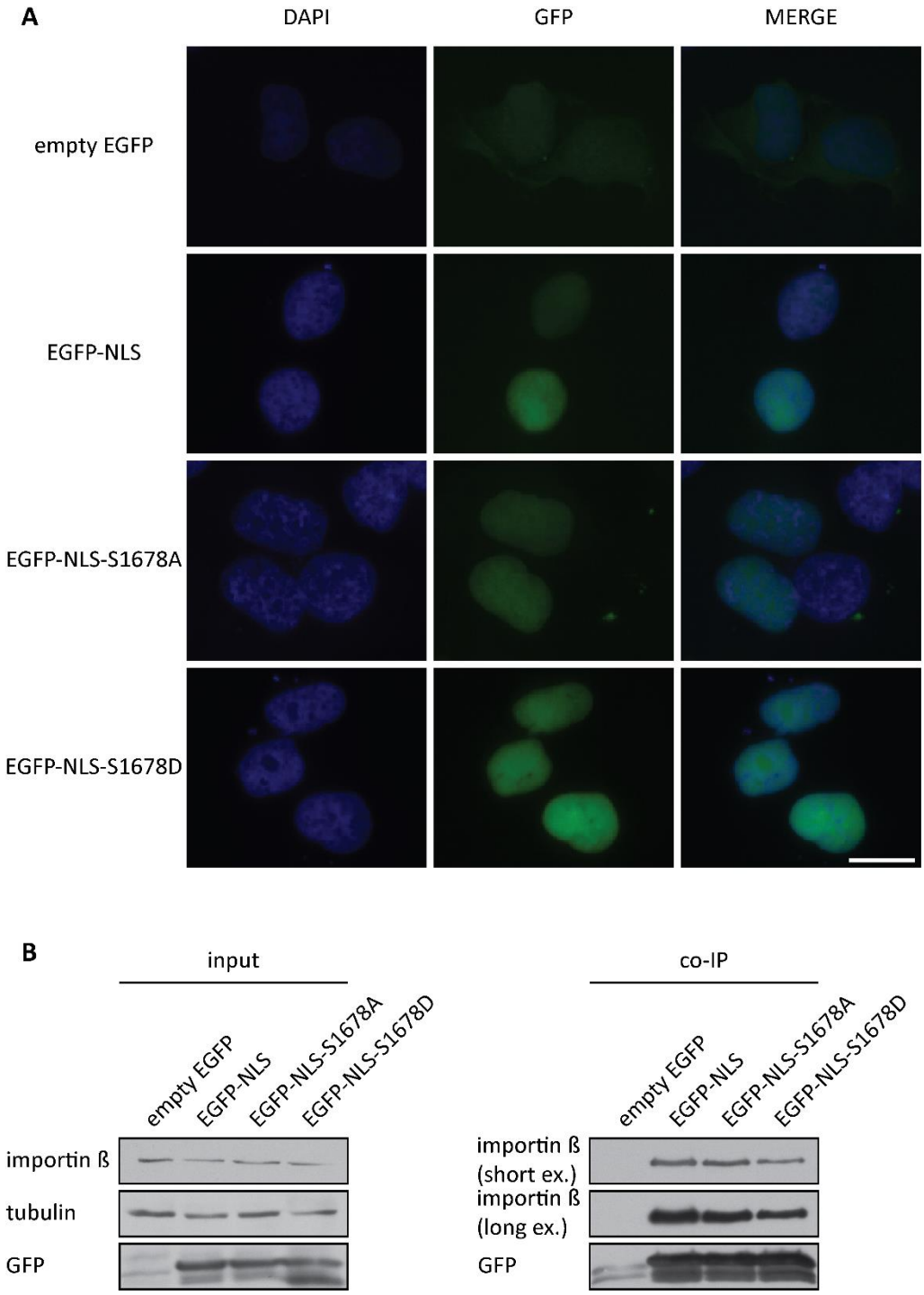


**Figure 10. Localization of EGFP-NLS-S1678A and EGFP-NLS-S1678D and their binding to importin ß.** U2OS cells were transfected with DNA constructs encoding empty EGFP, EGFP-NLS and EGFP-NLS-S1678A and EGFP-NLS-S1678D. Cells were fixed 48 h after transfection and processed for fluorescence microscopy examination (A) or lysed 24 h after transfection to perform co-IP (B). The results demonstrated that both EGFP-NLS-S1678A and EGFP-NLS-S1678D localize to the nucleus and interact with importin ß, albeit with lower affinity than EGFP-NLS. DAPI was used to visualize nuclei. Scale bar 20 µm.

### 5.2.6. Recruitment of EGFP-53BP1-S1678A and EGFP-53BP1-S1678D to DNA damage sites

Recruitment of EGFP-53BP1-S1678A and EGFP-53BP1-S1678D mutants to laser microirradiation induced DNA damage sites (Figure 11) and to DNA damage foci after γ-irradiation (Figure 12) was monitored. EGFP-53BP1-T1609D-S1618D, which mimics two well-described mitotic phosphorylations, and EGFP-53BP1-ΔNLS1, which lacks the C-terminal part of UDR motif, were used as negative controls. EGFP-53BP1-wt, EGFP-53BP1-S1678A and EGFP-53BP1-S1678D were recruited to laser microirradiation induced DNA damage sites during the first 5 min, while EGFP-53BP1-T1609D-S1618D and EGFP-53BP1-ΔNLS1 were not. Furthermore, DNA damage foci after γ-irradiation were quantified. Only 53BP1 foci co-localizing with γH2AX were counted and the average proportion of cells with >5 foci was calculated. Although significant difference among the groups was revealed (p=0.02, K-W), it was not noticed between EGFP-53BP1-wt and other groups by multiple comparisons test.

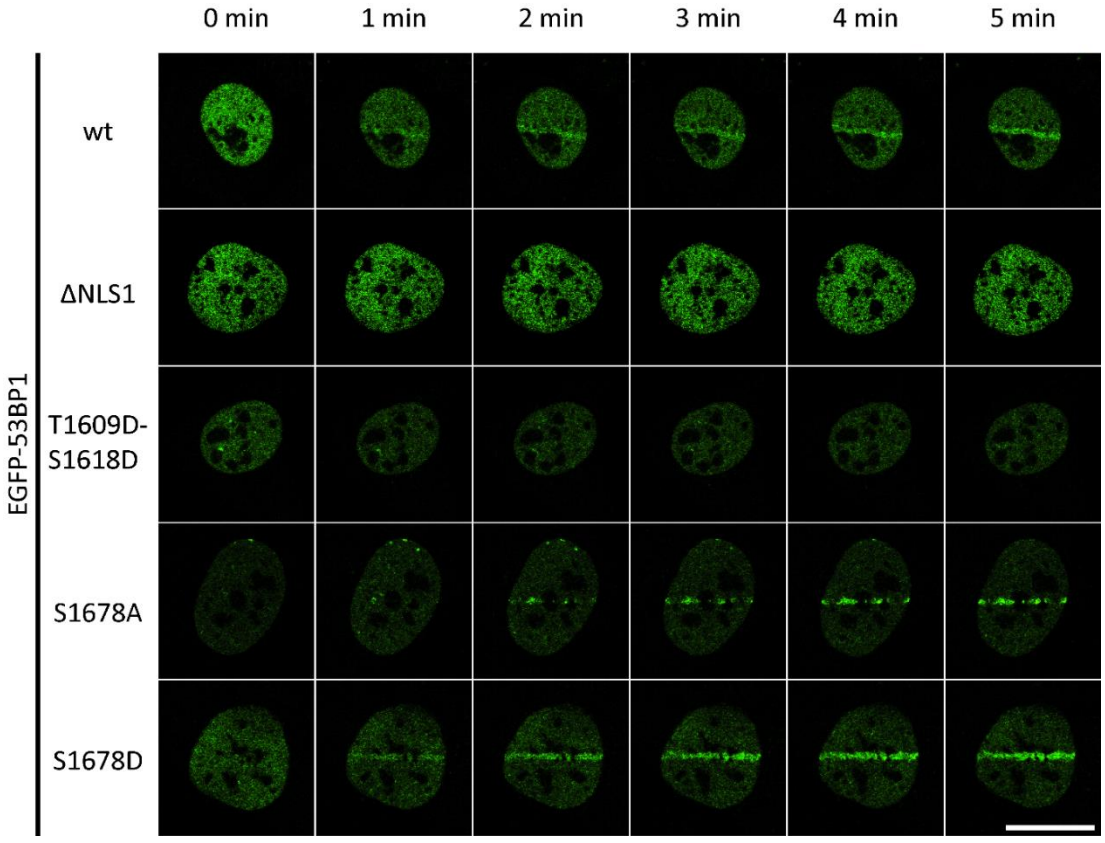


**Figure 11. Recruitment of EGFP-53BP1-S1678A and EGFP-53BP1-S1678D to laser microirradiation induced DNA damage sites.** U2OS cells were transfected with DNA constructs encoding indicated EGFP-53BP1 mutants, sensitised by BrdU and processed for live cell confocal imaging. Laser microirrradiation was employed to induce DNA damage. The recruitment of EGFP-53BP1 mutants to laser microirradiated tracks was monitored during the first 5 min. The live cell imaging showed that EGFP-53BP1-S1678A and EGFP-53BP1-S1678D do not have impaired recruitment to laser microirradiation induced DNA damage sites.

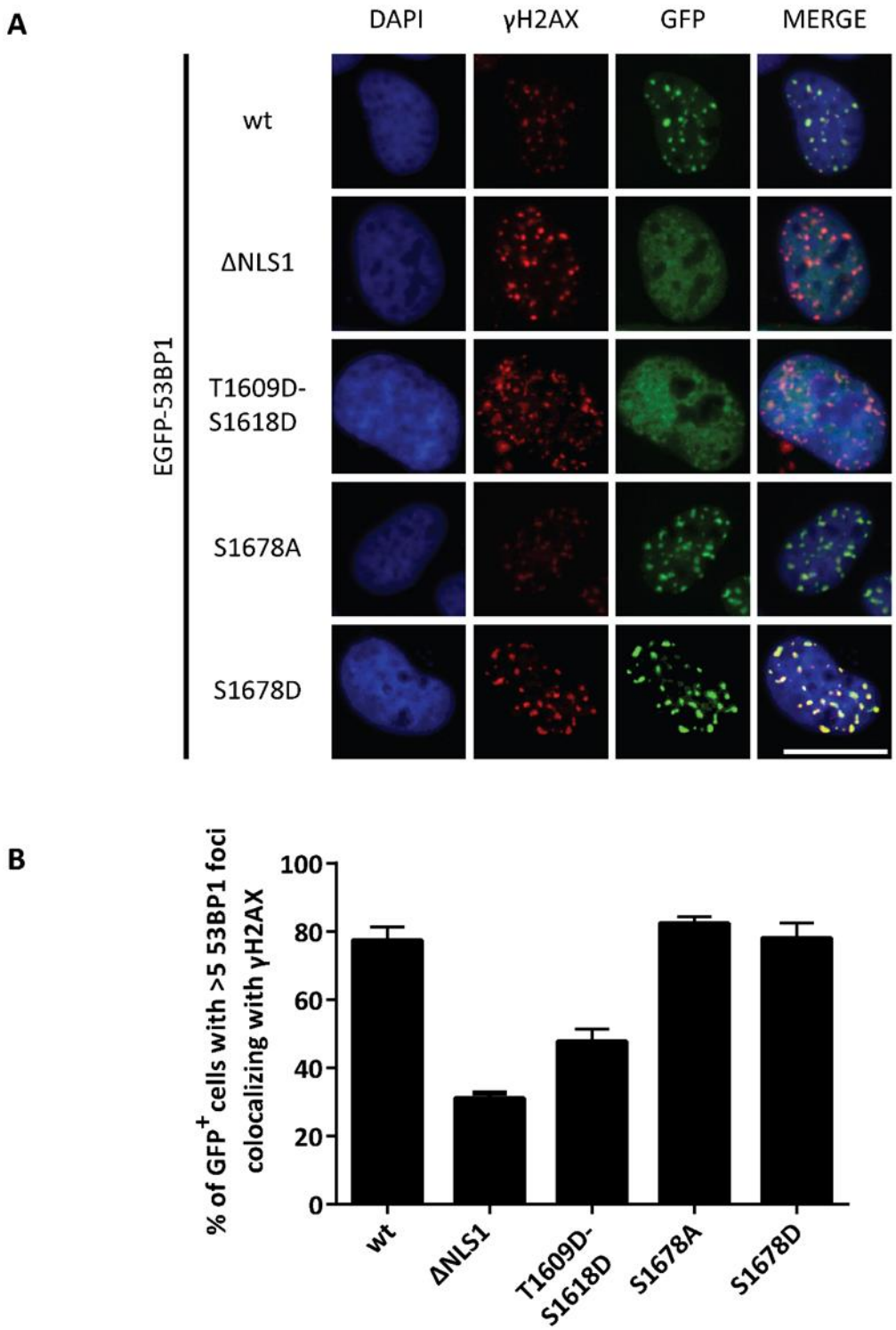


**Figure 12. Recruitment of EGFP-53BP1-S1678A and EGFP-53BP1-S1678D to DNA damage foci after γ-irradiation.** U2OS cells were transfected with DNA constructs encoding indicated EGFP-53BP1 mutants, γ-irradiated (3 Gy), fixed 3 h later and stained with γH2AX antibody. DAPI was used to visualize nuclei. The images were captured using automated high-content microscopy and processed by spot detection module. Representative images are shown in (A). Average percentage of cells with more than five 53BP1 foci co-localizing with γH2AX (n = 3, error bars indicate standard deviation) is shown in (B). The results suggested that the localization of EGFP-53BP1-S1678A and EGFP-53BP1-S1678D to DNA damage foci is not impaired.

## 5.3. Potential regulation of 53BP1 NLS by acetylation

Identification of 53BP1 NLS also enabled the examination of its potential regulation by acetylation. Among the residues within or adjacent to 53BP1 NLS, only K1667 is reported in PhosphoSitePlus database to be acetylated (Hornbeck et al. 2015). Therefore, we decided to try detecting an acetylation within EGFP-NLS using the acetylated lysine antibody (Figure 13). This antibody recognized acetylated lysine residue(s) within EGFP-NLS, while only low background signal was detected with EGFP-FLAG.

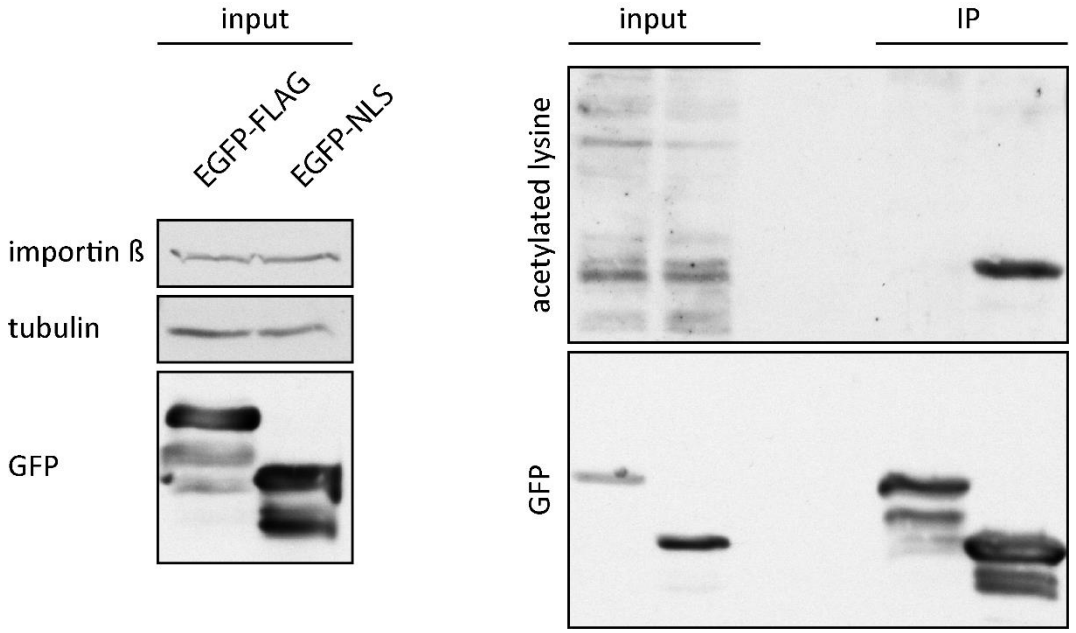


**Figure 13. Detection of EGFP-NLS acetylation.** U2OS cells were transfected with DNA constructs encoding EGFP-FLAG or EGFP-NLS and lysed 24 h later. IP of EGFP-FLAG or EGFP-NLS was performed. Acetylated lysine antibody was used to detect acetylation. This preliminary result suggested that there might be an acetylated lysine within NLS sequence.

# 6. Discussion

## 6.1. 53BP1 NLS

53BP1 is a large nuclear protein, whose nuclear transport has been insufficiently examined so far. The characterisation of 53BP1 NLS would lead to better understanding of 53BP1 nuclear import pathway. However, the nature of 53BP1 NLS and its position within 53BP1 sequence has not been experimentally determined yet.

The NLS is usually short sequence that must meet four criteria: (1) the NLS must be necessary for import, (2) the NLS must be sufficient to target an unrelated protein to the nucleus, (3) the interaction of cargo with its import receptor must be mediated by the NLS and (4) disruption of the cargo import pathway must prevent cargo import to the nucleus (Lange et al., 2007). Recently, it was demonstrated that 53BP1 nuclear import depends on importin ß (Moudry et al., 2012). 53BP1 interacts with importin ß and the disruption of importin ß import pathway prevents 53BP1 import to the nucleus (Moudry et al., 2012).

NLS prediction tools provided numerous putative NLSs within 53BP1 sequence (Dinkel et al., 2016; Kosugi et al., 2009b; Nguyen Ba et al., 2009). To identify 53BP1 sequence necessary for its import, the set of DNA constructs encoding EGFP-53BP1 mutants, which have the core residues of putative NLSs substituted with alanine residues, was prepared and their sub-cellular steady-state localization was determined. However, this steady-state protein distribution between the cytoplasm and the nucleus can be a result of protein import, protein export and protein degradation. That is why the ability of the EGFP-53BP1 mutants to interact with importin ß was assessed in co-IP experiments. The sequence that was identified to be necessary for 53BP1 import was tested whether it is sufficient to target GFP to the nucleus and to interact with importin ß. Taken together, this integrative approach should lead to identification of functional 53BP1 NLS(s).

I have identified two linear motifs within 53BP1 sequence that are both necessary for its nuclear import. Substitution of 1667-KRK-1669 or 1681-KRGRK-1685 linear motifs of 53BP1 with alanine residues disrupted its interaction with importin ß and resulted in its steady-state cytoplasmic localization. The 1658-RASMGVLSG**KRK**LITSEEERSPA**KRGRK**SA-1687 sequence derived from 53BP1 that includes these two linear motifs (highlighted in bold) was sufficient to target GFP to the nucleus and for interaction with importin ß. The requirement of two basic linear motifs separated by a short intervening linker implies that 53BP1 has a classical bipartite NLS (Robbins et al., 1991).

Consistently, one of the several putative instances of 53BP1 NLSs obtained from ELM prediction was a classical bipartite NLS with the sequence 1667-KRKLITSEEERSPAKRGRK-1685 and there are numerous already annotated instances of similar NLSs in the ELM database (Dinkel et al., 2016). Fur-

thermore, results obtained from cNLS Mapper (Kosugi et al., 2009b) indicated that only classical bipartite NLS with the sequence 1666-GKRKLITSEEERSPAKRGRKS-1686 can account for 53BP1 nuclear localization. Consensus sequence of the classical bipartite NLS was defined as $KRX_{10–12}K(KR)(KR)$ or $KRX_{10–12}K(K/R)X(K/R)$ and additional optional criteria for its optimal activity were determined (Kosugi et al., 2009a). Acidic residues should be rich in the central linker region and rare in the terminal linker region. Basic and hydrophobic residues should be rare in the central region and proline residues are preferred in the terminal linker region (Kosugi et al., 2009a). 1658-RASMGVLSG**KRKLITSEEERSPAKRGR**KSA-1687 sequence fits the consensus of the classical bipartite NLS (highlighted in bold) and meets the optional criteria.

During the analysis, several putative 53BP1 NLSs were found not to be relevant for its nuclear import. As deletion of the 53BP1 region 1626-1692 disrupted its interaction with importin ß and caused its steady-state cytoplasmic localization, the putative non-classical NLS in the 53BP1 region 1386-1407 (Nguyen Ba et al., 2009) was further excluded from the analysis. In the region 1626-1692, four distinct classical NLSs were predicted based on the consensus sequence search by ELM prediction (Dinkel et al., 2016). Except the bipartite NLS described above, the remaining three putative classical NLS obtained low scores in cNLS Mapper and were anticipated to cause nucleocytoplasmic distribution of 53BP1 (Kosugi et al., 2009b). Substitution of 1626-KRKRR-1630 linear motif of 53BP1 with alanines did not influence its interaction with importin ß or nuclear localization and therefore this motif is not necessary for 53BP1 nuclear import. 53BP1 mutants that have substituted 1667-KRK-1669 or 1681-KRGRK-1685 linear motifs had steady-state cytoplasmic localization and did not detectably interact with importin ß. Thus, 1626-KRKRR-1630 linear motif is not sufficient for detectable binding to importin ß and nucleocytoplasmic distribution of 53BP1 in the absence of the functional bipartite NLS. The same was true also for 53BP1 mutants that have intact 1651-RK-1652 and 1667-KRK-1669 or 1681-KRGRK-1685 linear motifs in the absence of the functional bipartite NLS. This indicates that putative monopartite NLSs with the core 1626-KRKRR-1630 or 1681-KRGRK-1685 linear motifs and a putative bipartite NLS with 1651-RK-1652 and 1667-KRK-1669 core linear motifs are not able to mediate 53BP1 nuclear import. However, I cannot rule out the possibility that some of these putative NLSs may be important for 53BP1 nuclear import under different experimental conditions (e.g. in different cell lines or in response to some signal).

ELM prediction, which employs consensus sequence similarity search, provided a lot of false positive results (Dinkel et al., 2016). This prediction applies globular domain, structural and context filters and displays unlikely results in a separate table to consider the whole-protein context. Nevertheless, the classical bipartite NLS identified in this study had been assessed as an unlikely one by ELM prediction, whereas other putative NLSs showed in this study as not being able to mediate 53BP1 nuclear import had been assessed as probable ones (Dinkel et al., 2016). cNLS Mapper, which employs

classical NLS search based on calculating NLS activity, proved to be more accurate in 53BP1 NLS prediction (Kosugi et al., 2009b). This prediction generally calculates the ability of the putative classical NLS to be imported to the nucleus using a dataset obtained in budding yeast import assays. Thus, the cNLS Mapper is not considering the whole-protein context and the prediction accuracy might be weaker for human NLSs. Nevertheless, only 53BP1 bipartite NLS identified in this study had been assessed to be able caused exclusive 53BP1 nuclear localization by cNLS Mapper (Kosugi et al., 2009b). The other putative classical NLSs obtained low scores (Kosugi et al., 2009b). Although they might be able to bind weakly to importin ß and mediate partial nuclear localization themselves, they did not exhibit this action in the context of the whole 53BP1 (as discussed above). Therefore, they seem not to be accessible enough or to be recognised too weakly by human nuclear import machinery.

Importin ß mediates the translocation of its cargos to the nucleus by several distinct ways. The identification of the bipartite classical NLS indicates that 53BP1 is indirectly recognised by importin ß *via* importin α. In agreement with this, I repeatedly observed approximately 60 kDa protein (the size of importin α) in a complex with importin ß and EGFP-NLS when I performed the co-IP experiments (not shown). To confirm that 53BP1 is imported to the nucleus by importin ß – importin α pathway, it would require: (1) a demonstration of interaction between 53BP1 and importin α and (2) a demonstration that the disruption of importin α pathway prevent 53BP1 nuclear import. This is complicated by the fact that there are six isoforms of importin α in humans (Goldfarb et al., 2004).

Importin α associates with importin ß through its IBB domain (Cingolani et al., 1999). In the importin α/ß heterodimer, importin ß is responsible for the translocation through the NPCs, whereas importin α binds cargo bearing classical bipartite NLS simultaneously by both the minor and major NLS binding grooves (Fontes et al., 2000). Several crystallographic analyses provided structural basic for the interaction of various classical bipartite NLSs with importin α (Conti and Kuriyan, 2000; Fontes et al., 2000, 2003a, 2003b). The crucial residues in the N-terminal basic linear motif of classical bipartite NLS, which bind to the minor NLS binding groove of importin α, are denoted P1' and P2'. The P1' and P2' positions must be occupied by lysine or arginine. Lysine is preferred at position P1', whereas arginine at position P2'. The crucial residues in the C-terminal basic linear motif of classical bipartite NLS bind to the major NLS binding groove and are denoted P2 to P6. At least three basic residues must be present at these positions. The P2 position is the most crucial for the activity of the NLS and must be occupied by lysine. The P3 and P5 positions display the preference for arginine or lysine residues. The P4 position is the most tolerant and can be occupied by various amino acids (except the negatively charged). The linker regions separating these two basic linear motifs are not conserved and vary in their length. They adopt different conformations and also make specific contacts with importin α, thereby also contributing to the efficiency of nuclear import (Conti and Kuriyan, 2000; Fontes et al., 2000, 2003a).

If the 53BP1 NLS is indeed recognised by importin α, the sequence 1667-**KR**KLITSEEERSPA**KRGR**-1684 (P1'-P2' and P2-P5 positions are highlighted in bold) should be sufficient for interaction with importin α/ß. Nevertheless, the NLS flanking regions have also been shown to contribute to the interaction with importin α (Fontes et al., 2003b). That is the reason why I used the longer sequence (1658-RASMGVLSGK**RK**LITSEEERSPA**KRGR**KSA-1687) to confirm the ability of the classical bipartite NLS of 53BP1 to mediate nuclear import. Thus, the precise boundary of 53BP1 NLS cannot be delineated based on this study. This would require extensive amino acid replacement analysis to determine which amino acids outside the 1667-**KR**KLITSEEERSPA**KRGR**-1684 sequence are still needed for 53BP1 nuclear import.

## 6.2. Potential regulation of 53BP1 NLS by phosphorylation

Identification of 53BP1 NLS, provided herein, facilitates the exploration of potential regulation of the 53BP1 nuclear import. Protein phosphorylation is the most common way of the protein import regulation (Nardozzi et al., 2010). The activity of NLSs can be regulated either by the phosphorylation of distant residues in the region flanking the NLSs (Hübner et al., 1997; Rihs et al., 1991) or by phosphorylation of the residues directly adjacent or within NLSs (Harreman et al., 2004; Jeong et al., 2015). This can either decrease or increase the affinity of the cargo protein for its import receptor. Subsequent downregulation or upregulation of the cargo nuclear import can change the distribution of the cargo protein between the cytoplasm and the nucleus (Harreman et al., 2004; Kitamura et al., 2006).

S1678 was an ideal candidate for a residue that can regulate the 53BP1 NLS activity when phosphorylated. It lies within 53BP1 NLS and overlaps with the CDK consensus phosphorylation site [pS/pT]PX[K/R]. Therefore, the 53BP1 import could be regulated by phosphorylation at S1678 during the cell cycle progression. However, this site also overlaps with consensus phosphorylation sites of other protein kinases (Xue et al., 2005) and could be phosphorylated in response to different stimuli than the cell cycle progression. Moreover, there are numerous records in the PhosphoSitePlus database, in which this residue was assigned to be phosphorylated by mass spectrometry analyses (Hornbeck et al., 2015).

S1678 phosphorylation status in cells was monitored using phospho-MAPK/CDK substrates antibody, which recognised PXpSP or pSPXR/K sites. In the context of full-length 53BP1, it was noticed that the phosphorylation of these sites is up-regulated in mitosis, but S1678 was not the dominantly recognised site. When the phosphorylation status of EGFP-NLS was tested, no specific signal was obtained (not shown). Certain substrates require for their efficient recognition and phosphorylation by cyclin-CDK complexes not only phosphorylation consensus motif but also cyclin docking motif (Schulman et al., 1998). EGFP-NLS did not interact with cyclin A or B, whereas EGFP-53BP1-wt did (not

shown). Therefore, the reason why EGFP-NLS was not phosphorylated could be its short length, which could cause its insufficient recognition by cyclin-CDK complexes in cells. Taken together, phospho-MAPK/CDK substrates antibody turned up to be unsuitable for detection of S1678 phosphorylation status in my experiments. Because of this, I was not able to determine whether phosphorylation status of S1678 changes during the cell cycle progression or under which conditions S1678 is phosphorylated. This would require raising the specific antibody against the peptide derived from 53BP1 containing the phosphorylated S1678.

The ability of 53BP1 to be imported to the nucleus was assessed during different cell cycle stages. Import of 53BP1 to the nucleus depends on importin ß and NUP153 and the interactions between 53BP1 and importin ß (regardless of the presence of NUP153) and between 53BP1 and NUP153 were previously established (Moudry et al., 2012). Differences in these interactions should reflect changes in 53BP1 import. Therefore, the co-IP experiments were employed. The attempts to use endogenous 53BP1 failed and so the interactions were finally assessed in cells transiently overexpressing EGFP-53BP1-wt. No difference in interactions between EGFP-53BP1-wt and importin ß was observed during the cell cycle progression. EGFP-53BP1-wt and NUP153 also interacted to the same extent in cells synchronized at G1/S boundary or in the S and G2 phases. In mitosis, NUP153 monoclonal antibody failed to recognise its epitope. This may be caused by NUP153 hyperphosphorylation in mitosis (Favreau et al., 1996) leading to masking the relevant epitope. In my experimental setting, 53BP1 seemed to be imported to the nucleus continuously during the cell cycle. However, this does not rule out the possibility that 53BP1 import is accelerated or inhibited in response to some specific stimuli or that its import is regulated in different cell lines.

The effect of S1678 phosphorylation on ability of 53BP1 to interact with importin ß was evaluated using 53BP1 mutants that mimic the phosphorylation or cannot be phosphorylated at this site. The substitution of S1678 to alanine residue weakened the interaction between 53BP1 and importin ß. When S1678 was substituted with negatively charged aspartate residue, the interaction was not detectable in asynchronous cells. This clearly demonstrates that the interaction between 53BP1 and importin ß is sensitive to amino acids changes at this position. Consistently, the crystallographic studies of classical bipartite NLSs bound to importin α suggest that the C-terminal portion of the linker region plays important role in binding to Importin α (Fontes et al., 2003a). Moreover, this also implies that the phosphorylation of S1678 could inhibit the interaction between 53BP1 and importin α/ß and inhibit its nuclear import.

It was demonstrated that the NLS affinity for its import receptor correlates with the steady-state accumulation of the cargo in the nucleus (Hodel et al., 2006). Consistently, a twofold increase in the number of cells with 53BP1 nucleocytoplasmic distribution was observed when the localization of EGFP-53BP1-S1678A was assessed compared to EGFP-53BP1-wt and even threefold increase in the

case of EGFP-53BP1-S1678D. The changes in localization were more apparent 24 h after transfection than 48 h. Therefore, they seem to be caused rather by reduced nuclear import efficiency than enhanced export of these 53BP1 mutants. Taken together, S1678 phosphorylation itself is not expected to completely block 53BP1 nuclear import. Instead of that, it would rather influence its efficiency or collaborate with other posttranslational modification(s) in regulation of 53BP1 import.

Interestingly, EGFP-53BP1-S1678D localized to the nucleus, albeit no detectable interaction with importin ß. To deal with this inconsistency, the effect of serine to alanine and serine to aspartate substitutions on the activity of 53BP1 NLS was tested. Both the EGFP-NLS-S1678A and the EGFP-NLS-S1678D localized to the nucleus. Importantly, EGFP-NLS-S1678D did interact with importin ß, but had the weakest interaction among all EGFP-NLS mutants. As expression of EGFP-NLS-S1678D was much more higher compared to EGFP-53BP1-S1678D, it is possible that the interaction between EGFP-53BP1-S1678D and importin ß was not detectable owing to reaching the lower detection limit of the method. As 53BP1 nuclear import clearly required the classical bipartite NLS and importin ß, it seems to be unlikely that EGFP-53BP1-S1678D is imported to the nucleus by some alternative nuclear import pathway.

S1678 was shown to be the major cyclin B-CDK1 complex phosphorylation site within the C-terminal part of 53BP1 (residues 1483-1972) *in vitro* (Benada et al., 2015). Furthermore, phosphorylations of S1673 and S1678 (both lies in the linker region of 53BP1 NLS) were detected to be upregulated in mitotic cells in quantitative mass spectrometry analysis of mitotic phosphorylations (Dephoure et al., 2008). These evidences suggested that S1678 could be phosphorylated in the M phase. Although the EGFP-53BP1-S1678D mutant (which mimics the phosphorylation) exhibited only weak interaction with importin ß in the M phase, strong interaction between EGFP-53BP1-wt and importin ß was detected even in the M phase. To further address this discrepancy, the dephosphorylation of mitotic lysate, which was expected to increase the 53BP1-importin ß interaction, was done. However, this assay did not yield conclusive results and needs to be further optimized in future experiments.

Phosphate moiety can be a direct binding determinant for import receptor as was demonstrated for EBNA-1 NLS (Kitamura et al., 2006). In this case, phosphorylation of S385 within EBNA-1 NLS increased binding affinity for importin α and thus up-regulated the cargo nuclear import, whereas serine to aspartate substitution decreased the binding affinity for importin α (Kitamura et al., 2006). In my experiments, the phosphorylation of S1678 seemed not to increase the ability of EGFP-53BP1-wt to bind importin ß in the M phase, as dephosphorylation of EGFP-53BP1-wt did not cause a decrease in the interaction. However, the efficiency of dephosphorylation of S1678 residue could not be determined and thus this possibility could not be definitely ruled out.

The discrepancy between EGFP-53BP1-S1678D and EGFP-53BP1-wt behaviour in the M phase can be explained in several ways: (1) the majority of S1678 could not have been phosphorylated in my

experiments (e.g. due to overexpression), (2) inhibitory effect of S1678 phosphorylation could have been compensated by the presence of additional posttranslational modifications in the M phase (e.g. phosphorylation of S1673), or (3) S1678 phosphorylation could not have influenced the binding to importin ß, while substitution to aspartate could.

## 6.3. Recruitment of EGFP-53BP1-S1678 mutants to DNA damage sites

In the M phase, 53BP1 recruitment to DNA damage sites is inhibited (Giunta et al., 2010). Mitotic kinases CDK1 and Plk1 phosphorylate its UDR motif at T1609 and S1618, respectively. These phosphorylations abolish the binding of 53BP1 to ubiquitinated histones and, therefore, inhibit its recruitment to DNA damage sites (Benada et al., 2015; Lee et al., 2014; Orthwein et al., 2014). 53BP1 mutants that mimic the phosphorylated residues or which cannot be phosphorylated at these residues were studied during interphase to assess the effect of the mitotic phosphorylation on 53BP1 recruitment to DNA damage sites (Benada et al., 2015; Lee et al., 2014; Orthwein et al., 2014). The mitotic phosphorylation of S1678 was recently also implicated in the inhibition of 53BP1 recruitment to DNA damage sites (Benada et al., 2015).

In my experiments, the live cell imaging showed that EGFP-53BP1-S1678A and EGFP-53BP1-S1678D did not have impaired recruitment to laser microirradiation-induced DNA damage sites within the first 5 minutes. Additionally, DNA damage foci quantification indicated that 53BP1-S1678A and 53BP1-S1678D localization to DNA damage foci was not impaired 3 hours after γ-irradiation. Taken together, the phosphorylation of S1678 seems not to have an inhibitory effect on 53BP1 recruitment to DNA damage sites.

## 6.4. Potential regulation of 53BP1 NLS by acetylation

Protein acetylation on lysine residues is involved in numerous cellular processes including the regulation of protein transport (Yang, 2004). In my experiments, detection of EGFP-NLS acetylation by the acetylated lysine antibody suggested that the 53BP1 NLS could be acetylated. Within the 1658-RASMGVLSGKRKLITSEEERSPAKRGRKSA-1687 sequence, only K1667 is reported in PhosphoSitePlus database to be acetylated (Hornbeck et al., 2015). The confirmation of K1667 acetylation would require the preparation of EGFP-NLS-K1667R mutant. EGFP-NLS-K1667R is expected to be able to bind importin α/ß heterodimer and to localize to the nucleus, while it should not be recognised by the acetylated lysine antibody.

Acetylation of lysine residue that is important for NLS activity was previously shown to disrupt the interaction of acetylated adenovirus-transforming protein E1A with importin α and inhibit its nuclear import. The non-acetylated E1A protein was found in the nuclear extract, whereas acetylated

E1A in the cytoplasm (Madison et al., 2002). As the residue K1667 of 53BP1 is at the P1' position of the classical bipartite NLS, which must be occupied by lysine or arginine residues, the acetylation of K1667 should disrupt the binding to importin α/ß heterodimer and also prevent 53BP1 nuclear import. There are several approaches how to test these predictions. The nuclear, cytoplasmic or nucleocytoplasmic localization of acetylated EGFP-NLS can be revealed by subcellular fractionalisation. EGFP-NLS-K1667Q and EGFP-53BP1-K1667Q mutants, which mimic the acetylated lysine, can further address the role of K1667 acetylation in the regulation of 53BP1 nuclear import.

Acetylation of lysine residues within NLS was also shown to be important for accumulation of certain proteins in the nucleus (Blanco-García et al., 2009; Soutoglou et al., 2000; Spilianakis et al., 2000). This can be achieved, for example, by inhibition of protein export caused by acetylation-induced change in protein conformation (Soutoglou et al., 2000). It is possible that the acetylation of K1667 occurs in the nucleus and it is important for 53BP1 nuclear retention. If 53BP1 is no shuttling between the nucleus and the cytoplasm, the 53BP1 NLS does not need to remain active after 53BP1 enters the nucleus. The acetylation within NLS can then have distinct roles independent from nuclear transport. Therefore, further exploration of the K1667 acetylation would bring new insight into not only the mechanism of 53BP1 nuclear transport. Moreover, this again emphasizes the importance of addressing the question whether there is or not 53BP1 shuttling between the cytoplasm and the nucleus.

# 7. Conclusion

53BP1 nuclear transport has been insufficiently explored so far. To gain more insight into the mechanisms of 53BP1 nuclear import, I used several approaches to identify 53BP1 NLS and to examine potential ways of its regulation.

First, I demonstrated that:

- 1667-**KRK**-1669 and 1681-**KRGRK**-1685 linear motifs of 53BP1 are both necessary for its interaction with importin ß and its nuclear import;
- 1658-RASMGVLSG**KRK**LITSEEERSPA**KRGRK**SA-1687 sequence derived from 53BP1 is sufficient for interaction with importin ß and targeting GFP to the nucleus.

Taken together, these evidences support the conclusion that 53BP1 has a NLS, which corresponds to $KRX_{10-12}K(KR)X(K/R)$ consensus sequence of the classical bipartite NLS recognised by importin α. Consequently, I implicate importin α in 53BP1 nuclear import.

Second, I demonstrated that:

- 53BP1 seems to be imported to the nucleus continuously during the cell cycle progression;
- mimicking a phosphorylation at S1678 (within the identified NLS) decreases binding affinity of 53BP1 NLS to importin ß and results in a mild defect in 53BP1 nuclear import;
- 53BP1 NLS might be regulated by acetylation.

These results indicate that 53BP1 enters the nucleus at constant rate during the cell cycle. Although the phosphorylation of S1678 itself cannot inhibit 53BP1 nuclear import, it can decrease 53BP1 import efficiency. I suggest a role for acetylation in regulation of 53BP1 nuclear import. Finally, I disproved previous speculation that phosphorylation of S1678 contributes to inhibition of 53BP1 recruitment to DNA damage sites.

In the summary, identification of 53BP1 NLS brought new information about 53BP1 import pathway. Attributes of classical bipartite NLS are well described. Therefore, the potential effects of 53BP1 posttranslational modifications or cancer mutations on its nuclear import and localization can now be easily estimated. In the future, it would be exciting to test the involvement of importin α in 53BP1 import, the potential regulation of 53BP1 NLS by acetylation and to explore whether 53BP1 shuttles between the nucleus and the cytoplasm.

# 8. References


**Acs, K., Luijsterburg, M.S., Ackermann, L., Salomons, F.A., Hoppe, T., Dantuma, N.P., 2011.** The AAA-ATPase VCP/p97 promotes 53BP1 recruitment by removing L3MBTL1 from DNA double-strand breaks. Nat. Struct. Mol. Biol. 18, 1345–50.

**Anderson, L., Henderson, C., Adachi, Y., 2001.** Phosphorylation and rapid relocalization of 53BP1 to nuclear foci upon DNA damage. Mol. Cell. Biol. 21, 1719–29.

**Arellano, M., Moreno, S., 1997.** Regulation of CDK/cyclin complexes during the cell cycle. Int. J. Biochem. Cell Biol. 29, 559–73.

**Baldock, R.A., Day, M., Wilkinson, O.J., Cloney, R., Jeggo, P.A., Oliver, A.W., Watts, F.Z., Pearl, L.H., 2015.** ATM Localization and Heterochromatin Repair Depend on Direct Interaction of the 53BP1-BRCT2 Domain with γH2AX. Cell Rep. 13, 2081–9.

**Bartek, J., Lukas, J., 2003.** Chk1 and Chk2 kinases in checkpoint control and cancer. Cancer Cell 3, 421–9.

**Bastos, R., Lin, A., Enarson, M., Burke, B., 1996.** Targeting and function in mRNA export of nuclear pore complex protein Nup153. J. Cell Biol. 134, 1141–56.

**Bayliss, R., Littlewood, T., Stewart, M., 2000.** Structural basis for the interaction between FxFG nucleoporin repeats and importin-beta in nuclear trafficking. Cell 102, 99–108.

**Benada, J., Burdová, K., Lidak, T., von Morgen, P., Macurek, L., 2015.** Polo-like kinase 1 inhibits DNA damage response during mitosis. Cell Cycle 14, 219–31.

**Bennardo, N., Cheng, A., Huang, N., Stark, J.M., 2008.** Alternative-NHEJ is a mechanistically distinct pathway of mammalian chromosome break repair. PLoS Genet. 4, e1000110.

**Bischoff, F.R., Görlich, D., 1997.** RanBP1 is crucial for the release of RanGTP from importin beta-related nuclear transport factors. FEBS Lett. 419, 249–54.

**Bischoff, F.R., Ponstingl, H., 1991**. Catalysis of guanine nucleotide exchange on Ran by the mitotic regulator RCC1. Nature 354, 80–2.

**Blanco-García, N., Asensio-Juan, E., de la Cruz, X., Martínez-Balbás, M.A., 2009.** Autoacetylation regulates P/CAF nuclear localization. J. Biol. Chem. 284, 1343–52.

**Boersma, V., Moatti, N., Segura-Bayona, S., Peuscher, M.H., van der Torre, J., Wevers, B.A., Orthwein, A., Durocher, D., Jacobs, J.J.L., 2015.** MAD2L2 controls DNA repair at telomeres and DNA breaks by inhibiting 5' end resection. Nature 521, 537–40.

**Bothmer, A., Robbiani, D.F., Di Virgilio, M., Bunting, S.F., Klein, I.A., Feldhahn, N., Barlow, J., Chen, H.T., Bosque, D., Callen, E., Nussenzweig, A., Nussenzweig, M.C., 2011.** Regulation of DNA end joining, resection, and immunoglobulin class switch recombination by 53BP1. Mol. Cell 42, 319–29.

**Bothmer, A., Robbiani, D.F., Feldhahn, N., Gazumyan, A., Nussenzweig, A., Nussenzweig, M.C., 2010.** 53BP1 regulates DNA resection and the choice between classical and alternative end joining during class switch recombination. J. Exp. Med. 207, 855–65.

**Botuyan, M.V., Lee, J., Ward, I.M., Kim, J.E., Thompson, J.R., Chen, J., Mer, G., 2006.** Structural basis for the methylation state-specific recognition of histone H4-K20 by 53BP1 and Crb2 in DNA repair. Cell 127, 1361–73.

**Bouwman, P., Aly, A., Escandell, J.M., Pieterse, M., Bartkova, J., van der Gulden, H., Hiddingh, S., Thanasoula, M., Kulkarni, A., Yang, Q., Haffty, B.G., Tommiska, J., Blomqvist, C., Drapkin, R., Adams, D.J., Nevanlinna, H., Bartek, J., Tarsounas, M., Ganesan, S., Jonkers, J., 2010.** 53BP1 loss rescues

BRCA1 deficiency and is associated with triple-negative and BRCA-mutated breast cancers. Nat. Struct. Mol. Biol. 17, 688–95.

**Bryant, H.E., Schultz, N., Thomas, H.D., Parker, K.M., Flower, D., Lopez, E., Kyle, S., Meuth, M., Curtin, N.J., Helleday, T., 2005.** Specific killing of BRCA2-deficient tumours with inhibitors of poly(ADP-ribose) polymerase. Nature 434, 913–7.

**Bunting, S.F., Callén, E., Wong, N., Chen, H.T., Polato, F., Gunn, A., Bothmer, A., Feldhahn, N., Fernandez-Capetillo, O., Cao, L., Xu, X., Deng, C.X., Finkel, T., Nussenzweig, M., Stark, J.M., Nussenzweig, A., 2010.** 53BP1 inhibits homologous recombination in Brca1-deficient cells by blocking resection of DNA breaks. Cell 141, 243–54.

**Callen, E., Di Virgilio, M., Kruhlak, M.J., Nieto-Soler, M., Wong, N., Chen, H.T., Faryabi, R.B., Polato, F., Santos, M., Starnes, L.M., Wesemann, D.R., Lee, J.E., Tubbs, A., Sleckman, B.P., Daniel, J.A., Ge, K., Alt, F.W., Fernandez-Capetillo, O., Nussenzweig, M.C., Nussenzweig, A., 2013.** 53BP1 mediates productive and mutagenic DNA repair through distinct phosphoprotein interactions. Cell 153, 1266–80.

**Cao, L., Xu, X., Bunting, S.F., Liu, J., Wang, R.H., Cao, L.L., Wu, J.J., Peng, T.N., Chen, J., Nussenzweig, A., Deng, C.X., Finkel, T., 2009.** A selective requirement for 53BP1 in the biological response to genomic instability induced by Brca1 deficiency. Mol. Cell 35, 534–41.

**Cautain, B., Hill, R., de Pedro, N., Link, W., 2015.** Components and regulation of nuclear transport processes. FEBS J. 282, 445–62.

**Ceccaldi, R., Rondinelli, B., D'Andrea, A.D., 2016.** Repair Pathway Choices and Consequences at the Double-Strand Break. Trends Cell Biol. 26, 52–64.

**Chapman, J.R., Barral, P., Vannier, J.B., Borel, V., Steger, M., Tomas-Loba, A., Sartori, A.A., Adams, I.R., Batista, F.D., Boulton, S.J., 2013.** RIF1 is essential for 53BP1-dependent nonhomologous end joining and suppression of DNA double-strand break resection. Mol. Cell 49, 858–71.

**Chen, S., Parmigiani, G., 2007.** Meta-analysis of BRCA1 and BRCA2 penetrance. J. Clin. Oncol. 25, 1329–33.

**Choi, S., Yamashita, E., Yasuhara, N., Song, J., Son, S.Y., Won, Y.H., Hong, H.R., Shin, Y.S., Sekimoto, T., Park, I.Y., Yoneda, Y., Lee, S.J., 2014.** Structural basis for the selective nuclear import of the C2H2 zinc-finger protein Snail by importin β. Acta Crystallogr. D. Biol. Crystallogr. 70, 1050–60.

**Chook, Y.M., Süel, K.E., 2011.** Nuclear import by karyopherin-βs: recognition and inhibition. Biochim. Biophys. Acta 1813, 1593–606.

**Cingolani, G., Bednenko, J., Gillespie, M.T., Gerace, L., 2002.** Molecular basis for the recognition of a nonclassical nuclear localization signal by importin beta. Mol. Cell 10, 1345–53.

**Cingolani, G., Petosa, C., Weis, K., Müller, C.W., 1999.** Structure of importin-beta bound to the IBB domain of importin-alpha. Nature 399, 221–9.

**Conti, E., Kuriyan, J., 2000.** Crystallographic analysis of the specific yet versatile recognition of distinct nuclear localization signals by karyopherin alpha. Structure 8, 329–38.

**Conti, E., Uy, M., Leighton, L., Blobel, G., Kuriyan, J., 1998.** Crystallographic analysis of the recognition of a nuclear localization signal by the nuclear import factor karyopherin alpha. Cell 94, 193–204.

**Dai, C., Gu, W., 2010.** p53 post-translational modification: deregulated in tumorigenesis. Trends Mol. Med. 16, 528–36.

**Daigle, N., Beaudouin, J., Hartnell, L., Imreh, G., Hallberg, E., Lippincott-Schwartz, J., Ellenberg, J., 2001.** Nuclear pore complexes form immobile networks and have a very low turnover in live mammalian cells. J. Cell Biol. 154, 71–84.

**Davis, A.J., Chen, D.J., 2013.** DNA double strand break repair via non-homologous end-joining. Transl. Cancer Res. 2, 130–143.

**Densham, R.M., Garvin, A.J., Stone, H.R., Strachan, J., Baldock, R.A., Daza-Martin, M., Fletcher, A., Blair-Reid, S., Beesley, J., Johal, B., Pearl, L.H., Neely, R., Keep, N.H., Watts, F.Z., Morris, J.R., 2016.** Human BRCA1-BARD1 ubiquitin ligase activity counteracts chromatin barriers to DNA resection. Nat. Struct. Mol. Biol. 23, 647–55.

**Dephoure, N., Zhou, C., Villén, J., Beausoleil, S.A., Bakalarski, C.E., Elledge, S.J., Gygi, S.P., 2008.** A quantitative atlas of mitotic phosphorylation. Proc. Natl. Acad. Sci. U. S. A. 105, 10762–7.

**di Bari, M.G., Ciuffini, L., Mingardi, M., Testi, R., Soddu, S., Barilà, D., 2006.** c-Abl acetylation by histone acetyltransferases regulates its nuclear-cytoplasmic localization. EMBO Rep. 7, 727–33.

**Di Virgilio, M., Callen, E., Yamane, A., Zhang, W., Jankovic, M., Gitlin, A.D., Feldhahn, N., Resch, W., Oliveira, T.Y., Chait, B.T., Nussenzweig, A., Casellas, R., Robbiani, D.F., Nussenzweig, M.C., 2013.** Rif1 prevents resection of DNA breaks and promotes immunoglobulin class switching. Science 339, 711–5.

**Difilippantonio, S., Gapud, E., Wong, N., Huang, C.Y., Mahowald, G., Chen, H.T., Kruhlak, M.J., Callen, E., Livak, F., Nussenzweig, M.C., Sleckman, B.P., Nussenzweig, A., 2008.** 53BP1 facilitates long-range DNA end-joining during V(D)J recombination. Nature 456, 529–33.

**Dimitrova, N., Chen, Y.C.M., Spector, D.L., de Lange, T., 2008.** 53BP1 promotes non-homologous end joining of telomeres by increasing chromatin mobility. Nature 456, 524–8.

**Dinkel, H., Michael, S., Weatheritt, R.J., Davey, N.E., Van Roey, K., Altenberg, B., Toedt, G., Uyar, B., Seiler, M., Budd, A., Jödicke, L., Dammert, M.A., Schroeter, C., Hammer, M., Schmidt, T., Jehl, P., McGuigan, C., Dymecka, M., Chica, C., Luck, K., Via, A., Chatr-Aryamontri, A., Haslam, N., Grebnev, G., Edwards, R.J., Steinmetz, M.O., Meiselbach, H., Diella, F., Gibson, T.J., 2012.** ELM--the database of eukaryotic linear motifs. Nucleic Acids Res. 40, D242–51.

**Dinkel, H., Van Roey, K., Michael, S., Kumar, M., Uyar, B., Altenberg, B., Milchevskaya, V., Schneider, M., Kühn, H., Behrendt, A., Dahl, S.L., Damerell, V., Diebel, S., Kalman, S., Klein, S., Knudsen, A.C., Mäder, C., Merrill, S., Staudt, A., Thiel, V., Welti, L., Davey, N.E., Diella, F., Gibson, T.J., 2016.** ELM 2016--data update and new functionality of the eukaryotic linear motif resource. Nucleic Acids Res. 44, D294–300.

**Dudley, D.D., Chaudhuri, J., Bassing, C.H., Alt, F.W., 2005.** Mechanism and control of V(D)J recombination versus class switch recombination: similarities and differences. Adv. Immunol. 86, 43–112.

**Dulić, V., Kaufmann, W.K., Wilson, S.J., Tlsty, T.D., Lees, E., Harper, J.W., Elledge, S.J., Reed, S.I., 1994.** p53-dependent inhibition of cyclin-dependent kinase activities in human fibroblasts during radiation-induced G1 arrest. Cell 76, 1013–23.

**Enarson, P., Enarson, M., Bastos, R., Burke, B., 1998.** Amino-terminal sequences that direct nucleoporin nup153 to the inner surface of the nuclear envelope. Chromosoma 107, 228–36.

**Escribano-Díaz, C., Orthwein, A., Fradet-Turcotte, A., Xing, M., Young, J.T.F., Tkáč, J., Cook, M. A., Rosebrock, A.P., Munro, M., Canny, M.D., Xu, D., Durocher, D., 2013.** A cell cycle-dependent regulatory circuit composed of 53BP1-RIF1 and BRCA1-CtIP controls DNA repair pathway choice. Mol. Cell 49, 872–83.

**Fahrenkrog, B., Maco, B., Fager, A.M., Köser, J., Sauder, U., Ullman, K.S., Aebi, U., 2002.** Domain-specific antibodies reveal multiple-site topology of Nup153 within the nuclear pore complex. J. Struct. Biol. 140, 254–67.

**Falck, J., Coates, J., Jackson, S.P., 2005.** Conserved modes of recruitment of ATM, ATR and DNA-PKcs to sites of DNA damage. Nature 434, 605–11.

**Falck, J., Mailand, N., Syljuåsen, R.G., Bartek, J., Lukas, J., 2001.** The ATM-Chk2-Cdc25A checkpoint pathway guards against radioresistant DNA synthesis. Nature 410, 842–7.

**Farmer, H., McCabe, N., Lord, C.J., Tutt, A.N.J., Johnson, D. a, Richardson, T.B., Santarosa, M., Dillon, K.J., Hickson, I., Knights, C., Martin, N.M.B., Jackson, S.P., Smith, G.C.M., Ashworth, A., 2005.** Targeting the DNA repair defect in BRCA mutant cells as a therapeutic strategy. Nature 434, 917–21.

**Favreau, C., Worman, H.J., Wozniak, R.W., Frappier, T., Courvalin, J.C., 1996.** Cell cycle-dependent phosphorylation of nucleoporins and nuclear pore membrane protein Gp210. Biochemistry 35, 8035–44.

**Feng, L., Fong, K.W., Wang, J., Wang, W., Chen, J., 2013.** RIF1 counteracts BRCA1-mediated end resection during DNA repair. J. Biol. Chem. 288, 11135–43.

**Fontes, M.R., Teh, T., Kobe, B., 2000.** Structural basis of recognition of monopartite and bipartite nuclear localization sequences by mammalian importin-alpha. J. Mol. Biol. 297, 1183–94.

**Fontes, M.R.M., Teh, T., Jans, D., Brinkworth, R.I., Kobe, B., 2003a.** Structural basis for the specificity of bipartite nuclear localization sequence binding by importin-alpha. J. Biol. Chem. 278, 27981–7.

**Fontes, M.R.M., Teh, T., Toth, G., John, A., Pavo, I., Jans, D.A., Kobe, B., 2003b.** Role of flanking sequences and phosphorylation in the recognition of the simian-virus-40 large T-antigen nuclear localization sequences by importin-alpha. Biochem. J. 375, 339–49.

**Fradet-Turcotte, A., Canny, M.D., Escribano-Díaz, C., Orthwein, A., Leung, C.C.Y., Huang, H., Landry, M.C., Kitevski-LeBlanc, J., Noordermeer, S.M., Sicheri, F., Durocher, D., 2013.** 53BP1 is a reader of the DNA-damage-induced H2A Lys 15 ubiquitin mark. Nature 499, 50–4.

**Frit, P., Barboule, N., Yuan, Y., Gomez, D., Calsou, P., 2014.** Alternative end-joining pathway(s): bricolage at DNA breaks. DNA Repair (Amst). 17, 81–97.

**Giunta, S., Belotserkovskaya, R., Jackson, S.P., 2010.** DNA damage signaling in response to double-strand breaks during mitosis. J. Cell Biol. 190, 197–207.

**Goldfarb, D.S., Corbett, A.H., Mason, D.A., Harreman, M.T., Adam, S.A., 2004.** Importin alpha: a multipurpose nuclear-transport receptor. Trends Cell Biol. 14, 505–14.

**Goodarzi, A.A., Kurka, T., Jeggo, P.A., 2011.** KAP-1 phosphorylation regulates CHD3 nucleosome remodeling during the DNA double-strand break response. Nat. Struct. Mol. Biol. 18, 831–9.

**Goodarzi, A.A., Noon, A.T., Deckbar, D., Ziv, Y., Shiloh, Y., Löbrich, M., Jeggo, P. A., 2008.** ATM signaling facilitates repair of DNA double-strand breaks associated with heterochromatin. Mol. Cell 31, 167–77.

**Hari, F.J., Spycher, C., Jungmichel, S., Pavic, L., Stucki, M., 2010.** A divalent FHA/BRCT-binding mechanism couples the MRE11-RAD50-NBS1 complex to damaged chromatin. EMBO Rep. 11, 387–92.

**Harreman, M.T., Kline, T.M., Milford, H.G., Harben, M.B., Hodel, A.E., Corbett, A.H., 2004.** Regulation of nuclear import by phosphorylation adjacent to nuclear localization signals. J. Biol. Chem. 279, 20613–21.

**Harrigan, J.A., Belotserkovskaya, R., Coates, J., Dimitrova, D.S., Polo, S.E., Bradshaw, C.R., Fraser, P., Jackson, S.P., 2011.** Replication stress induces 53BP1-containing OPT domains in G1 cells. J. Cell Biol. 193, 97–108.

**Heyer, W.D., Ehmsen, K.T., Liu, J., 2010.** Regulation of homologous recombination in eukaryotes. Annu. Rev. Genet. 44, 113–39.

**Hodel, A.E., Harreman, M.T., Pulliam, K.F., Harben, M.E., Holmes, J.S., Hodel, M.R., Berland, K.M., Corbett, A.H., 2006.** Nuclear localization signal receptor affinity correlates with in vivo localization in Saccharomyces cerevisiae. J. Biol. Chem. 281, 23545–56.

**Hornbeck, P. V., Zhang, B., Murray, B., Kornhauser, J.M., Latham, V., Skrzypek, E., 2015.** PhosphoSitePlus, 2014: mutations, PTMs and recalibrations. Nucleic Acids Res. 43, D512–20.

**Huber, J., Cronshagen, U., Kadokura, M., Marshallsay, C., Wada, T., Sekine, M., Lührmann, R., 1998.** Snurportin1, an m3G-cap-specific nuclear import receptor with a novel domain structure. EMBO J. 17, 4114–26.

**Hübner, S., Xiao, C.Y., Jans, D.A., 1997.** The protein kinase CK2 site (Ser111/112) enhances recognition of the simian virus 40 large T-antigen nuclear localization sequence by importin. J. Biol. Chem. 272, 17191–5.

**Huen, M.S.Y., Huang, J., Leung, J.W.C., Sy, S.M.H., Leung, K.M., Ching, Y.P., Tsao, S.W., Chen, J., 2010a.** Regulation of chromatin architecture by the PWWP domain-containing DNA damage-responsive factor EXPAND1/MUM1. Mol. Cell 37, 854–64.

**Huen, M.S.Y., Sy, S.M.H., Chen, J., 2010b.** BRCA1 and its toolbox for the maintenance of genome integrity. Nat. Rev. Mol. Cell Biol. 11, 138–48.

**Jackson, S.P., Bartek, J., 2009.** The DNA-damage response in human biology and disease. Nature 461, 1071–8.

**Jankovic, M., Feldhahn, N., Oliveira, T.Y., Silva, I.T., Kieffer-Kwon, K.R., Yamane, A., Resch, W., Klein, I., Robbiani, D.F., Casellas, R., Nussenzweig, M.C., 2013.** 53BP1 alters the landscape of DNA rearrangements and suppresses AID-induced B cell lymphoma. Mol. Cell 49, 623–31.

**Jaspers, J.E., Kersbergen, A., Boon, U., Sol, W., van Deemter, L., Zander, S.A., Drost, R., Wientjens, E., Ji, J., Aly, A., Doroshow, J.H., Cranston, A., Martin, N.M.B., Lau, A., O'Connor, M.J., Ganesan, S., Borst, P., Jonkers, J., Rottenberg, S., 2013.** Loss of 53BP1 causes PARP inhibitor resistance in Brca1-mutated mouse mammary tumors. Cancer Discov. 3, 68–81.

**Jazayeri, A., Falck, J., Lukas, C., Bartek, J., Smith, G.C.M., Lukas, J., Jackson, S.P., 2006.** ATM- and cell cycle-dependent regulation of ATR in response to DNA double-strand breaks. Nat. Cell Biol. 8, 37–45.

**Jeong, S.A., Kim, K., Lee, J.H., Cha, J.S., Khadka, P., Cho, H.S., Chung, I.K., 2015.** Akt-mediated phosphorylation increases the binding affinity of hTERT for importin α to promote nuclear translocation. J. Cell Sci. 128, 2287–301.

**Jin, J., Shirogane, T., Xu, L., Nalepa, G., Qin, J., Elledge, S.J., Harper, J.W., 2003.** SCFbeta-TRCP links Chk1 signaling to degradation of the Cdc25A protein phosphatase. Genes Dev. 17, 3062–74.

**Jowsey, P., Morrice, N.A., Hastie, C.J., McLauchlan, H., Toth, R., Rouse, J., 2007.** Characterisation of the sites of DNA damage-induced 53BP1 phosphorylation catalysed by ATM and ATR. DNA Repair (Amst). 6, 1536–44.

**Jullien, D., Görlich, D., Laemmli, U.K., Adachi, Y., 1999.** Nuclear import of RPA in Xenopus egg extracts requires a novel protein XRIPalpha but not importin alpha. EMBO J. 18, 4348–58.

**Jullien, D., Vagnarelli, P., Earnshaw, W.C., Adachi, Y., 2002.** Kinetochore localisation of the DNA damage response component 53BP1 during mitosis. J. Cell Sci. 115, 71–9.

**Kakarougkas, A., Ismail, A., Klement, K., Goodarzi, A.A., Conrad, S., Freire, R., Shibata, A., Lobrich, M., Jeggo, P.A., 2013.** Opposing roles for 53BP1 during homologous recombination. Nucleic Acids Res. 41, 9719–31.

**Kann, M., Sodeik, B., Vlachou, A., Gerlich, W.H., Helenius, A., 1999.** Phosphorylation-dependent binding of hepatitis B virus core particles to the nuclear pore complex. J. Cell Biol. 145, 45–55.

**Kim, S.T., Lim, D.S., Canman, C.E., Kastan, M.B., 1999.** Substrate specificities and identification of putative substrates of ATM kinase family members. J. Biol. Chem. 274, 37538–43.

**Kitamura, R., Sekimoto, T., Ito, S., Harada, S., Yamagata, H., Masai, H., Yoneda, Y., Yanagi, K., 2006.** Nuclear import of Epstein-Barr virus nuclear antigen 1 mediated by NPI-1 (Importin alpha5) is up- and down-regulated by phosphorylation of the nuclear localization signal for which Lys379 and Arg380 are essential. J. Virol. 80, 1979–91.

**Kleiner, R.E., Verma, P., Molloy, K.R., Chait, B.T., Kapoor, T.M., 2015.** Chemical proteomics reveals a γH2AX-53BP1 interaction in the DNA damage response. Nat. Chem. Biol. 11, 807–14.

**Knobel, P.A., Belotserkovskaya, R., Galanty, Y., Schmidt, C.K., Jackson, S.P., Stracker, T.H., 2014.** USP28 is recruited to sites of DNA damage by the tandem BRCT domains of 53BP1 but plays a minor role in double-strand break metabolism. Mol. Cell. Biol. 34, 2062–74.

**Knockenhauer, K.E., Schwartz, T.U., 2016.** The Nuclear Pore Complex as a Flexible and Dynamic Gate. Cell 164, 1162–71.

**Kobe, B., 1999.** Autoinhibition by an internal nuclear localization signal revealed by the crystal structure of mammalian importin alpha. Nat. Struct. Biol. 6, 388–97.

**Kondoh, K., Terasawa, K., Morimoto, H., Nishida, E., 2006.** Regulation of nuclear translocation of extracellular signal-regulated kinase 5 by active nuclear import and export mechanisms. Mol. Cell. Biol. 26, 1679–90.

**Kortlever, R.M., Higgins, P.J., Bernards, R., 2006.** Plasminogen activator inhibitor-1 is a critical downstream target of p53 in the induction of replicative senescence. Nat. Cell Biol. 8, 877–84.

**Kosugi, S., Hasebe, M., Matsumura, N., Takashima, H., Miyamoto-Sato, E., Tomita, M., Yanagawa, H., 2009a.** Six classes of nuclear localization signals specific to different binding grooves of importin alpha. J. Biol. Chem. 284, 478–85.

**Kosugi, S., Hasebe, M., Tomita, M., Yanagawa, H., 2009b.** Systematic identification of cell cycle-dependent yeast nucleocytoplasmic shuttling proteins by prediction of composite motifs. Proc. Natl. Acad. Sci. U. S. A. 106, 10171–6.

**Kutay, U., Bischoff, F.R., Kostka, S., Kraft, R., Görlich, D., 1997.** Export of importin alpha from the nucleus is mediated by a specific nuclear transport factor. Cell 90, 1061–71.

**Lange, A., Mills, R.E., Lange, C.J., Stewart, M., Devine, S.E., Corbett, A.H., 2007.** Classical nuclear localization signals: definition, function, and interaction with importin alpha. J. Biol. Chem. 282, 5101–5.

**Lee, D.H., Acharya, S.S., Kwon, M., Drane, P., Guan, Y., Adelmant, G., Kalev, P., Shah, J., Pellman, D., Marto, J.A., Chowdhury, D., 2014.** Dephosphorylation enables the recruitment of 53BP1 to double-strand DNA breaks. Mol. Cell 54, 512–25.

**Lee, J.H., Goodarzi, A.A., Jeggo, P.A., Paull, T.T., 2010.** 53BP1 promotes ATM activity through direct interactions with the MRN complex. EMBO J. 29, 574–85.

**Lee, S.J., Matsuura, Y., Liu, S.M., Stewart, M., 2005.** Structural basis for nuclear import complex dissociation by RanGTP. Nature 435, 693–6.

**Lee, S.J., Sekimoto, T., Yamashita, E., Nagoshi, E., Nakagawa, A., Imamoto, N., Yoshimura, M., Sakai, H., Chong, K.T., Tsukihara, T., Yoneda, Y., 2003.** The structure of importin-beta bound to SREBP-2: nuclear import of a transcription factor. Science 302, 1571–5.

**Lemaître, C., Fischer, B., Kalousi, A., Hoffbeck, A.S., Guirouilh-Barbat, J., Shahar, O.D., Genet, D., Goldberg, M., Betrand, P., Lopez, B., Brino, L., Soutoglou, E., 2012.** The nucleoporin 153, a novel factor in double-strand break repair and DNA damage response. Oncogene 31, 4803–9.

**Leung, C.C.Y., Glover, J.N.M., 2011.** BRCT domains: easy as one, two, three. Cell Cycle 10, 2461–70.

**Li, T., Diner, B.A., Chen, J., Cristea, I.M., 2012.** Acetylation modulates cellular distribution and DNA sensing ability of interferon-inducible protein IFI16. Proc. Natl. Acad. Sci. U. S. A. 109, 10558–63.

**Liu, X., Jiang, W., Dubois, R.L., Yamamoto, K., Wolner, Z., Zha, S., 2012.** Overlapping functions between XLF repair protein and 53BP1 DNA damage response factor in end joining and lymphocyte development. Proc. Natl. Acad. Sci. U. S. A. 109, 3903–8.

**Lott, K., Cingolani, G., 2011.** The importin β binding domain as a master regulator of nucleocytoplasmic transport. Biochim. Biophys. Acta 1813, 1578–92.

**Lottersberger, F., Bothmer, A., Robbiani, D.F., Nussenzweig, M.C., de Lange, T., 2013.** Role of 53BP1 oligomerization in regulating double-strand break repair. Proc. Natl. Acad. Sci. U. S. A. 110, 2146–51.

**Lottersberger, F., Karssemeijer, R.A., Dimitrova, N., de Lange, T., 2015.** 53BP1 and the LINC Complex Promote Microtubule-Dependent DSB Mobility and DNA Repair. Cell 163, 880–93.

**Lukas, C., Falck, J., Bartkova, J., Bartek, J., Lukas, J., 2003.** Distinct spatiotemporal dynamics of mammalian checkpoint regulators induced by DNA damage. Nat. Cell Biol. 5, 255–60.

**Lukas, C., Savic, V., Bekker-Jensen, S., Doil, C., Neumann, B., Pedersen, R.S., Grøfte, M., Chan, K.L., Hickson, I.D., Bartek, J., Lukas, J., 2011.** 53BP1 nuclear bodies form around DNA lesions generated by mitotic transmission of chromosomes under replication stress. Nat. Cell Biol. 13, 243–53.

**Mackay, D.R., Elgort, S.W., Ullman, K.S., 2009.** The nucleoporin Nup153 has separable roles in both early mitotic progression and the resolution of mitosis. Mol. Biol. Cell 20, 1652–60.

**Macůrek, L., Lindqvist, A., Lim, D., Lampson, M.A., Klompmaker, R., Freire, R., Clouin, C., Taylor, S.S., Yaffe, M.B., Medema, R.H., 2008.** Polo-like kinase-1 is activated by aurora A to promote checkpoint recovery. Nature 455, 119–23.

**Madison, D.L., Yaciuk, P., Kwok, R.P.S., Lundblad, J.R., 2002.** Acetylation of the adenovirus-transforming protein E1A determines nuclear localization by disrupting association with importin-alpha. J. Biol. Chem. 277, 38755–63.

**Mailand, N., Bekker-Jensen, S., Faustrup, H., Melander, F., Bartek, J., Lukas, C., Lukas, J., 2007.** RNF8 ubiquitylates histones at DNA double-strand breaks and promotes assembly of repair proteins. Cell 131, 887–900.

**Mallette, F.A., Mattiroli, F., Cui, G., Young, L.C., Hendzel, M.J., Mer, G., Sixma, T.K., Richard, S., 2012.** RNF8- and RNF168-dependent degradation of KDM4A/JMJD2A triggers 53BP1 recruitment to DNA damage sites. EMBO J. 31, 1865–78.

**Manis, J.P., Morales, J.C., Xia, Z., Kutok, J.L., Alt, F.W., Carpenter, P.B., 2004.** 53BP1 links DNA damage-response pathways to immunoglobulin heavy chain class-switch recombination. Nat. Immunol. 5, 481–7.

**Matsuoka, S., Ballif, B.A., Smogorzewska, A., McDonald, E.R., Hurov, K.E., Luo, J., Bakalarski, C.E., Zhao, Z., Solimini, N., Lerenthal, Y., Shiloh, Y., Gygi, S.P., Elledge, S.J., 2007.** ATM and ATR substrate analysis reveals extensive protein networks responsive to DNA damage. Science 316, 1160–6.

**Matsuura, Y., Stewart, M., 2005.** Nup50/Npap60 function in nuclear protein import complex disassembly and importin recycling. EMBO J. 24, 3681–9.

**Mattiroli, F., Vissers, J.H.A., van Dijk, W.J., Ikpa, P., Citterio, E., Vermeulen, W., Marteijn, J.A., Sixma, T.K., 2012.** RNF168 ubiquitinates K13-15 on H2A/H2AX to drive DNA damage signaling. Cell 150, 1182–95.

**McBride, K.M., Banninger, G., McDonald, C., Reich, N.C., 2002.** Regulated nuclear import of the STAT1 transcription factor by direct binding of importin-alpha. EMBO J. 21, 1754–63.

**Meerang, M., Ritz, D., Paliwal, S., Garajova, Z., Bosshard, M., Mailand, N., Janscak, P., Hübscher, U., Meyer, H., Ramadan, K., 2011.** The ubiquitin-selective segregase VCP/p97 orchestrates the response to DNA double-strand breaks. Nat. Cell Biol. 13, 1376–1382.

**Miki, Y., Swensen, J., Shattuck-Eidens, D., Futreal, P.A., Harshman, K., Tavtigian, S., Liu, Q., Cochran, C., Bennett, L.M., Ding, W., 1994.** A strong candidate for the breast and ovarian cancer susceptibility gene BRCA1. Science 266, 66–71.

**Miyashita, T., Krajewski, S., Krajewska, M., Wang, H.G., Lin, H.K., Liebermann, D.A., Hoffman, B., Reed, J.C., 1994.** Tumor suppressor p53 is a regulator of bcl-2 and bax gene expression in vitro and in vivo. Oncogene 9, 1799–805.

**Mohapatra, S., Yannone, S.M., Lee, S.H., Hromas, R.A., Akopiants, K., Menon, V., Ramsden, D.A., Povirk, L.F., 2013.** Trimming of damaged 3' overhangs of DNA double-strand breaks by the Metnase and Artemis endonucleases. DNA Repair (Amst). 12, 422–32.

**Morales, J.C., Franco, S., Murphy, M.M., Bassing, C.H., Mills, K.D., Adams, M.M., Walsh, N.C., Manis, J.P., Rassidakis, G.Z., Alt, F.W., Carpenter, P.B., 2006.** 53BP1 and p53 synergize to suppress genomic instability and lymphomagenesis. Proc. Natl. Acad. Sci. U. S. A. 103, 3310–5.

**Morales, J.C., Xia, Z., Lu, T., Aldrich, M.B., Wang, B., Rosales, C., Kellems, R.E., Hittelman, W.N., Elledge, S.J., Carpenter, P.B., 2003.** Role for the BRCA1 C-terminal repeats (BRCT) protein 53BP1 in maintaining genomic stability. J. Biol. Chem. 278, 14971–7.

**Moudry, P., Lukas, C., Macurek, L., Neumann, B., Heriche, J.K., Pepperkok, R., Ellenberg, J., Hodny, Z., Lukas, J., Bartek, J., 2012.** Nucleoporin NUP153 guards genome integrity by promoting nuclear import of 53BP1. Cell Death Differ. 19, 798–807.

**Munoz, I.M., Jowsey, P. a, Toth, R., Rouse, J., 2007.** Phospho-epitope binding by the BRCT domains of hPTIP controls multiple aspects of the cellular response to DNA damage. Nucleic Acids Res. 35, 5312–22.

**Nakano, K., Vousden, K.H., 2001.** PUMA, a novel proapoptotic gene, is induced by p53. Mol. Cell 7, 683–94.

**Nardozzi, J.D., Lott, K., Cingolani, G., 2010.** Phosphorylation meets nuclear import: a review. Cell Commun. Signal. 8, 32.

**Nguyen Ba, A.N., Pogoutse, A., Provart, N., Moses, A.M., 2009.** NLStradamus: a simple Hidden Markov Model for nuclear localization signal prediction. BMC Bioinformatics 10, 202.

**Noon, A.T., Shibata, A., Rief, N., Löbrich, M., Stewart, G.S., Jeggo, P. a, Goodarzi, A. a, 2010.** 53BP1-dependent robust localized KAP-1 phosphorylation is essential for heterochromatic DNA double-strand break repair. Nat. Cell Biol. 12, 177–84.

**Ogawa, Y., Miyamoto, Y., Oka, M., Yoneda, Y., 2012.** The interaction between importin-α and Nup153 promotes importin-α/β-mediated nuclear import. Traffic 13, 934–46.

**Ochs, F., Somyajit, K., Altmeyer, M., Rask, M.-B., Lukas, J., Lukas, C., 2016.** 53BP1 fosters fidelity of homology-directed DNA repair. Nat. Struct. Mol. Biol. 23, 714–21.

**Oksenych, V., Alt, F.W., Kumar, V., Schwer, B., Wesemann, D.R., Hansen, E., Patel, H., Su, A., Guo, C., 2012.** Functional redundancy between repair factor XLF and damage response mediator 53BP1 in V(D)J recombination and DNA repair. Proc. Natl. Acad. Sci. U. S. A. 109, 2455–60.

**Orthwein, A., Fradet-Turcotte, A., Noordermeer, S.M., Canny, M.D., Brun, C.M., Strecker, J., Escribano-Diaz, C., Durocher, D., 2014.** Mitosis inhibits DNA double-strand break repair to guard against telomere fusions. Science 344, 189–93.

**Paraskeva, E., Izaurralde, E., Bischoff, F.R., Huber, J., Kutay, U., Hartmann, E., Lührmann, R., Görlich, D., 1999.** CRM1-mediated recycling of snurportin 1 to the cytoplasm. J. Cell Biol. 145, 255–64.

**Peng, C.Y., Graves, P.R., Thoma, R.S., Wu, Z., Shaw, A.S., Piwnica-Worms, H., 1997.** Mitotic and G2 checkpoint control: regulation of 14-3-3 protein binding by phosphorylation of Cdc25C on serine-216. Science 277, 1501–5.

**Pfeiffer, P., Goedecke, W., Obe, G., 2000.** Mechanisms of DNA double-strand break repair and their potential to induce chromosomal aberrations. Mutagenesis 15, 289–302.

**Prunuske, A.J., Liu, J., Elgort, S., Joseph, J., Dasso, M., Ullman, K.S., 2006.** Nuclear envelope breakdown is coordinated by both Nup358/RanBP2 and Nup153, two nucleoporins with zinc finger modules. Mol. Biol. Cell 17, 760–9.

**Rappold, I., Iwabuchi, K., Date, T., Chen, J., 2001.** Tumor suppressor p53 binding protein 1 (53BP1) is involved in DNA damage-signaling pathways. J. Cell Biol. 153, 613–20.

**Reina-San-Martin, B., Chen, J., Nussenzweig, A., Nussenzweig, M.C., 2007.** Enhanced intra-switch region recombination during immunoglobulin class switch recombination in 53BP1-/- B cells. Eur. J. Immunol. 37, 235–9.

**Ribbeck, K., Lipowsky, G., Kent, H.M., Stewart, M., Görlich, D., 1998.** NTF2 mediates nuclear import of Ran. EMBO J. 17, 6587–98.

**Rihs, H.P., Jans, D. a, Fan, H., Peters, R., 1991.** The rate of nuclear cytoplasmic protein transport is determined by the casein kinase II site flanking the nuclear localization sequence of the SV40 T-antigen. EMBO J. 10, 633–9.

**Robbins, J., Dilworth, S.M., Laskey, R.A., Dingwall, C., 1991.** Two interdependent basic domains in nucleoplasmin nuclear targeting sequence: identification of a class of bipartite nuclear targeting sequence. Cell 64, 615–23.

**Rogakou, E.P., Boon, C., Redon, C., Bonner, W.M., 1999.** Megabase chromatin domains involved in DNA double-strand breaks in vivo. J. Cell Biol. 146, 905–16.

**Rogakou, E.P., Pilch, D.R., Orr, A.H., Ivanova, V.S., Bonner, W.M., 1998.** DNA double-stranded breaks induce histone H2AX phosphorylation on serine 139. J. Biol. Chem. 273, 5858–68.

**Rost, B., Yachdav, G., Liu, J., 2004.** The PredictProtein server. Nucleic Acids Res. 32, W321–6.

**Rottenberg, S., Jaspers, J.E., Kersbergen, A., van der Burg, E., Nygren, A.O.H., Zander, S.A.L., Derksen, P.W.B., de Bruin, M., Zevenhoven, J., Lau, A., Boulter, R., Cranston, A., O'Connor, M.J., Martin, N.M.B., Borst, P., Jonkers, J., 2008.** High sensitivity of BRCA1-deficient mammary tumors to the PARP inhibitor AZD2281 alone and in combination with platinum drugs. Proc. Natl. Acad. Sci. 105, 17079–17084.

**Sanchez, Y., Wong, C., Thoma, R.S., Richman, R., Wu, Z., Piwnica-Worms, H., Elledge, S.J., 1997.** Conservation of the Chk1 checkpoint pathway in mammals: linkage of DNA damage to Cdk regulation through Cdc25. Science 277, 1497–501.

**Shah, S., Forbes, D.J., 1998.** Separate nuclear import pathways converge on the nucleoporin Nup153 and can be dissected with dominant-negative inhibitors. Curr. Biol. 8, 1376–86.

**Schulman, B.A., Lindstrom, D.L., Harlow, E., 1998**. Substrate recruitment to cyclin-dependent kinase 2 by a multipurpose docking site on cyclin A. Proc. Natl. Acad. Sci. U. S. A. 95, 10453–8.

**Schultz, L.B., Chehab, N.H., Malikzay, A., Halazonetis, T.D., 2000.** p53 binding protein 1 (53BP1) is an early participant in the cellular response to DNA double-strand breaks. J. Cell Biol. 151, 1381–90.

**Smits, V.A.J., Reaper, P.M., Jackson, S.P., 2006.** Rapid PIKK-dependent release of Chk1 from chromatin promotes the DNA-damage checkpoint response. Curr. Biol. 16, 150–9.

**Songyang, Z., Blechner, S., Hoagland, N., Hoekstra, M.F., Piwnica-Worms, H., Cantley, L.C., 1994.** Use of an oriented peptide library to determine the optimal substrates of protein kinases. Curr. Biol. 4, 973–82.

**Sonnenblick, A., de Azambuja, E., Azim, H.A., Piccart, M., 2015.** An update on PARP inhibitors--moving to the adjuvant setting. Nat. Rev. Clin. Oncol. 12, 27–41.

**Soutoglou, E., Katrakili, N., Talianidis, I., 2000.** Acetylation regulates transcription factor activity at multiple levels. Mol. Cell 5, 745–51.

**Spilianakis, C., Papamatheakis, J., Kretsovali, A., 2000.** Acetylation by PCAF enhances CIITA nuclear accumulation and transactivation of major histocompatibility complex class II genes. Mol. Cell. Biol. 20, 8489–98.

**Stavnezer, J., Guikema, J.E.J., Schrader, C.E., 2008.** Mechanism and regulation of class switch recombination. Annu. Rev. Immunol. 26, 261–92.

**Stewart, G.S., Panier, S., Townsend, K., Al-Hakim, A.K., Kolas, N.K., Miller, E.S., Nakada, S., Ylanko, J., Olivarius, S., Mendez, M., Oldreive, C., Wildenhain, J., Tagliaferro, A., Pelletier, L., Taubenheim, N., Durandy, A., Byrd, P.J., Stankovic, T., Taylor, a M.R., Durocher, D., 2009.** The RIDDLE syndrome protein mediates a ubiquitin-dependent signaling cascade at sites of DNA damage. Cell 136, 420–34.

**Stewart, G.S., Stankovic, T., Byrd, P.J., Wechsler, T., Miller, E.S., Huissoon, A., Drayson, M.T., West, S.C., Elledge, S.J., Taylor, a M.R., 2007.** RIDDLE immunodeficiency syndrome is linked to defects in 53BP1-mediated DNA damage signaling. Proc. Natl. Acad. Sci. U. S. A. 104, 16910–5.

**Stiff, T., O'Driscoll, M., Rief, N., Iwabuchi, K., Löbrich, M., Jeggo, P.A., 2004.** ATM and DNA-PK function redundantly to phosphorylate H2AX after exposure to ionizing radiation. Cancer Res. 64, 2390–6.

**Stucki, M., Clapperton, J.A., Mohammad, D., Yaffe, M.B., Smerdon, S.J., Jackson, S.P., 2005.** MDC1 directly binds phosphorylated histone H2AX to regulate cellular responses to DNA double-strand breaks. Cell 123, 1213–26.

**Sukegawa, J., Blobel, G., 1993.** A nuclear pore complex protein that contains zinc finger motifs, binds DNA, and faces the nucleoplasm. Cell 72, 29–38.

**Takeyama, K., Monti, S., Manis, J.P., Dal Cin, P., Getz, G., Beroukhim, R., Dutt, S., Aster, J.C., Alt, F.W., Golub, T.R., Shipp, M. a, 2008.** Integrative analysis reveals 53BP1 copy loss and decreased expression in a subset of human diffuse large B-cell lymphomas. Oncogene 27, 318–22.

**Thorslund, T., Ripplinger, A., Hoffmann, S., Wild, T., Uckelmann, M., Villumsen, B., Narita, T., Sixma, T.K., Choudhary, C., Bekker-Jensen, S., Mailand, N., 2015.** Histone H1 couples initiation and amplification of ubiquitin signalling after DNA damage. Nature 527, 389–93.

**Truong, L.N., Li, Y., Shi, L.Z., Hwang, P.Y.H., He, J., Wang, H., Razavian, N., Berns, M.W., Wu, X., 2013.** Microhomology-mediated End Joining and Homologous Recombination share the initial end resection step to repair DNA double-strand breaks in mammalian cells. Proc. Natl. Acad. Sci. U. S. A. 110, 7720–5.

**Ullman, K.S., Shah, S., Powers, M.A., Forbes, D.J., 1999.** The nucleoporin nup153 plays a critical role in multiple types of nuclear export. Mol. Biol. Cell 10, 649–64.

**Vetter, I.R., Arndt, A., Kutay, U., Görlich, D., Wittinghofer, A., 1999.** Structural view of the Ran-Importin beta interaction at 2.3 A resolution. Cell 97, 635–46.

**Vollmer, B., Lorenz, M., Moreno-Andrés, D., Bodenhöfer, M., De Magistris, P., Astrinidis, S.A., Schooley, A., Flötenmeyer, M., Leptihn, S., Antonin, W., 2015.** Nup153 Recruits the Nup107-160 Complex to the Inner Nuclear Membrane for Interphasic Nuclear Pore Complex Assembly. Dev. Cell 33, 717–28.

**Walther, T.C., Fornerod, M., Pickersgill, H., Goldberg, M., Allen, T.D., Mattaj, I.W., 2001.** The nucleoporin Nup153 is required for nuclear pore basket formation, nuclear pore complex anchoring and import of a subset of nuclear proteins. EMBO J. 20, 5703–14.

**Wang, J., Aroumougame, A., Lobrich, M., Li, Y., Chen, D., Chenj, J., Gong, Z., 2014.** PTIP associates with artemis to dictate DNA repair pathway choice. Genes Dev. 28, 2693–2698.

**Ward, I., Kim, J.E., Minn, K., Chini, C.C., Mer, G., Chen, J., 2006.** The tandem BRCT domain of 53BP1 is not required for its repair function. J. Biol. Chem. 281, 38472–7.

**Ward, I.M., Difilippantonio, S., Minn, K., Mueller, M.D., Molina, J.R., Yu, X., Frisk, C.S., Ried, T., Nussenzweig, A., Chen, J., 2005.** 53BP1 cooperates with p53 and functions as a haploinsufficient tumor suppressor in mice. Mol. Cell. Biol. 25, 10079–86.

**Ward, I.M., Minn, K., van Deursen, J., Chen, J., 2003.** p53 Binding protein 53BP1 is required for DNA damage responses and tumor suppression in mice. Mol. Cell. Biol. 23, 2556–63.

**Ward, I.M., Reina-San-Martin, B., Olaru, A., Minn, K., Tamada, K., Lau, J.S., Cascalho, M., Chen, L., Nussenzweig, A., Livak, F., Nussenzweig, M.C., Chen, J., 2004.** 53BP1 is required for class switch recombination. J. Cell Biol. 165, 459–64.

**Xia, Z., Morales, J.C., Dunphy, W.G., Carpenter, P.B., 2001.** Negative cell cycle regulation and DNA damage-inducible phosphorylation of the BRCT protein 53BP1. J. Biol. Chem. 276, 2708–18.

**Xu, G., Chapman, J.R., Brandsma, I., Yuan, J., Mistrik, M., Bouwman, P., Bartkova, J., Gogola, E., Warmerdam, D., Barazas, M., Jaspers, J.E., Watanabe, K., Pieterse, M., Kersbergen, A., Sol, W., Celie, P.H.N., Schouten, P.C., van den Broek, B., Salman, A., Nieuwland, M., de Rink, I., de Ronde, J., Jalink, K., Boulton, S.J., Chen, J., van Gent, D.C., Bartek, J., Jonkers, J., Borst, P., Rottenberg, S., 2015.** REV7 counteracts DNA double-strand break resection and affects PARP inhibition. Nature 521, 541–4.

**Xue, Y., Zhou, F., Zhu, M., Ahmed, K., Chen, G., Yao, X., 2005.** GPS: a comprehensive www server for phosphorylation sites prediction. Nucleic Acids Res. 33, W184–7.

**Yan, W., Shao, Z., Li, F., Niu, L., Shi, Y., Teng, M., Li, X., 2011.** Structural basis of γH2AX recognition by human PTIP BRCT5-BRCT6 domains in the DNA damage response pathway. FEBS Lett. 585, 3874–9.

**Yang, X.J., 2004.** Lysine acetylation and the bromodomain: a new partnership for signaling. Bioessays 26, 1076–87.

**Zgheib, O., Pataky, K., Brugger, J., Halazonetis, T.D., 2009**. An oligomerized 53BP1 tudor domain suffices for recognition of DNA double-strand breaks. Mol. Cell. Biol. 29, 1050–8.

**Zhang, H., Liu, H., Chen, Y., Yang, X., Wang, P., Liu, T., Deng, M., Qin, B., Correia, C., Lee, S., Kim, J., Sparks, M., Nair, A.A., Evans, D.L., Kalari, K.R., Zhang, P., Wang, L., You, Z., Kaufmann, S.H., Lou, Z., Pei, H., 2016.** A cell cycle-dependent BRCA1-UHRF1 cascade regulates DNA double-strand break repair pathway choice. Nat. Commun. 7, 10201.

**Zimmermann, M., Lottersberger, F., Buonomo, S.B., Sfeir, A., de Lange, T., 2013.** 53BP1 regulates DSB repair using Rif1 to control 5’ end resection. Science 339, 700–4.

# 9. Supplementary information

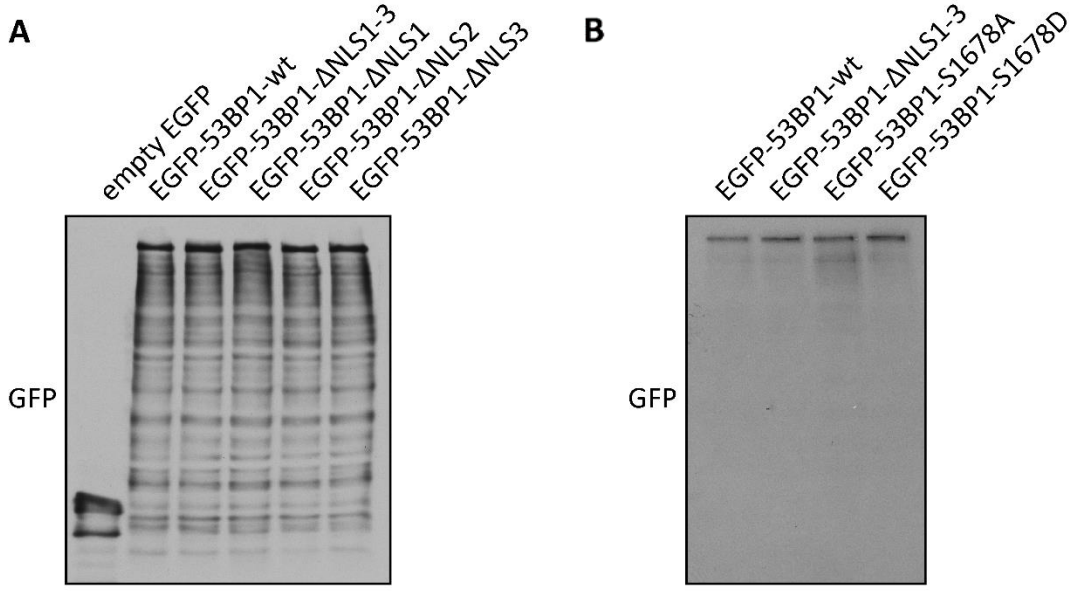


**Supplementary Figure 1. Representative whole cell lysates demonstrating the same expressing of empty EGFP and EGFP-53BP1 mutants in my experiments.** Protein samples were separated on gradient gel prepared by casting mixed 6%—15% separating gel solution.

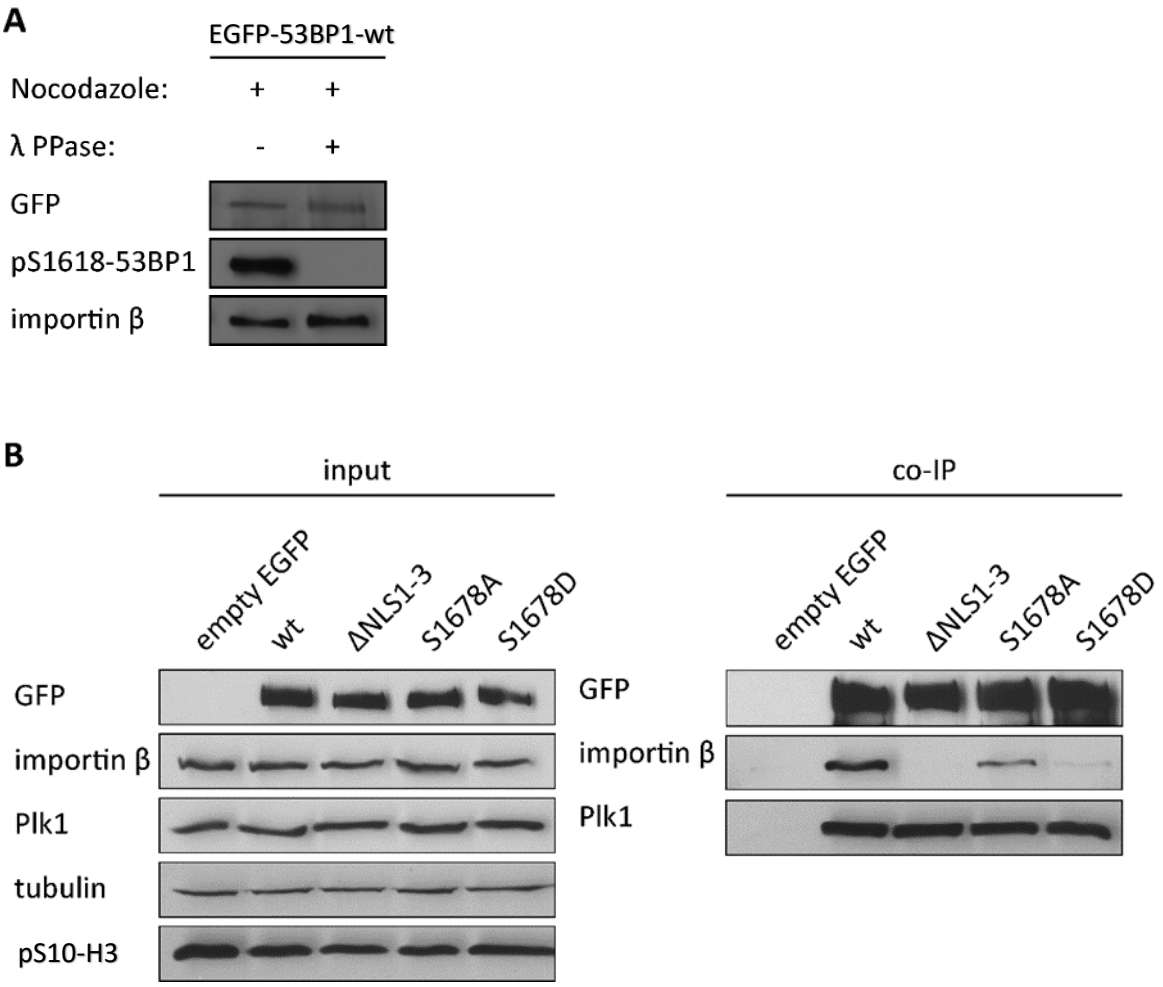


**Supplementary Figure 2. Interactions between EGFP-53BP1 mutants and importin ß in the M phase.** U2OS cells were transfected with DNA constructs encoding EGFP-53BP1-wt or indicated EGFP-53BP1 mutants, synchronised by thymidine-nocodazole block and harvested by mitotic shake-off prior to lysis. Lambda phosphatase assay was employed to test a phospho-dependent increase in interaction between EGFP-53BP-wt and importin ß (A). Interactions between indicated EGFP-53BP1 mutants and importin ß were evaluated by co-IP (B). The well-established interaction with Plk1 was used as a positive control. The results suggested that there is not phospho-dependent increase in interaction between EGFP-53BP1-wt and importin ß in the M phase. Furthermore, the results showed that EGFP-53BP1-S1678D interacts weakly with importin ß in the M phase, whereas strong interaction between EGFP-53BP1-wt and importin ß occurs even in the M phase.

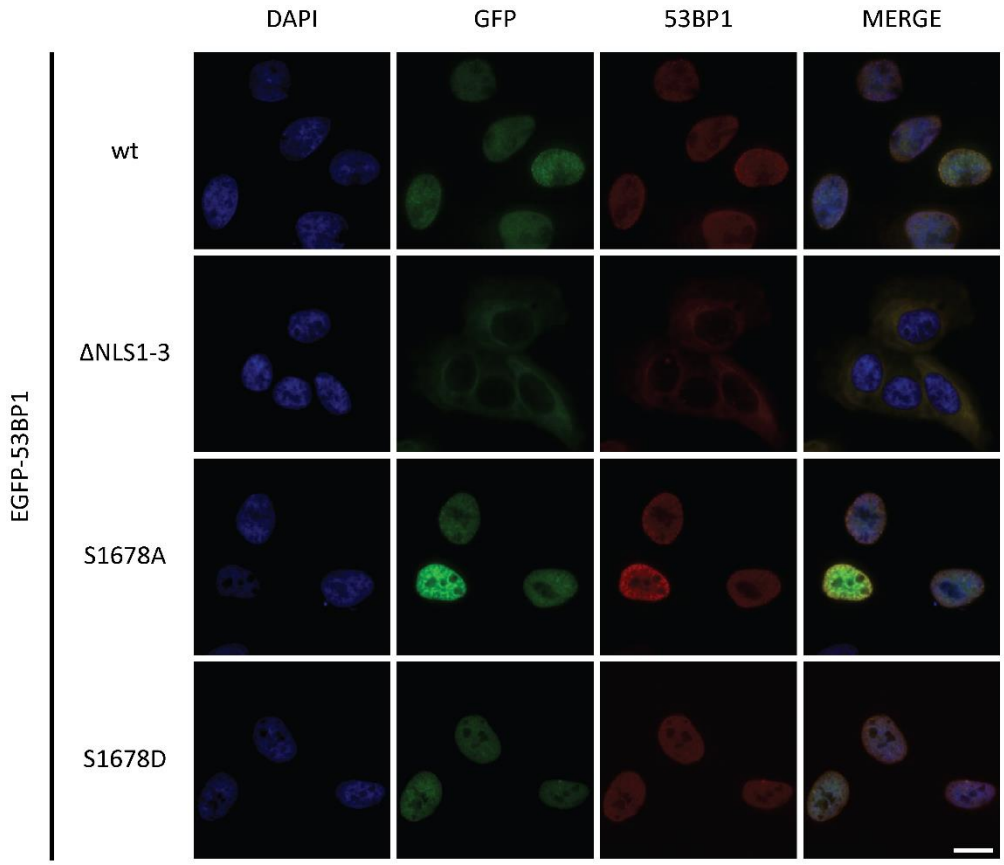


**Supplementary Figure 3. Nuclear localization of EGFP-53BP1-S1678A and EGFP-53BP1-S1678D mutants.** U2OS cells were transfected with DNA constructs encoding indicated EGFP-53BP1 mutants. Cells were fixed 48 h after transfection and stained with 53BP1 antibody (to confirm that EGFP signal corresponds to 53BP1). DAPI was used to visualize nuclei. The results demonstrated that EGFP-53BP1-S1678A and EGFP-53BP1-S1678D mutants are both able to localise to the nucleus. Scale bar 20 µm.